Late Jurassic magmatism, metamorphism, and deformation in the Blue Mountains Province, northeast Oregon

Joshua J. Schwartz[1,†], Arthur W. Snoke[2], Fabrice Cordey[3], Kenneth Johnson[4], Carol D. Frost[2], Calvin G. Barnes[5], Todd A. LaMaskin[6], and Joseph L. Wooden[7]

[1]*Department of Geological Sciences, University of Alabama, Tuscaloosa, Alabama 35487, USA*
[2]*Department of Geology and Geophysics, University of Wyoming, Laramie, Wyoming 82071, USA*
[3]*Laboratoire de géologie de Lyon, Centre National de la Recherche Scientifique CNRS unit 5276, Université Claude Bernard Lyon 1, 69622 Villeurbanne, France*
[4]*Department of Natural Sciences, University of Houston–Downtown, Houston, Texas 77002, USA*
[5]*Department of Geosciences, Texas Tech University, Lubbock, Texas 79409-1053, USA*
[6]*Department of Geological Sciences, University of Oregon, Eugene, Oregon 97403, USA*
[7]*Stanford University, Department of Geological and Environmental Sciences, Stanford, California 94305, USA*

ABSTRACT

An early to mid-Mesozoic record of sedimentation, magmatism, and metamorphism is well developed in the Blue Mountains Province of northeast Oregon. Detailed studies both north and south of the Blue Mountains Province (e.g., terranes of the Intermontane belt, Klamath Mountains, and western Sierra Nevada) have documented a complex Middle to Late Jurassic orogenic evolution. However, the timing of magmatic, metamorphic, and deformational events in the Blue Mountains, and the significance of these events in relationship to other terranes in the western North American Cordillera remain poorly understood. In this study, we investigate the structural, magmatic, and metamorphic histories of brittle to semibrittle deformation zones that indicate widespread Late Jurassic orogenesis in the Blue Mountains Province. Folding and faulting associated with contractional deformation are primarily localized along terrane boundaries (e.g., Baker-Wallowa and Baker–Izee–Olds Ferry boundaries) and within the composite Baker oceanic mélange terrane (e.g., Bourne-Greenhorn subterrane boundary). These brittle to semibrittle deformation zones are broadly characterized by the development of E-W–oriented slaty to spaced cleavage in fine-grained metasedimentary rocks of the Baker terrane (e.g., Elkhorn Ridge Argillite), approximately N-S–divergent folding, and N- and S-dipping reverse and thrust faulting on opposite flanks of the Baker terrane.

Similarly oriented contractional features are also present in late Middle Triassic to early Late Jurassic (i.e., Oxfordian Stage, ca. 159 Ma) sedimentary rocks of the John Day and Huntington areas of northeast Oregon. Radiometric age constraints from youngest detrital zircons in deformed sedimentary rocks and crystallization ages of postkinematic plutons, which intrude the deformation zones, limit deformation to between ca. 159 and ca. 154 Ma. We suggest that the widespread, approximately N-S–directed contractional features in the Blue Mountains Province record a short-lived, intense early Late Jurassic deformational event and preserve an example of upper-crustal strain localization associated with terminal arc-arc collision between the Olds Ferry and Wallowa island-arc terranes. The age interval of deformation in the Blue Mountains Province is younger than Middle Jurassic deformation in the Canadian Cordillera and Klamath Mountains (Siskiyou orogeny) and predates classic Nevadan orogenesis.

INTRODUCTION

Middle to Late Jurassic magmatism, metamorphism, and deformation are well documented in the accreted terranes of the Klamath Mountains of southwestern Oregon and northwestern California, as well as in the western Sierra Nevada of east-central California (e.g., Schweickert and Cowan, 1975; Schweickert et al., 1984; Wright and Fahan, 1988; Hacker et al., 1995). For decades, Jurassic orogenesis in the western North American Cordillera was generally referred to as the "Nevada orogeny" (Blackwelder, 1914; Taliaferro, 1942; Lanphere et al., 1968; Schweickert et al., 1984); however, widespread use of radiometric dating, especially U-Pb (zircon) geochronology, has led to the recognition of distinct orogenic episodes during the Jurassic Period (Coleman et al., 1988; Wright and Fahan, 1988; Hacker et al., 1995). In the Klamath Mountains, the classic Nevadan orogeny has been restricted to the Late Jurassic (ca. 153–150 Ma; Harper and Wright, 1984; Chamberlain et al., 2006), and an important Middle Jurassic orogeny has been referred to as the Siskiyou orogeny (ca. 169–161 Ma; Coleman et al., 1988; Barnes et al., 2006; Snoke and Barnes, 2006). These regional contractional events were separated by a widespread extensional episode manifested by the development of ophiolitic assemblages (e.g., Preston Peak, Josephine ophiolites: Snoke, 1977; Saleeby et al., 1982; Harper and Wright, 1984; Harper et al., 1994; Snoke and Barnes, 2006). Although early Mesozoic rocks in northeast Oregon are believed to be a northward continuation of the greater Klamath-Sierra arc trend (e.g., Dickinson, 2004; LaMaskin et al., 2008b), extrapolation of Jurassic orogenesis northward into the Blue Mountains Province, northeast Oregon, has been problematic in part due to a lack of well-constrained geochronological data within a detailed geologic context.

In this article, we summarize new structural, geochronological, and geochemical data with implications for Late Jurassic orogenesis in the Blue Mountains Province. We describe several anastomosing, brittle to semibrittle fault zones within the Baker oceanic mélange terrane (Bourne-Greenhorn subterrane fault zone; Figs. 1–3), as well as along terrane boundaries (e.g.,
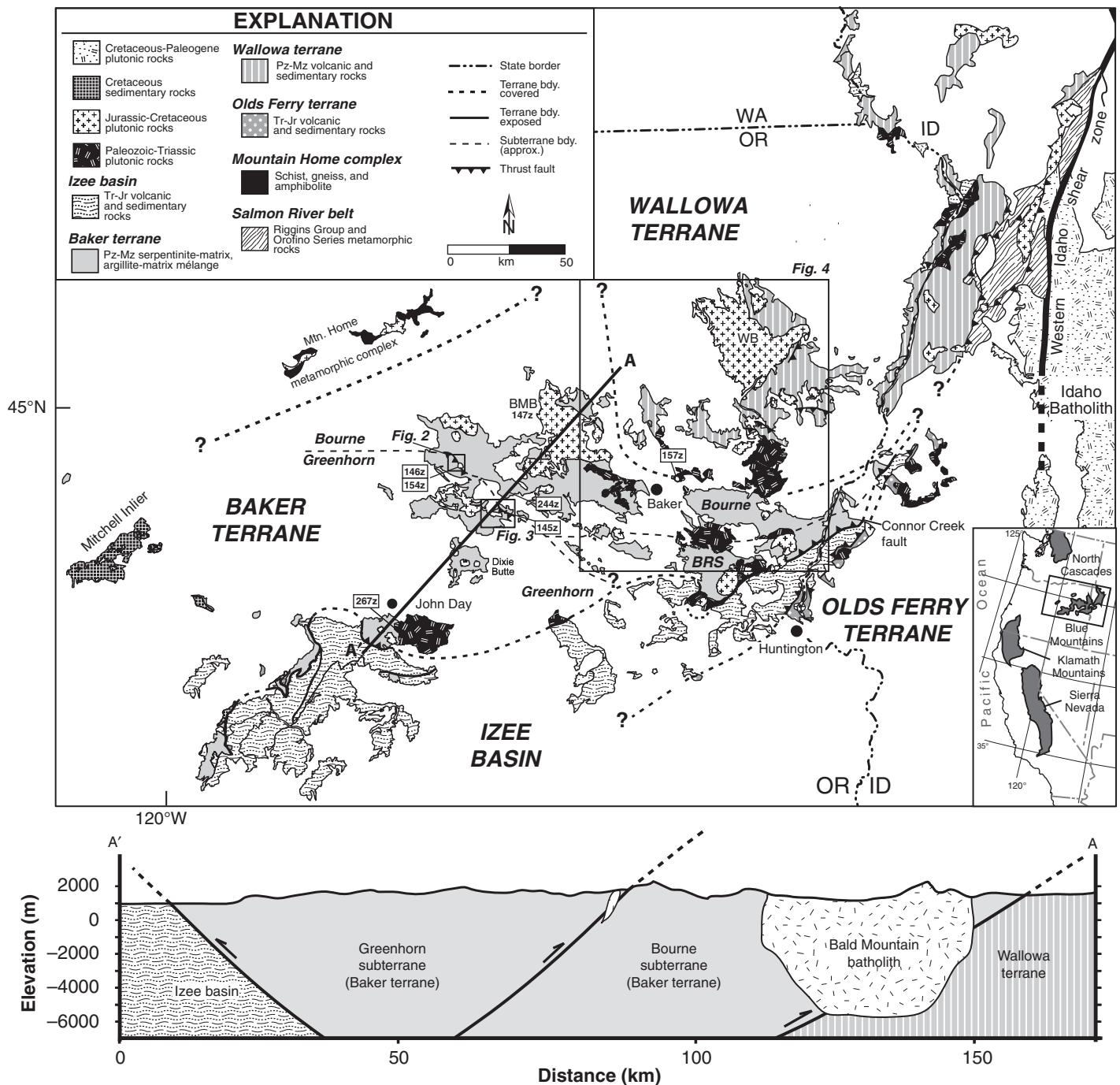
†E-mail: jschwartz@geo.ua.edu

Figure 1. Regional map of the Blue Mountains Province, northeast Oregon and western Idaho, showing the locations of the various terranes and subterranes (modified from LaMaskin et al., 2009b). Locations of Figures 2–4 are shown for reference. The ^{206}Pb/^{238}U zircon ages of igneous rocks are shown in white boxes. Inset map shows location of the Blue Mountains Province with respect to other Paleozoic–Mesozoic accreted terranes of the North American Cordillera. WB—Wallowa batholith; BMB—Bald Mountain batholith; BRS—Burnt River Schist.

Baker-Wallowa and Baker–Izee–Olds Ferry boundaries; Figs. 1 and 4) in the Blue Mountains Province. These fault zones accommodated significant contractional strain at upper-crust levels within a broad area encompassing an accretionary complex, forearc, and arc terranes. We propose that the Late Jurassic structural features that we observe in the Blue Mountains Province are related to a short-lived, intense, collisional event (159–154 Ma) between the Olds Ferry and Wallowa island-arc terranes synchronous with bivergent thrusting of rocks of the Baker terrane onto the colliding island arcs. This process of tectonic back flow (see Hamilton, 1979, his figure 99, p. 192–193) of the Baker mélange wedge onto the flanks of the arc terranes accommodated a significant amount of upper-crustal contractional strain, but another important

Late Jurassic orogenesis in the Blue Mountains Province
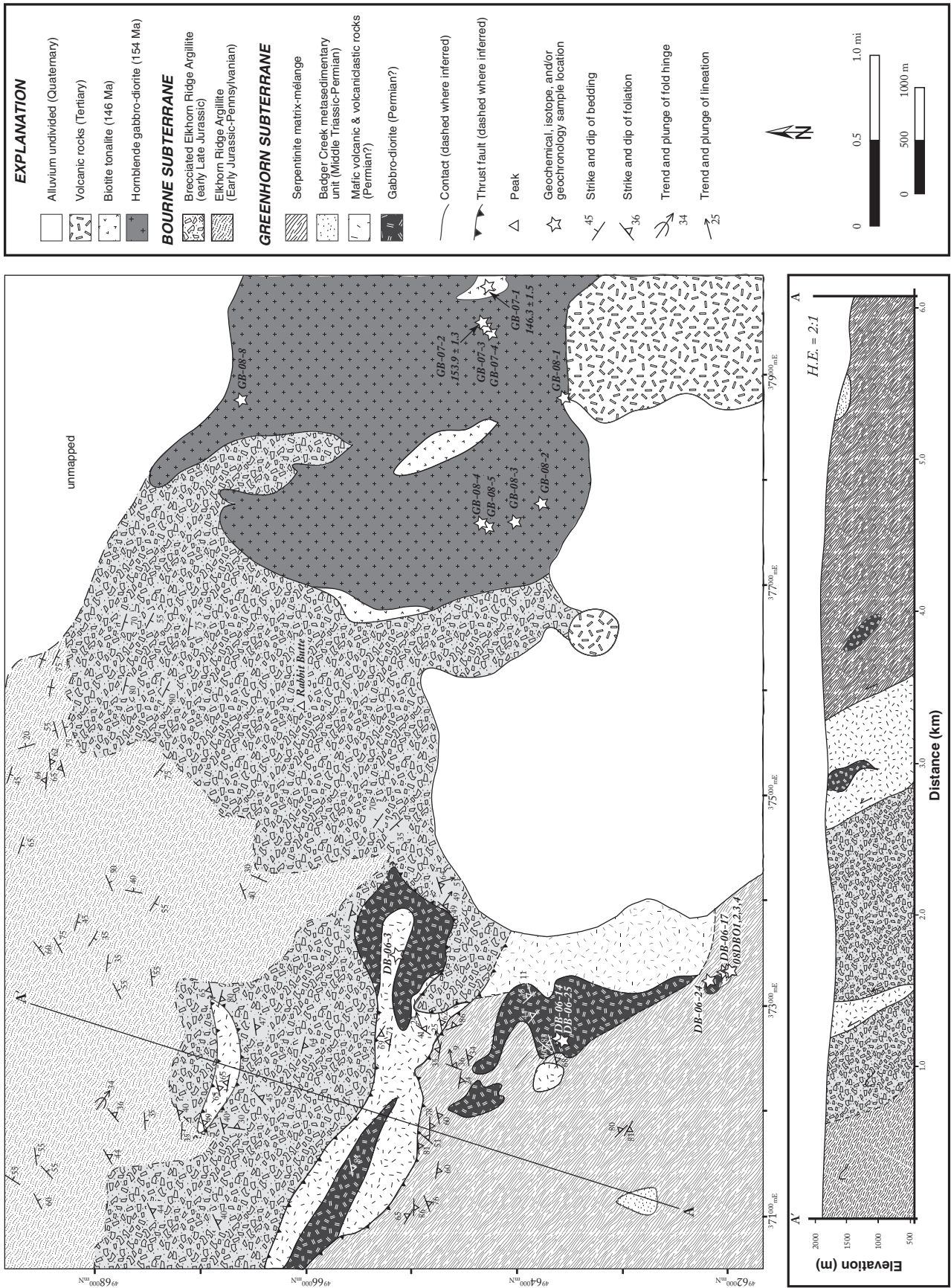
Figure 2. Simplified geologic map of the Desolation Butte area, which spans the Greenhorn subterrane (south) and Bourne subterrane (north)(after Evans, 1995). The Greenhorn subterrane is characterized by serpentinite-matrix mélange, whereas the Bourne subterrane contains chiefly Elkhorn Ridge Argillite. At this subterrane contact, the Greenhorn subterrane is thrust over the Bourne subterrane along a moderately S-dipping, greenschist-facies fault zone. Locations of samples discussed in text are shown by stars. H.E.—horizontal exaggeration.

element in this arc-arc collisional process was tectonic slicing of rocks of the Wallowa terrane into the Baker terrane (Ferns and Brooks, 1995; Schwartz et al., 2010). The age interval of deformation in the Blue Mountains Province is younger than Middle Jurassic deformation in the Canadian Cordillera and Klamath Mountains (Siskiyou orogeny), but it also apparently predates classic Nevadan orogenesis.

GEOLOGIC FRAMEWORK OF THE BLUE MOUNTAINS PROVINCE

The Blue Mountains Province of northeast Oregon and western Idaho (Fig. 1) consists of three distinct terrane types, which record over ~140 m.y. of sedimentation, magmatism, and deformation from the Early Permian through Early Cretaceous (Fig. 1; Brooks and Vallier, 1978; Dickinson and Thayer, 1978; Dickinson et al., 1979; Walker, 1986; Silberling et al., 1987; LaMaskin et al., 2009a). These terranes include the Wallowa and Olds Ferry island arc–related terranes, Baker oceanic mélange terrane, and Izee forearc or collisional basin (Dickinson and Thayer, 1978; Dickinson, 1979; Dorsey and LaMaskin, 2007; LaMaskin et al., 2008a, 2011). Late Jurassic to Early Cretaceous magmatic rocks intrude the Baker terrane and Wallowa island-arc terrane (Fig. 1), as well as the Izee–Olds Ferry terranes, and Salmon River suture zone (e.g., Lund, 1995; Snee et al., 1995; Gray and Oldow, 2005; Johnson and Schwartz, 2009).

Wallowa Island-Arc Terrane

The Wallowa terrane is a composite island-arc system consisting of a Permian island-arc complex overlain and/or intruded by Upper Triassic to Lower Jurassic sedimentary, volcanic, volcaniclastic, and plutonic rocks (Vallier, 1977, 1995; Vallier et al., 1977; Vallier and Batiza, 1978; Kays et al., 2006). Plutonic basement rocks range in age from ca. 264 to 215 Ma (Walker, 1986, 1995; Kurz et al., 2009; Schwartz et al., 2010). High-precision U-Pb ages from syndeformational sphene neoblasts in the Cougar Creek complex record left-lateral mylonitic fabric development from 260 to 220 Ma, synchronous with igneous activity (Kurz et al., 2009). Lower Permian to Upper Triassic volcanic rocks consist of keratophyre and spilite interbedded within volcaniclastic rocks (Seven Devils Group; Vallier, 1977). Upper Triassic well-sorted conglomerate and breccia ("Lower Sedimentary Series" of Prostka and Bateman, 1962), massive to thin-bedded limestone (e.g., Martin Bridge Formation; Stanley et al., 2008), and an Upper Triassic to Lower Jurassic clastic sequence (Hurwal Formation) are unconformably overlain by Upper Jurassic to Upper Cretaceous sedimentary rocks (e.g., Coon Hollow Formation; Brooks and Vallier, 1978; Dorsey and LaMaskin, 2007; LaMaskin et al., 2008b, 2009a). The Wallowa terrane is intruded by Early Cretaceous plutonic rocks of the Wallowa batholith (e.g., Taubeneck, 1964, 1967, 1995; Walker, 1989; Johnson et al., 1997; Johnson and Schwartz, 2009), as well as by smaller Jurassic–Cretaceous plutons (White, 1973; Johnson et al., 2007; Unruh et al., 2008; Johnson and Schwartz, 2009; Schwartz and Johnson, 2009).

Olds Ferry Island-Arc Terrane

The Olds Ferry island-arc terrane consists chiefly of Middle Triassic to Lower Jurassic weakly metamorphosed, volcanic, volcaniclastic, and sedimentary rocks of the Huntington Formation (Brooks and Vallier, 1978; Brooks, 1979; Tumpane and Schmitz, 2009). These volcanogenic rocks are dominantly andesitic in composition, but they range from basalt to rhyolite and record arc-related plutonism and volcanic activity from Middle Triassic to Early Jurassic time (Walker, 1995; Tumpane and Schmitz, 2009). Volcanic and volcaniclastic rocks of the Huntington Formation are locally in fault contact with penetratively deformed Jurassic sedimentary rocks of the Lower to Middle Jurassic Weatherby Formation, which has southeast-vergent folds (Avé Lallemant, 1983). Previous workers have also interpreted this contact as an unconformity (cf. Brooks and Vallier, 1978; Dickinson, 1979); however, it likely has a composite history as a faulted unconformity. If this interpretation is correct, the tectonic displacement along this boundary may be relatively minor, especially as compared to the complex fault zones that mark the boundary of the Baker terrane with the Wallowa and Olds Ferry island-arc terranes (see following). The Weatherby Formation is, in turn, bound on the northwest by the reverse-sense, northeast-striking, northwest-dipping Connor Creek fault (Brooks and Vallier, 1978; Avé Lallemant, 1983), which emplaced rocks of the Baker terrane onto the younger, Jurassic footwall rocks (cf. Fig. 1).

Baker Terrane

The Baker terrane is the focus of this study and lies between the Wallowa and Olds Ferry island-arc terranes (Fig. 1). It is the oldest and most structurally complex terrane in the Blue Mountains Province, containing fragments of ocean-floor (non-arc) and island-arc volcanic, plutonic, and sedimentary rocks ranging in age from Early Permian to Early Jurassic (Nestell, 1983; Walker, 1986, 1995; Blome and Nestell, 1991; Carpenter and Walker, 1992; Ferns and Brooks, 1995; Nestell et al., 1995; Nestell and Nestell, 1998; Nestell and Orchard, 2000; Schwartz et al., 2010; this paper). Previous workers have recognized three subterranes (Bourne and Greenhorn subterranes and Burnt River Schist; Fig. 1), which preserve a complex history of deposition, magmatism, metamorphism, and structural processes marginal to the Wallowa and Olds Ferry arc terranes (Ferns and Brooks, 1995; Schwartz et al., 2010).

Bourne Subterrane

The dominant lithologic unit of the Bourne subterrane is the Elkhorn Ridge Argillite (Pardee and Hewett, 1914; Gilluly, 1937; Coward, 1983), which contains dominantly disrupted chert and argillite with lesser blocks of coherent, bedded argillite and ribbon chert. These rocks are commonly tightly folded and cut by a penetrative slaty to spaced cleavage, faults, and/or zones of cataclasite. Fusulinids, conodonts, corals, and crinoids in limestones are Middle Devonian to Late Triassic age (Vallier et al., 1977; Wardlaw et al., 1982; Nestell, 1983; Nestell et al., 1995; Nestell and Nestell, 1998; Nestell and Orchard, 2000), whereas cherts contain Permian to Early Jurassic radiolarian fauna (Coward, 1983; Blome et al., 1986; Ferns et al., 1987; F. Cordey, 2005–2010, personal commun.). Both Tethyan- and McCloud-affinity fusulinids are reported from the Bourne subterrane (Bostwick and Koch, 1962; Bostwick and Nestell, 1965; Nestell, 1983).

Fault-bounded slabs or slices of Middle to Late Triassic arc-related plutonic/hypabyssal, volcaniclastic, and sedimentary rocks also occur within the Elkhorn Ridge Argillite near the boundary with the Wallowa terrane (Stimson, 1980; Brooks et al., 1982a, 1982b; Ferns et al., 1987; Bishop, 1995b; Evans, 1995; Ferns and Brooks, 1995; Walker, 1995; Schwartz et al., 2010). These slabs/slices are faulted into Elkhorn Ridge Argillite along moderate- to low-angle, southward-dipping, reverse-sense faults (Ferns and Brooks, 1995). Ferns and Brooks (1995) and Schwartz et al. (2010) have suggested that these slabs of meta-igneous and metasedimentary rocks may represent imbricated fragments of the nearby Wallowa island-arc terrane, which became tectonically intercalated into the Baker terrane in post–Late Triassic time.

Tectonic slices of alkalic pillow basalts and related volcaniclastic and metasedimentary rocks are also present within the Bourne subterrane at the tectonic boundary between the Bourne and Greenhorn subterranes (Fig. 3; Olive Creek unit of Ferns and Brooks, 1995). Radiolarian-bearing cherts associated with these slices contain Permian fauna (Ferns and Brooks, 1995). These
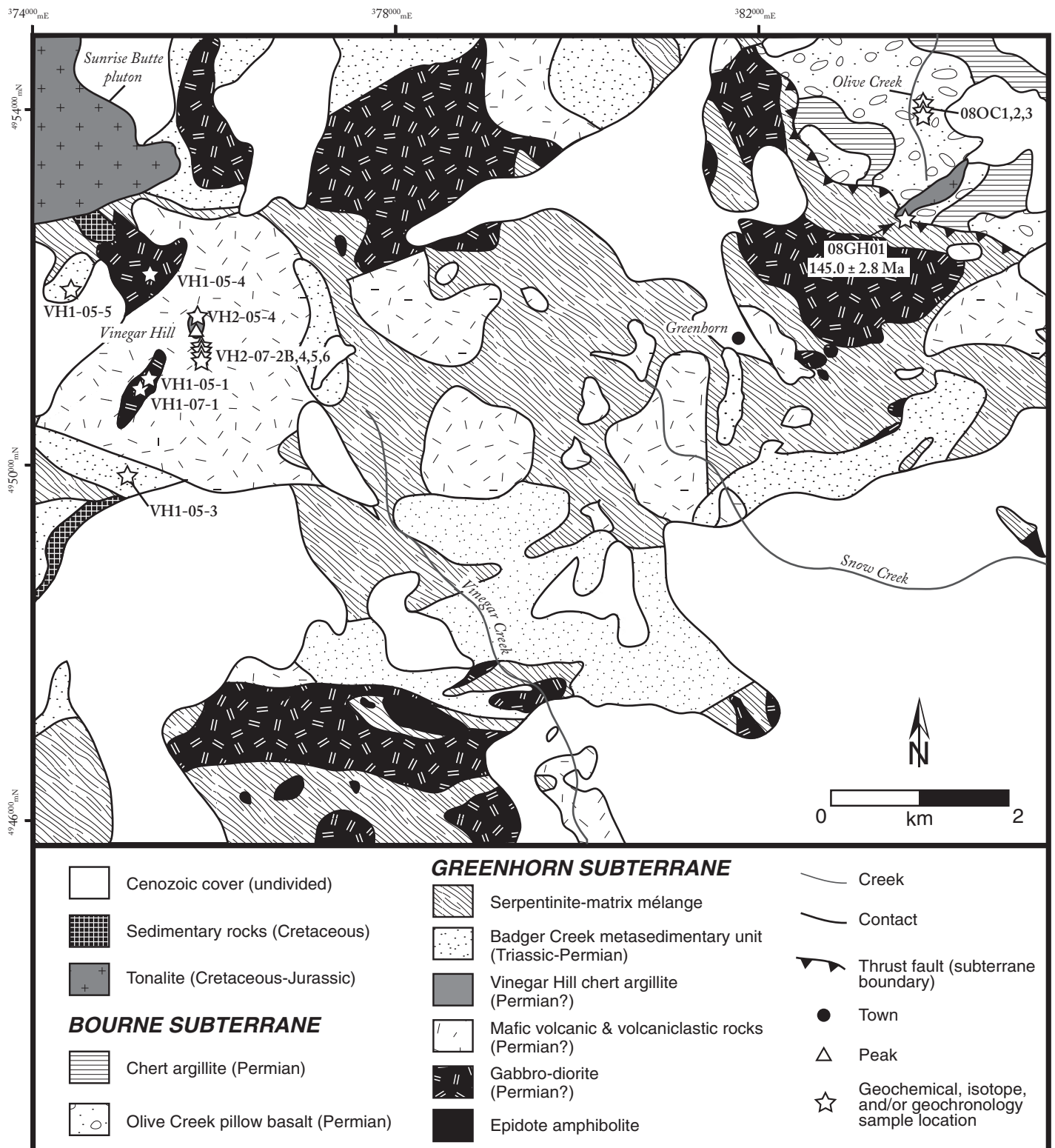
Figure 3. Simplified geologic map of the Bourne-Greenhorn subterrane boundary near the town of Greenhorn (modified from Ferns and Brooks, 1995). Locations of samples discussed in text are shown by stars.
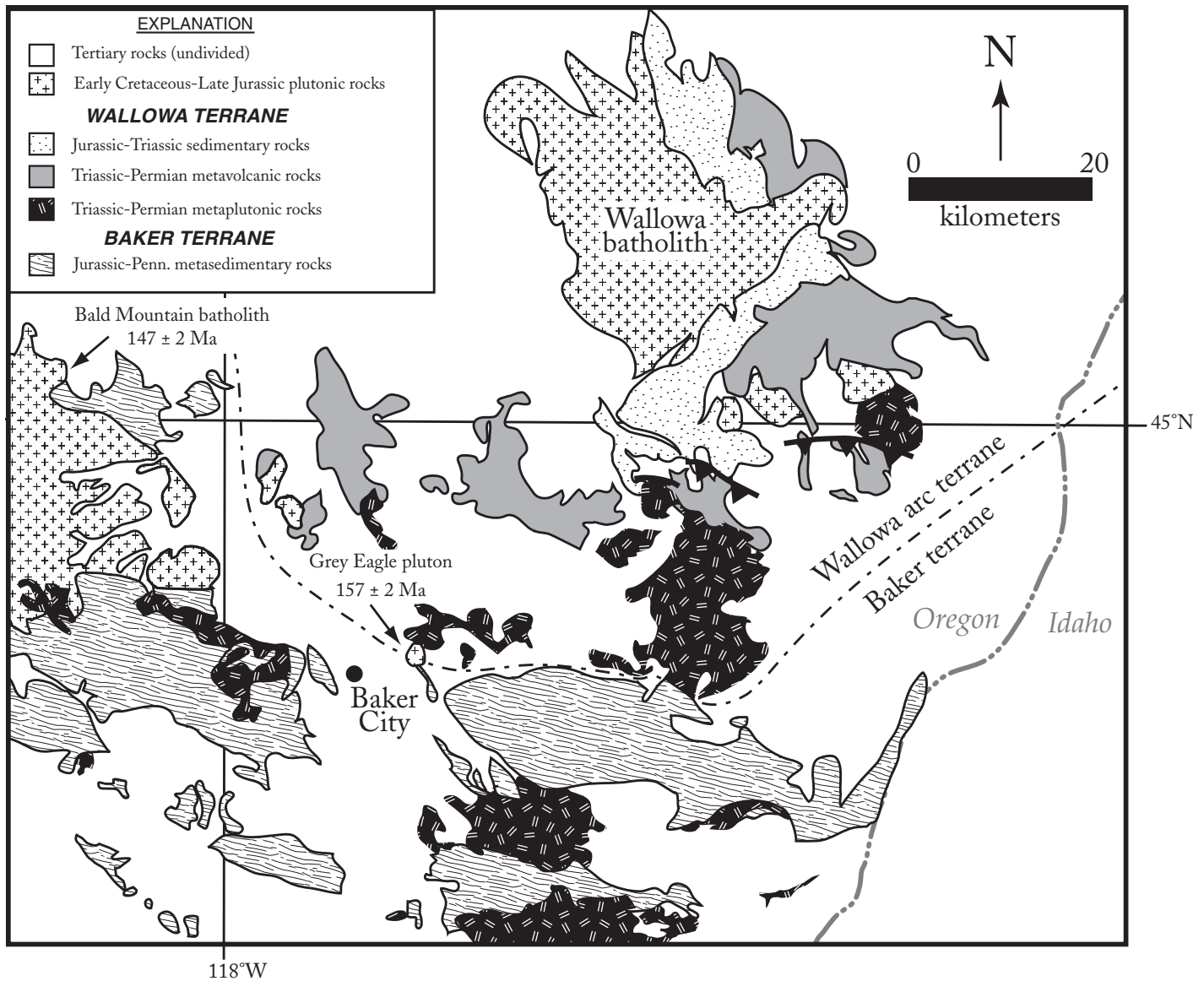
Figure 4. Geologic map of the Baker-Wallowa terrane boundary (modified from Schwartz et al., 2010). Meta-igneous thrust slices (black) occur throughout the Bourne subterrane and are interpreted to be imbricated fragments of the adjacent Wallowa island arc tectonically emplaced into the Baker terrane during Late Jurassic contractional deformation.

volcanic rocks are geochemically distinct from the arc-related, meta-igneous rocks distributed along the Baker-Wallowa terrane margin and may represent slices of enriched oceanic crust faulted into the Baker terrane during a period of collision between the Wallowa and Olds Ferry terranes (Ferns and Brooks, 1995).

Greenhorn Subterrane

The Greenhorn subterrane consists of serpentinite-matrix mélange and includes large blocks of arc-related metaplutonic, metavolcanic (locally pillowed), and metavolcaniclastic rocks, brecciated chert-argillite, and amphibolitic rocks. These rocks are overlain by Permian–Triassic conglomerate, sandstone, argillite, and limestone of the Badger Creek metasedimentary unit (Wheeler, 1976; Mullen, 1978; Ferns and Brooks, 1995). An upper age for mélange development is indicated by the presence of altered clasts of ultramafic rocks (ophicalcite) in the Permian–Triassic Badger Creek unit, suggesting that mélange development occurred prior to and/or during deposition of the overlying metasedimentary unit (Carpenter and Walker, 1992; Ferns and Brooks, 1995). In contrast to the Bourne subterrane, where both Tethyan and McCloud fusulinids are present, the Greenhorn subterrane apparently contains only fusulinids of McCloud affinity (Mullen, 1978). A well-preserved radiolarian fauna of Early and Middle Jurassic age from a block of black chert in serpentinite-matrix mélange (i.e., Miller Mountain mélange) indicates that deposition of chert-argillite sequences in the Greenhorn subterrane may have occurred into mid-Mesozoic time (Jones et al., 1977).

The Canyon Mountain complex has been included in the Greenhorn subterrane by several authors, who interpret it as a large tectonic slab within serpentinite-matrix mélange (e.g., Brooks and Vallier, 1978; Dickinson and

Thayer, 1978; Dickinson et al., 1979; Mullen, 1983, 1985; Bishop, 1995b; Walker, 1995). Alternatively, it may represent the Permian part of the Olds Ferry volcanic island-arc terrane (Avé Lallemant, 1995). Multigrain U-Pb zircon fractions range from 276 to 268 Ma, with some highly discordant ages possibly suggesting the presence of older components (Walker, 1995). Major-, minor-, and trace-element studies on various rocks are consistent with formation in a suprasubduction-zone environment (Gerlach et al., 1981; Leeman et al., 1995).

Burnt River Schist Subterrane

The Burnt River Schist (Gilluly, 1937; Ashley, 1966, 1995) is a heterogeneous suite of rocks chiefly dominated by fine-grained metasedimentary rocks (e.g., slaty argillite and siliceous phyllite), but it also includes mappable bodies of greenschist-facies metavolcanic rocks, mafic to felsic metaplutonic rocks (i.e., Blue Spring Gulch), and impure marble. The Burnt River Schist has been correlated with the Elkhorn Ridge Argillite and has commonly been considered to be a slightly higher-grade equivalent (Ashley, 1995). However, new isotopic data (Mailloux et al., 2009) indicate that such a straightforward correlation is unlikely because the Burnt River Schist is isotopically distinct from the Elkhorn Ridge Argillite. Paleontological data also suggest a distinction between the Elkhorn Ridge Argillite and Burnt River Schist. For example, impure calcite marble at one locality (near French Spring) in Burnt River Canyon yielded Middle to Late Triassic conodonts (Morris and Wardlaw, 1986), and the Nelson Marble (an equivalent unit exposed to the east near Durkee, Oregon) also yielded Middle to Late Triassic conodonts (Morris and Wardlaw, 1986). On the other hand, the Elkhorn Ridge Argillite has yielded very diverse faunas, which broadly range in age from Permian through Early Jurassic (Vallier et al., 1977; Wardlaw et al., 1982; Nestell, 1983; Nestell et al., 1995; Nestell and Nestell, 1998; Nestell and Orchard, 2000).

The Burnt River Schist experienced polyphase deformation during moderately high-pressure, low-grade regional metamorphism (Ashley, 1966, 1995). A penetrative slaty to phyllitic foliation (S_1) is the most characteristic structural fabric in the fine-grained metasedimentary rocks of the Burnt River Schist. This foliation is locally folded by late to postmetamorphic folds, which are nearly coaxial to the first-phase folds (Ashley, 1995). Tight to isoclinal folds (F_1) are related to the penetrative foliation (S_1), and a prominent elongation lineation is locally developed in the metasedimentary rocks in Burnt River Schist. For example, lithic clasts in meta-conglomerate layers are blade shaped, indicating a strong component of elongation strain during the D_1 deformation phase. In other outcrops of the slaty to phyllitic metasedimentary rocks, intersection lineations ($S_1 \times S_2$) are common, occasionally form mullion structure (Fig. 12.10 *in* Ashley, 1995, p. 479), and are subparallel to the hinge lines of F_2 folds.

Greenschist-facies regional metamorphism is indicated by metamorphic mineral assemblages in both the metasedimentary and metavolcanic rocks of the Burnt River Schist. Biotite-grade metamorphic mineral assemblages (upper greenschist facies) are present in the Deer Creek phyllite unit of the Burnt River Schist, whereas lower-greenschist-facies metamorphic mineral assemblages occur in the Campbell Gulch phyllite unit of the Burnt River Schist (cf. Figs. 12.3 and 12.4 *in* Ashley, 1995). Greenstones (meta-lavas or scarce meta-tuff) in the Burnt River Schist typically contain: albite, quartz, actinolite, chlorite, clinozoisite/epidote, white mica, calcite, and leucoxene, indicative of greenschist-facies metamorphism. Scarce pumpellyite also occurs in the metavolcanic rocks. Relict igneous minerals, such as clinopyroxene and hornblende, are common in the mafic metavolcanic rocks (Ashley, 1995). Locally, the rocks of the Burnt River Schist were contact-metamorphosed, reaching hornblende to hornblende-pyroxene-hornfels facies adjacent to Jurassic(?)–Cretaceous plutons, which intruded this generally low-grade metamorphic terrane. Ashley (1995) concluded that the Burnt River Schist was developed in a subduction complex during Permian–Triassic time.

Middle Jurassic–Early Cretaceous Plutonism

Middle Jurassic to Early Cretaceous magmatism in the Blue Mountains Province consists of three distinct pulses of plutonism, which occurred between 162 and 154 Ma, 148 and 141 Ma, and 125 and 111 Ma (Walker, 1986, 1989, 1995; Johnson and Barnes, 2002; Johnson et al., 2007; Unruh et al., 2008; Johnson and Schwartz, 2009; Schwartz and Johnson, 2009). These plutons form spatially distinct belts that were emplaced prior to ~60° of post–Early Cretaceous clockwise rotation (Wilson and Cox, 1980; Housen and Dorsey, 2005; Housen, 2007). The oldest magmatic rocks (ca, 162–154 Ma) consist of late Middle–early Late Jurassic plutons in the Wallowa terrane (Unruh et al., 2008) and Greenhorn subterrane of the Baker terrane (Parker et al., 2008; Johnson and Schwartz, 2009; Schwartz and Johnson, 2009). These plutons are typically <3 km^2 in areal extent and range in composition from gabbro to quartz diorite. Geochemically, they are characterized as magnesian, calcic to calc-alkalic, and metaluminous (Frost et al., 2001), and they contain relatively low Na, Al, and Sr concentrations, but high Y concentrations.

A second distinct phase of magmatism occurred in the Baker and Wallowa terranes, with U-Pb zircon ages ranging from ca. 148 to 141 Ma. This phase of magmatism consists of two spatially and geochemically distinct belts of relatively sodic and aluminous tonalite-trondhjemite-granodiorite (TTG) plutons with high Sr/Y (Tulloch and Kimbrough, 2003) in the Greenhorn subterrane of the Baker terrane, and low Sr/Y TTG plutons and batholiths in the Bourne subterrane (Baker terrane) and Wallowa terrane (Johnson and Schwartz, 2009; Schwartz and Johnson, 2009).

The last episode of magmatism in the region (pre–Idaho batholith emplacement) consists of small plutons of tonalitic and trondhjemitic composition that intrude the Wallowa, Baker, and Izee–Olds Ferry terranes. This group consists of two subgroups: (1) 124–120 Ma metaluminous hornblende-biotite tonalite plutons in a NE-SW–trending belt eastward (inboard) of the Late Jurassic belt, and (2) 125–111 Ma, strongly peraluminous tonalite and trondhjemite plutons that mostly occur in a belt subparallel to the initial Sr isotopic 0.706 line in western Idaho (Johnson and Schwartz, 2009).

METHODS

Major-, Trace-Element, and Isotope Geochemistry

Samples for major- and trace-element, and Rb-Sr and Sm-Nd isotope geochemistry were selected to represent the major rocks types of the Bourne and Greenhorn subterranes. Samples were collected from the least-altered and least-deformed rocks to minimize effects of late-stage, low-grade alteration. Rock chips were handpicked at the University of Wyoming and University of Alabama, and weathered surfaces and veins were discarded. Samples collected for geochemical analysis consisted of six samples of metaplutonic rocks and eight samples of metavolcanic rocks from the Bourne-Greenhorn boundary, three plutonic rocks and one quartz keratophyre from the Canyon Mountain complex, 12 samples of terrane-stitching plutonic rocks, and four samples of metasedimentary rocks from the Badger Creek unit and Vinegar Hill chert-argillite unit. Samples for isotopic analyses were selected from the metasedimentary rocks. Samples collected for U-Pb geochronology consist of a volcaniclastic breccia from the Bourne subterrane near the Bourne-

Greenhorn subterrane boundary, a hornblende diorite that intrudes Elkhorn Ridge Argillite and meta-igneous slices at the Bourne subterrane–Wallowa terrane boundary, a biotite-hornblende diorite and biotite tonalite from the Gold Bug pluton that intrudes the Bourne-Greenhorn subterrane boundary (Fig. 2), a muscovite-biotite tonalite that intrudes the Bourne-Greenhorn subterrane boundary (Fig. 3), and a biotite-hornblende tonalite from the Bald Mountain batholith (Fig. 4). Detrital zircon U-Pb ages from a deformed sample of the Lonesome Formation in the John Day region were used to constrain the maximum age of deformation that affected that area (LaMaskin et al., 2011). Sample locations are shown on Figures 1–4, and UTM locations are given in GSA Data Repository Table A1.[1] Data for these samples are presented in Tables 1–4. Additional analytical details are given in the GSA Data Repository (see footnote 1).

Radiolarian Micropaleontology

Radiolarian-bearing cherts were sampled to determine the timing and duration of sedimentation in the Baker terrane. Due to both regional greenschist-facies and localized contact metamorphism, careful field selection of suitable radiolarian-bearing chert beds and appropriate hydrofluoric acid methods in the laboratory were necessary for obtaining diagnostic fauna. Chert samples for radiolarian analysis were collected from visibly bedded strata and are interpreted to represent primary depositional ages.

RESULTS

Field Observations and Petrography of the Bourne-Greenhorn Subterrane Fault Zone

Structural field mapping and sample collection were conducted in two brittle to semi-brittle fault zones within the Baker terrane (the Bourne-Greenhorn subterrane boundary; Figs. 2 and 3) to evaluate structural features, metamorphic mineral assemblages, and primary intrusive relationships. In these areas, the Greenhorn subterrane (hanging wall) is thrust over the Bourne subterrane (footwall) along a series of anastomosing, moderately to steeply dipping faults. Footwall rocks of the Bourne subterrane consist chiefly of Elkhorn Ridge Argillite and intercalated meta-igneous fault slices, whereas hanging-wall rocks of the Greenhorn subterrane contain a diverse assemblage of meta-peridotite, serpentinite,

amphibolite, metasedimentary rocks (Badger Creek unit), and meta-igneous rocks. Both subterranes are intruded by syn- to postkinematic plutons. Descriptions of primary rock units observed and sampled for geochemical and geochronologic analyses are presented next.

Serpentinite-Matrix Mélange (Greenhorn Subterrane)

The dark olive-green to black serpentinite matrix of the Greenhorn subterrane makes up over 50% of surface exposures (Figs. 2 and 3). Serpentinite varies from massive to foliated, and both types occur in close spatial proximity. Massive serpentinite commonly forms ridges and is easily distinguished by its characteristic red-brown weathering and less abundant vegetation (e.g., east of Vinegar Hill; Fig. 3) compared to other areas not underlain by serpentinite. Foliated serpentinite commonly wraps around more massive serpentinite and displays a strong, variably oriented schistose foliation. Internally unsheared phacoids of serpentinite are found in more intensely deformed areas and range up to tens of centimeters in length. Phacoids are surrounded by foliated and anastomosing serpentinite, which defines a spaced cleavage. Near blocks of metaplutonic and metavolcaniclastic rocks, deformational fabrics are more intense and show more consistent orientations.

Metasomatic reaction rinds (i.e., rodingites) at serpentinite–mafic rock contacts are uncommon, only occurring locally around margins of some gabbroic blocks (Ferns and Brooks, 1995). These reaction rinds form during the serpentinization process from elemental exchange with mafic rocks, possibly in response to silica activity gradients (e.g., Coleman, 1963; Frost and Beard, 2007). The lack of these reaction rinds in the metavolcanic rocks and their rarity in the metaplutonic rocks suggest that metavolcanic and metaplutonic rocks were tectonically incorporated into the serpentinite-matrix mélange relatively late and after initial serpentinization.

Ultramafic Rocks (Greenhorn Subterrane)

Small exposures of peridotite and pyroxenite are preserved in the massive serpentinite. These ultramafic rocks weather to a brown and reddish-orange color and locally preserve vestiges of primary minerals on weathered surfaces. Olivine is almost entirely altered to serpentine-group minerals, although small, unaltered kernels are locally preserved. Pyroxenes are less altered and range from tens of millimeters to centimeters in size. Clinopyroxene grains display lobate boundaries and are generally undeformed. No plagioclase was observed. Alteration minerals are serpentine-group minerals, chlorite, talc, carbonate, and magnetite.

Meta-lavas and Metavolcaniclastic Rocks (Greenhorn Subterrane)

Metamorphosed lavas and metavolcaniclastic rocks are well exposed on Vinegar Hill and are the dominant rock type in the area (Fig. 3). These metavolcanic rocks include basalt and andesite flows. Metavolcaniclastic rocks are more abundant than meta-lavas and typically are massive, heterogeneous deposits consisting of clasts of basalt (locally pillowed), plagioclase-phyric andesite, scoria, diabase, gabbro, diorite, argillite, siliceous argillite, and limestone. Basaltic pillow breccias were found near the summit of Vinegar Hill and are sometimes encased in a muddy red matrix (Fig. 5A). Carbonate infillings are also common in the pillow breccias. All the metavolcanogenic rocks are crosscut by cataclastic shear zones associated with chlorite and clinozoisite veins.

Metaplutonic Rocks (Greenhorn Subterrane)

Metaplutonic rocks consist of a heterogeneous assemblage of hornblende gabbro to hornblende quartz diorite. Pegmatitic gabbros are particularly well exposed on Black Butte (SW Vinegar Hill; Fig. 3) and are locally crosscut by fine-grained dioritic dikes and porphyritic gabbros. Coarse-grained gabbros commonly have a high-temperature deformational fabric defined by alignment of plagioclase. Magmatic mineral assemblages in these rocks include plagioclase + clinopyroxene + hornblende ± quartz ± apatite ± sphene. Clinopyroxene is almost always pseudomorphosed by green amphibole and chlorite. Relict clinopyroxene displays lobate and intercumulate textures between plagioclase.

All metaplutonic rocks are strongly overprinted by upper-greenschist- to lower-amphibolite-facies metamorphic assemblages including green hornblende + clinozoisite + chlorite + epidote. Metamorphic veins of clinozoisite and chlorite are ubiquitous features forming an anastomosing network throughout the metaplutonic rocks (Fig. 5B). These metamorphic mineral assemblages are crosscut by zones of cataclastic deformation and brittle fractures (Fig. 5B).

Metasedimentary Rocks (Bourne and Greenhorn Subterranes)

Elkhorn Ridge Argillite is the dominant lithologic unit of the Bourne subterrane (Ferns and Brooks, 1995; Schwartz et al., 2010) and consists of fine-grained argillaceous rocks containing quartz + plagioclase + carbonate ± chlorite ± white mica. Grain sizes for these rocks are typically <5 μm; however, in the Desolation Butte area (Fig. 2), coarse sandstones and pebble conglomerates are locally present. These rocks

---

Late Jurassic orogenesis in the Blue Mountains Province

TABLE 1. WHOLE-ROCK MAJOR- AND TRACE-ELEMENT GEOCHEMICAL DATA

	Meta-igneous rocks from Vinegar Hill and Desolation Butte																Meta-igneous rocks from Canyon Mtn.			
Sample:	VH1-05-1	VH1-05-4	VH1-07-1*	VH2-07-2B	VH2-07-5	VH2-07-6	08DBO1	08DBO2	08DBO4	DB-06-3	DB-06-14	DB-06-24	DB-06-25	08OC-1	08OC-2	08OC-3	CM2-05-1	CM2-05-2	CM2-05-3	CM2-05-4
SiO_2 (wt%)	51.31	47.27	49.13	n.d	54.18	n.d	51.51	49.14	49.54	54.11	52.23	50.24	51.34	45.70	47.06	45.54	48.91	49.51	76.28	76.92
TiO_2	0.69	0.30	0.29	n.d	0.80	n.d	1.35	1.42	1.38	0.79	0.17	1.30	0.14	2.35	2.11	2.08	0.32	0.36	0.16	0.17
Al_2O_3	18.07	16.11	14.25	n.d	13.97	n.d	13.97	13.90	13.86	15.59	19.19	14.84	20.72	15.64	16.73	15.45	16.85	19.75	12.21	12.02
Fe_2O_3	8.22	7.27	8.19	n.d	9.79	n.d	11.55	11.67	10.57	9.79	7.34	11.30	4.58	10.79	9.36	9.15	7.30	6.43	2.59	3.13
MnO	0.15	0.12	0.14	n.d	0.19	n.d	0.20	0.19	0.18	0.18	0.16	0.19	0.09	0.17	0.16	0.15	0.13	0.11	0.01	0.01
MgO	6.74	12.89	12.43	n.d	7.20	n.d	6.70	6.26	6.34	6.59	8.74	7.08	5.54	5.01	4.54	4.81	9.85	8.16	0.37	0.35
CaO	10.39	14.41	13.02	n.d	9.18	n.d	9.67	12.56	13.27	7.36	7.45	10.71	13.99	15.24	13.72	17.53	14.48	13.24	2.88	1.87
Na_2O	4.33	1.53	2.54	n.d	4.45	n.d	3.91	3.63	3.81	5.42	2.91	4.09	3.48	4.34	5.07	4.46	2.11	2.35	5.41	5.44
K_2O	0.08	0.09	0.00	n.d	0.18	n.d	1.01	1.08	0.90	0.11	1.80	0.13	0.11	0.36	0.86	0.50	0.03	0.08	0.06	0.06
P_2O_5	0.01	0.01	0.00	n.d	0.08	n.d	0.13	0.16	0.15	0.06	0.02	0.11	0.02	0.40	0.39	0.34	0.01	0.01	0.03	0.03
LOI	2.23	1.44	2.63	n.d.	0.71	n.d.	2.75	5.11	4.24	2.85	2.81	3.20	2.65	9.28	8.42	9.87	2.62	2.50	0.92	0.73
V (ppm)	207.20	153.20	167.20	263.20	279.40	263.20	283.60	271.40	301.40	252.60	133.40	264.20	84.20	243.80	231.00	239.00	160.60	159.60	12.80	9.60
Cr	28.60	985.60	531.40	270.00	265.60	255.80	184.20	185.40	169.20	107.20	164.80	100.00	127.00	469.20	410.00	381.80	221.60	295.00	b.d.	b.d.
Ni	43.80	233.60	177.40	86.80	80.60	84.00	62.60	64.80	63.00	50.60	65.80	60.00	52.00	247.20	199.00	204.80	113.20	146.60	4.00	5.20
Cu	8.00	84.00	76.20	11.00	92.20	42.00	119.00	112.40	94.60	85.00	96.80	143.00	15.20	73.60	72.00	79.60	52.60	64.60	14.00	7.60
Zn	53.00	38.00	44.80	177.60	70.20	78.20	88.20	94.40	72.80	71.20	54.60	76.40	26.60	80.40	69.00	65.20	32.20	33.00	25.80	5.20
Sr	264.80	172.20	238.20	502.20	212.40	194.40	162.60	197.80	200.00	195.60	208.80	163.60	275.00	343.40	406.00	536.60	143.60	167.80	49.60	59.20
Y	9.60	9.00	9.20	29.40	25.00	21.20	30.20	34.60	32.60	18.00	7.20	30.60	4.80	35.60	34.00	31.80	8.80	5.80	58.80	55.80
Zr	25.00	17.20	21.20	125.60	50.40	48.20	90.40	98.40	96.80	63.00	18.20	86.20	26.40	228.00	217.00	222.80	13.00	14.00	129.00	163.20
Nb	2.40	2.20	2.40	4.20	3.40	3.80	4.40	4.80	4.60	2.40	1.80	4.80	2.80	25.40	22.80	22.60	2.20	2.00	0.60	b.d.
Ba	51.60	22.40	35.40	59.00	157.20	152.00	57.40	55.40	56.80	95.40	383.60	61.40	88.00	78.00	184.40	109.00	22.80	15.80	3.80	14.00
Rb	1.31	1.53	0.62	1.33	3.45	2.43	16.27	16.02	13.83	1.95	49.93	2.46	2.28	5.85	11.49	7.02	0.90	0.98	0.67	0.43
Pb	1.17	0.33	0.41	4.59	0.75	0.62	0.43	0.48	0.60	0.93	0.46	0.26	0.70	1.57	1.20	1.39	0.50	0.18	0.68	0.09
Th	0.06	0.01	0.01	0.32	0.22	0.19	0.30	0.36	0.33	0.18	0.05	0.23	0.04	1.96	1.57	1.73	0.02	0.01	0.27	0.33
U	0.02	0.00	0.00	0.11	0.22	0.12	0.22	0.55	0.43	0.18	0.02	0.61	0.02	0.39	0.35	0.40	0.01	0.01	0.08	0.08
La	0.44	0.24	0.14	4.29	1.95	1.14	3.36	3.91	3.97	2.12	0.69	4.96	1.25	17.06	15.87	15.78	0.12	0.09	5.63	5.38
Ce	1.44	1.02	0.78	12.26	6.55	3.19	9.82	10.08	10.63	5.60	2.00	11.83	2.89	38.11	34.09	34.68	0.60	0.53	18.32	17.13
Pr	0.29	0.20	0.16	1.92	0.96	0.52	1.52	1.68	1.66	1.04	0.27	2.06	0.37	4.93	4.38	4.43	0.12	0.09	3.10	2.91
Nd	1.50	1.18	1.05	10.22	5.59	3.10	8.23	9.22	8.99	4.34	1.40	10.54	1.56	22.86	20.13	20.30	0.70	0.53	16.07	15.51
Sm	0.77	0.65	0.56	3.25	2.17	1.32	2.73	3.02	2.94	1.68	0.49	3.32	0.50	5.55	4.78	4.84	0.52	0.59	5.36	5.50
Eu	0.45	0.29	0.22	1.15	0.55	0.40	0.86	0.93	1.09	0.61	0.20	1.14	0.30	1.74	1.39	1.63	0.33	0.35	1.01	0.87
Gd	1.21	1.05	0.95	4.15	3.42	2.12	3.71	4.07	3.93	2.32	0.80	4.84	0.63	5.66	4.92	4.97	0.92	0.57	6.97	7.40
Tb	0.22	0.18	0.16	0.68	0.57	0.36	0.60	0.66	0.63	0.53	0.13	0.87	0.10	0.86	0.72	0.72	0.16	0.10	1.23	1.27
Dy	1.47	1.26	1.20	4.63	4.29	2.74	4.25	4.72	4.45	3.51	1.00	5.79	0.70	5.54	4.72	4.78	1.17	0.69	8.27	8.21
Ho	0.31	0.25	0.31	1.13	1.18	0.76	1.01	1.15	1.10	0.75	0.27	1.21	0.14	1.21	1.07	1.12	0.30	0.18	2.03	1.82
Er	0.90	0.77	0.95	3.32	3.71	2.43	3.03	3.50	3.32	1.97	0.88	3.24	0.44	3.34	2.97	3.20	0.92	0.53	5.99	5.07
Tm	0.14	0.10	0.13	0.46	0.51	0.34	0.39	0.46	0.44	0.31	0.12	0.49	0.06	0.45	0.37	0.41	0.12	0.07	0.87	0.70
Yb	0.80	0.67	0.85	2.83	3.47	2.38	2.57	3.08	2.85	1.74	0.89	2.88	0.44	2.68	2.30	2.63	0.76	0.45	5.54	4.36
Lu	0.13	0.09	0.11	0.37	0.46	0.33	0.30	0.39	0.35	0.25	0.12	0.43	0.06	0.34	0.27	0.32	0.10	0.06	0.78	0.55
Sc	34.15	49.60	55.02	37.66	60.76	51.80	43.76	46.43	44.05	41.50	41.52	46.14	24.89	29.91	26.67	28.23	45.61	26.06	6.26	10.35

(continued)

Schwartz et al.

TABLE 1. WHOLE-ROCK MAJOR- AND TRACE-ELEMENT GEOCHEMICAL DATA (*continued*)

Sample:	Terrane-stitching plutonic rocks												Metasedimentary rocks				
	GB-07-1*	GB-07-2*	GB-07-3*	GB-07-4*	GB-08-1	GB-08-2	GB-08-3	GB-08-4	GB-08-5	GB-08-8	08GH01	08DBO3	DB-06-17	VH1-05-3†	VH1-05-5†	VH2-05-4†	VH1-07-4*
SiO₂ (wt%)	71.92	55.35	51.76	54.97	53.07	63.09	56.11	61.96	52.24	65.14	73.17	51.58	51.11	76.94	68.21	84.09	89.33
TiO₂	0.33	0.81	1.30	1.07	0.85	0.73	0.79	0.78	0.86	0.72	0.17	1.12	1.11	0.65	0.88	0.41	0.22
Al₂O₃	14.73	11.80	18.05	17.42	15.61	17.05	17.45	17.51	15.65	16.31	15.13	19.41	19.38	10.91	13.19	6.33	5.21
Fe₂O₃	2.31	9.04	8.37	9.05	9.00	5.71	8.76	6.21	8.51	5.80	2.02	9.37	9.80	5.32	8.09	4.07	1.05
MnO	0.05	0.18	0.14	0.20	0.18	0.10	0.18	0.12	0.17	0.11	0.10	0.17	0.19	0.06	0.09	0.24	0.02
MgO	0.82	10.10	6.01	4.29	8.09	1.96	3.83	2.25	9.25	1.42	0.63	3.92	3.90	2.33	4.54	1.71	0.88
CaO	2.36	9.91	10.24	7.57	10.05	5.07	7.34	5.31	10.03	4.30	2.12	7.90	8.32	0.61	1.25	1.24	0.67
Na₂O	3.56	1.76	3.18	3.54	1.90	3.97	3.91	3.94	2.32	3.86	3.83	4.52	4.45	0.89	2.25	1.42	2.58
K₂O	3.84	0.94	0.74	1.71	1.17	2.20	1.48	1.78	0.85	2.18	2.76	1.74	1.49	2.20	1.38	0.45	0.04
P₂O₅	0.08	0.12	0.22	0.18	0.09	0.14	0.15	0.14	0.12	0.14	0.08	0.28	0.27	0.09	0.12	0.05	0.01
LOI	0.83	1.55	1.13	0.72	2.35	0.71	0.51	1.28	3.01	1.24	1.39	2.02	2.06	2.25	2.16	0.96	0.53
V (ppm)	23.22	276.02	200.22	161.87	n.d.	83.80	157.40	101.20	198.40	73.60	15.80	229.20	227.60	112.00	162.00	64.00	35.39
Cr	3.89	426.96	55.08	b.d.	n.d.	11.20	26.40	18.60	600.40	b.d.	b.d.	b.d.	b.d.	62.00	224.00	59.00	16.84
Ni	4.62	89.67	6.81	b.d.	n.d.	5.40	8.40	6.00	136.20	3.20	1.80	5.00	3.40	28.00	108.00	38.00	23.88
Cu	7.76	34.64	24.17	19.43	n.d.	11.20	19.00	6.60	26.80	5.20	3.40	4.60	4.80	45.00	58.00	56.00	3.97
Zn	45.19	98.18	72.47	95.37	n.d.	72.60	98.40	76.20	66.60	80.60	41.00	96.20	101.80	108.00	138.00	63.00	7.00
Sr	322.75	282.59	410.51	340.39	n.d.	255.40	245.20	278.60	279.20	254.40	398.60	669.00	627.60	65.00	138.00	184.00	28.56
Y	17.58	21.18	27.01	27.24	n.d.	34.80	52.40	31.60	19.20	33.00	11.00	23.40	22.80	21.00	21.60	14.60	8.17
Zr	180.67	78.53	91.22	138.08	n.d.	172.00	129.40	144.80	79.00	172.80	119.20	133.00	127.80	141.00	137.00	84.00	57.84
Nb	16.63	24.78	24.17	17.77	n.d.	8.60	8.80	9.00	7.40	9.80	9.20	7.60	7.20	4.00	5.00	4.00	13.22
Ba	1427.68	387.17	297.22	585.85	n.d.	855.80	643.60	862.80	303.80	1146.20	1049.00	434.60	394.80	1199.00	816.00	88.00	24.27
Rb	117.02	15.35	16.75	n.d.	37.01	64.27	66.54	39.40	25.23	65.13	45.16	37.43	31.18	64.00	38.00	12.00	0.96
Pb	13.69	2.44	4.04	n.d.	3.70	9.25	13.97	7.69	2.59	9.51	9.13	3.76	4.21	7.34	8.52	8.51	0.49
Th	10.59	1.63	1.56	n.d.	2.21	4.93	8.72	4.63	1.03	3.01	4.63	1.83	1.86	4.42	3.47	2.39	3.08
U	3.89	0.48	0.46	n.d.	0.73	1.74	2.38	1.31	0.28	0.94	2.02	0.68	0.68	1.00	1.19	0.52	0.44
La	28.75	11.47	14.57	n.d.	9.81	16.21	33.37	19.65	7.02	13.85	18.35	13.94	13.57	15.25	22.38	10.16	7.16
Ce	68.50	34.16	32.41	n.d.	28.84	34.25	82.16	40.27	15.34	31.34	34.25	31.04	30.20	31.27	47.61	27.54	27.62
Pr	5.92	3.36	4.23	n.d.	2.97	4.38	11.39	4.91	2.07	4.10	3.79	4.04	3.90	4.13	5.47	2.61	1.81
Nd	21.59	14.41	20.17	n.d.	13.43	24.78	48.60	19.95	9.31	17.65	13.28	18.68	17.90	17.67	21.53	11.01	7.30
Sm	3.96	3.56	4.92	n.d.	3.54	4.23	11.97	4.73	2.53	4.39	2.07	4.19	3.96	3.71	4.04	2.49	1.63
Eu	0.81	0.87	1.37	n.d.	0.96	1.06	2.34	1.22	0.89	1.07	0.53	1.27	1.22	0.73	1.10	0.58	0.34
Gd	2.90	3.73	5.07	n.d.	3.89	4.54	12.32	4.91	3.00	4.64	1.37	3.89	3.62	3.34	3.18	2.26	1.29
Tb	0.45	0.62	0.75	n.d.	0.64	0.75	2.05	0.82	0.50	0.76	0.21	0.55	0.51	0.50	0.47	0.36	0.22
Dy	2.59	3.98	5.03	n.d.	4.11	4.73	13.23	5.05	3.19	4.83	1.20	3.63	3.38	3.03	1.71	2.43	1.43
Ho	0.48	0.83	0.95	n.d.	0.85	1.14	2.86	1.02	0.65	0.98	0.23	0.85	0.85	0.52	0.25	0.60	0.33
Er	1.31	2.34	2.86	n.d.	2.42	3.23	8.47	2.87	1.88	2.83	0.63	2.47	2.50	1.45	0.57	1.83	0.98
Tm	0.21	0.34	0.38	n.d.	0.35	0.47	1.27	0.43	0.27	0.41	0.09	0.32	0.32	0.21	0.09	0.25	0.13
Yb	1.31	2.19	2.51	n.d.	2.17	2.99	8.46	2.66	1.76	2.64	0.68	2.09	2.13	1.37	0.53	1.72	0.96
Lu	0.20	0.32	0.33	n.d.	0.32	0.43	1.25	0.41	0.26	0.39	0.11	0.25	0.26	0.20	0.09	0.22	0.12
Sc	4.76	37.27	31.24	22.05	50.04	13.59	54.60	16.42	34.31	13.34	2.82	22.04	21.64	16.75	22.98	13.00	7.00

Note: Analytical details: Unless indicated, major and minor elements were analyzed on glass beads, whereas V, Cr, Ni, Cu, Zn, Sr, Y, Zr, Nb, and Ba were analyzed on pressed pellets by X-ray fluorescence (XRF) at the University of Alabama. Rb, Pb, Th, U, Sc, and rare earth elements were analyzed by inductively coupled plasma–mass spectrometry (ICP-MS) at the University of Alabama. Glass beads for XRF analysis were fused in lithium metaborates. Samples for ICP were fused in lithium metaborates and dissolved in 50 mL of 5% HCl solution. Samples for ICP-MS analysis were digested in HF-HNO₃, and converted to chlorides and then nitrates for analysis. Relative uncertainties at the 95% confidence level are <1% for Si and Al; <2% for V; <3% for Ti, Fe, Mn, Ca, Na, Sr, Ba, and Zr; <5% for K, Mg, Y, and Rb; <10% for P, Sc, Cu, and Zn; <15% for Nb, Cr, and Ni; and <20% for Pb, Th, U, and rare earth elements. B.d.—below detection; n.d.—not determined.
*Major elements analyzed by ICP at the University of Houston—Downtown.
†Major elements analyzed by ICP atomic emission spectrometry (AES) at Texas Tech University.

TABLE 2. Nd AND Sr ISOTOPIC DATA FOR METASEDIMENTARY ROCKS OF THE GREENHORN SUBTERRANE

Sample	Rb (ppm)	Sr (ppm)	$^{87}Rb/^{86}Sr$	$^{87}Sr/^{86}Sr$ (present)	$^{87}Sr/^{86}Sr$ (initial)	Sm (ppm)	Nd (ppm)	$^{147}Sm/^{144}Nd$	$^{143}Nd/^{144}Nd$ (present)	$^{143}Nd/^{144}Nd$ (initial)	Initial ε_{Nd}	Nd model age (Ga)
Greenhorn subterrane (Badger Creek metasedimentary sequence)												
VH1-05-3	71.71	64.72	3.20955	0.71734	0.70730	3.78	16.70	0.13688	0.512357	0.512160	−3.80	1.6
VH1-05-5	37.53	128.51	8.45295	0.70988	0.70724	3.54	16.68	0.12828	0.512400	0.512215	−2.73	1.3
Greenhorn subterrane (Vinegar Hill Chert Argillite)												
VH2-05-4	12.62	176.87	0.20616	0.70680	0.70616	2.69	11.79	0.13780	0.512341	0.512233	−2.39	1.5

Note: Initial Nd and Sr isotopic ratios were calculated at 220 Ma for metasedimentary rocks. Analytical details: ~80 to 100 mg of sample were dissolved in HF-HNO₃. After conversion to chlorides, 1/3 of sample was spiked with ^{87}Rb, ^{84}Sr, ^{149}Sm, and ^{146}Nd. Rb, Sr, and rare earth elements were separated by conventional cation-exchange procedures. Sm and Nd were further separated in diethyl-hexylorthophosphoric acid columns. All isotopic measurements were made on a VG Sector multicollector mass spectrometer at the University of Wyoming. An average $^{87}Sr/^{86}Sr$ isotopic ratio of 0.710251 ± 20 (2σ) was measured for NBS 987 Sr, and an average $^{143}Nd/^{144}Nd$ ratio of 0.511846 ± 11 (2s) was measured for the La Jolla Nd standard. Uncertainties in Sr isotopic ratio measurements are ±0.00002, and uncertainties in Nd isotopic ratio measurements are ±0.00001 (2σ). Blanks are <50 pg for Rb, Sr, Nd, and Sm, and no blank correction was made. Uncertainties in Rb, Sr, Nd, and Sm concentrations are ±2% of the measured value; uncertainties on initial ε_{Nd} are ±0.3 epsilon units. Nd model ages were calculated based upon the depleted mantle model of Goldstein et al. (1984).

contain lithic clasts consisting of black chert, and silicic plutonic rocks. Graded bedding is locally visible within sandstone units. Radiolarian tests are commonly observed in the Elkhorn Ridge Argillite. They are typically poorly preserved due to subsequent regional greenschist-facies metamorphism and the effects of localized contact metamorphism resulting from Middle to Late Jurassic plutonism. As preservation varies locally, micropaleontology field detection techniques are necessary to successfully collect diagnostic fauna.

The Greenhorn subterrane contains at least two metasedimentary units, and possibly others (Mullen, 1978). The oldest of these metasedimentary units is informally here termed the "Vinegar Hill chert-argillite unit" (cf. Figs. 3 and 5C). It consists primarily of laterally discontinuous and finely laminated siliceous argillite. It almost exclusively crops out on the pinnacle of Vinegar Hill, although smaller and less extensive outcrops appear on the eastern flank of Vinegar Hill and in the southern Dixie Butte area (Fig. 1). These rocks are distinctively massive in appearance and are folded and brecciated (e.g., Fig. 5C). Brecciated chert-argillites in the Dixie Butte area contain Early to Late Permian radiolaria (Brooks et al., 1984; Ferns and Brooks, 1995; this paper).

A second sedimentary unit, the Badger Creek unit, is exposed discontinuously over an area of ~155 km² in the Greenhorn subterrane (Ferns and Brooks, 1995). It consists of conglomerate, fine- to medium-grained sandstone, argillite, and bedded limestone (Wheeler, 1976; Mullen, 1978; Ferns and Brooks, 1995). Polymict conglomerates in the Badger Creek unit contain clasts of metamorphosed and lineated gabbro, greenstone, chert, siliceous argillite, argillite, limestone, sandstone, white quartzite, and serpentinite- and talc-matrix rocks (Fig. 5D; Ferns and Ramp, 1988), all of which (except quartzite) are locally exposed in the map area. Chert pebbles are well-rounded and typically range from 1 to 5 cm in diameter. Subangular to subrounded lithic framework grains in sandstone include

chert, argillite, mafic volcanic, and silicic plutonic rock fragments. Additional framework grains are mono- and polycrystalline quartz and plagioclase.

Modal compositions of three sandstone samples from the Badger Creek metasedimentary unit are plotted on a Qp-Lv-Ls provenance discrimination diagram of Dickinson (1982) in Figure 6. Modal compositions are dominated by a high percent of polycrystalline quartz grains (>60%), which are chiefly metachert lithic fragments. Monocrystalline quartz grains (not plotted on this diagram) make up a low percentage (<10%). High modal percent of polycrystalline quartz grains and a relatively low modal percent of monocrystalline quartz grains were first recognized in the Blue Mountain province and are considered characteristic of sediment derived from oceanic mélange sources (i.e., Dickinson and Thayer, 1978; Dickinson, 1979; Dickinson et al., 1979).

Faunal ages from the Badger Creek metasedimentary unit range from Pennsylvanian to Late (?) Triassic (Ferns and Brooks, 1995). Late Permian (Guadalupian) radiolarians were reported from the Granite Boulder Creek area southwest of Vinegar Hill (Ferns and Brooks, 1995). Fusulinid assemblages from the Badger Creek unit are similar to those reported from the McCloud area in the Klamath Mountains of northern California and are distinct from Tethyan varieties in similar-age limestone in the Elkhorn Ridge Argillite of the Bourne subterrane (Mullen, 1978).

Amphibolitic Rocks (Greenhorn Subterrane)

Epidote amphibolites are exposed southeast of Vinegar Hill (Fig. 3), and they display tightly crenulated foliations within sheared serpentinites. They typically occur along major fault zones or along margins of metagabbro blocks. Blue amphibole occurs in some amphibolites southeast of Vinegar Hill (Mullen, 1978, 1980; Ferns et al., 1983). According to Mullen (1978, 1980) and Bishop (1995a), these amphiboles record two periods of metamorphism: an early

high-pressure, low-temperature event (~350 °C and 6–7 kbar), and a later, moderate-temperature, moderate-pressure event (~400 °C and 4–5 kbar).

Terrane and Subterrane Stitching Plutonic Rocks (Bourne and Greenhorn Subterranes)

In the Desolation Butte area (Fig. 2), the Gold Bug pluton intruded and metamorphosed brecciated Elkhorn Ridge Argillite in the footwall of the Greenhorn-Bourne subterrane fault zone. Plutonic rocks consist of undeformed and unmetamorphosed biotite-hornblende gabbro, biotite-hornblende diorite, biotite-hornblende quartz diorite, and minor biotite-hornblende tonalite and granodiorite. Biotite-hornblende gabbro occasionally preserves cores of augite surrounded by hornblende. The gabbro-diorite-tonalite suite is intruded by small (<1 km²) stocks of undeformed and unmetamorphosed, muscovite-biotite tonalite and granodiorite (Fig. 2).

A small (<1 km²), early Late Jurassic pluton intrudes the Bourne-Wallowa boundary at the Grey Eagle mine in the Virtue Hills area east of Baker City (Fig. 1). This pluton consists of chiefly biotite-hornblende diorite and intrudes both Elkhorn Ridge Argillite of the Bourne subterrane and meta-igneous fault slices that have been interpreted to represent imbricated fault slices of the nearby Wallowa terrane (Ferns and Brooks, 1995; Schwartz et al., 2010).

In the Olive Creek area, northeast of the town of Greenhorn (Fig. 3), small (<500 m²) Late Jurassic plutons intrude the Bourne-Greenhorn subterrane boundary. These plutons consist of muscovite-biotite tonalite and granodiorite.

Primary and Structural Features

Primary Features in the Metasedimentary Rocks

Bedding is locally preserved in the Badger Creek metasedimentary and Vinegar Hill chert-argillite units (Fig. 2). In the Badger Creek unit, primary stratification consists of graded beds, sometimes inverted due to tight to isoclinal,

synmetamorphic folding (see "Penetrative fabric development" section for a detailed description). In the Vinegar Hill chert-argillite unit, the direction of younging could not be determined from relict bedding features. Brecciation in the Vinegar Hill argillite is localized and is especially prominent near the summit of Vinegar Hill. This brecciation either postdates folding, or both features (i.e., folding and brecciation) may have formed together in a semilithified state during submarine slumping. This suggestion of widespread soft-sediment deformation in the chert-argillite unit of the Vinegar Hill area is supported by a lack of similar deformation in the immediately underlying and adjacent metavolcanic and metavolcaniclastic rocks.

Penetrative Fabric Development

Bedding in metasedimentary rock units is transposed by a NE-SW–striking, moderately to steeply-dipping penetrative slaty to spaced cleavage (S_1; Fig. 7). Isoclinal folding is also locally observed. In some cases, bedding and S_1 are obliquely oriented to each other, whereas in other cases they are parallel or subparallel (as observed in the isoclinal folds). In contrast, penetrative S_1 foliation (cleavage) is poorly developed in metavolcanic and metavolcaniclastic rocks on Vinegar Hill but is more common in the Desolation Butte area (Fig. 7). In this area, S_1 foliations strike roughly E-W with moderate to steep dips. Strongly sheared serpentinite also displays similar orientations to metavolcanic rocks along major shear zones within the Greenhorn subterrane and near structural contacts with the Bourne subterrane (e.g., Figs. 2 and 6). At the Bourne-Greenhorn subterrane boundary (Fig. 2), Elkhorn Ridge Argillite also displays a well-developed, E-W–striking, moderately to steeply dipping, slaty to spaced cleavage. The similarity in orientation of these fabrics suggests that they developed together.

Brittle to Semibrittle Fault Zones and Cataclasis

The E-W–oriented, penetrative slaty to spaced cleavage in both subterranes is overprinted by brittle faults, intense brecciation, and extensive networks of cataclastic shear zones. Along the contact between the two subterranes, a greenschist-facies shear zone separates serpentinite, metavolcanic, and metaplutonic rocks of the Greenhorn subterrane from the Elkhorn Ridge Argillite of the Bourne subterrane (central area of Fig. 2). The orientation of this fault zone ranges from approximately NW-SE in the Desolation Butte area, to nearly E-W in other areas (Evans, 1989, 1995; Ferns and Brooks, 1995). Fault surfaces in the Desolation Butte area dip to the S-SW, with slickenside orientations

TABLE 3. U-PB SENSITIVE HIGH-RESOLUTION ION MICROPROBE (SHRIMP) ISOTOPIC ANALYSES AND AGES

Grain	Concentrations U (ppm)	Th (ppm)	Th/U	Pb† (ppm)	f206§ (%)	Atomic ratios* $^{238}U/^{206}Pb^*$	% err (1σ)	$^{207}Pb/^{206}Pb^\#$	% err (1σ)	$^{206}Pb/^{238}U^{**}$	err abs (1σ)	Age (Ma) $^{206}Pb/^{238}U^{\dagger\dagger}$	err abs (1σ)	Weighted average age (Ma, 2σ)
Gold Bug biotite tonalite														
GB1-1	210.11	73.34	0.35	4.17	−0.06	43.24	0.99	0.0485	3.82	0.02314	0.0002	147.48	1.49	**146.3 ± 1.5**
GB1-2	353.05	141.52	0.40	6.96	−0.08	43.60	0.76	0.0483	3.05	0.02296	0.0002	146.31	1.14	**MSWD = 0.70**
GB1-3	272.83	108.83	0.40	5.37	0.09	43.61	0.87	0.0497	3.32	0.02291	0.0002	146.04	1.29	
GB1-4	323.13	189.11	0.59	6.30	−0.19	44.09	0.82	0.0474	3.19	0.02272	0.0002	144.84	1.21	
GB1-5	264.52	122.07	0.46	5.21	−0.16	43.66	0.89	0.0477	3.46	0.02294	0.0002	146.23	1.33	
GB1-6	707.39	195.63	0.28	14.98	0.93	40.56	0.57	0.0565	2.09	0.02443	0.0001	155.56	0.90	
GB1-7	339.81	132.05	0.39	6.75	−0.02	43.24	0.78	0.0489	3.00	0.02313	0.0002	147.42	1.18	
Bald Mountain batholith biotite-hornblende tonalite (Granodiorite of Anthony Lakes: Taubeneck, 1995)														
BMO1-1	58.06	18.32	0.32	1.15	0.56	43.31	2.19	0.0535	6.12	0.02296	0.0005	146.33	3.23	**146.7 ± 2.1**
BMO1-2	48.78	20.10	0.41	0.99	−0.10	42.37	2.32	0.0483	7.02	0.02363	0.0006	150.54	3.53	**MSWD = 1.25**
BMO1-3	166.12	75.04	0.45	3.14	0.14	45.41	1.55	0.0499	3.77	0.02199	0.0003	140.22	2.18	
BMO1-4	107.96	31.01	0.29	2.09	−0.16	44.28	1.72	0.0476	4.80	0.02262	0.0004	144.20	2.50	
BMO1-5	125.03	41.12	0.33	2.43	0.00	44.14	1.65	0.0489	4.33	0.02266	0.0004	144.42	2.39	
BMO1-6	83.66	30.23	0.36	1.65	−0.30	43.57	1.83	0.0466	10.09	0.02302	0.0004	146.73	2.80	
BMO1-7	72.78	23.95	0.33	1.46	0.09	42.84	1.91	0.0497	5.67	0.02332	0.0005	148.61	2.86	
BMO1-8	125.84	35.86	0.28	2.50	0.51	43.27	1.63	0.0530	4.11	0.02299	0.0004	146.55	2.41	
BMO1-9	75.25	25.75	0.34	1.46	−0.34	44.14	1.90	0.0462	5.89	0.02273	0.0004	144.89	2.77	
BMO1-10	79.91	26.85	0.34	1.66	−0.04	41.43	1.84	0.0488	5.35	0.02415	0.0005	153.83	2.86	
BMO1-11	62.51	18.48	0.30	1.25	−0.21	43.01	2.00	0.0473	6.14	0.02330	0.0005	148.47	3.00	
BMO1-12	124.27	40.60	0.33	2.41	0.58	44.22	1.66	0.0535	4.22	0.02248	0.0004	143.34	2.39	
Gold Bug biotite-hornblende diorite														
GB2-1	473.17	101.33	0.21	9.88	0.02	41.14	0.67	0.0493	2.56	0.02430	0.0002	154.80	1.06	**153.9 ± 1.3**
GB2-2	592.35	160.90	0.27	12.65	0.35	40.23	0.62	0.0520	2.30	0.02477	0.0002	157.71	1.00	**MSWD = 0.87**
GB2-3	1328.19	628.97	0.47	27.67	0.06	41.23	0.40	0.0496	1.51	0.02424	0.0001	154.39	0.63	
GB2-4	102.76	16.40	0.16	2.09	0.13	42.20	1.70	0.0501	5.60	0.02366	0.0004	150.78	2.60	
GB2-5	1650.37	828.80	0.50	34.32	0.15	41.31	0.36	0.0503	1.34	0.02417	0.0001	153.97	0.56	
GB2-6	165.80	51.20	0.31	3.45	0.33	41.31	1.12	0.0518	4.38	0.02412	0.0003	153.67	1.76	
GB2-7	135.99	25.43	0.19	2.99	−0.04	39.83	1.23	0.0489	4.63	0.02512	0.0003	159.91	2.00	
GB2-8	331.93	88.39	0.27	6.83	0.40	41.75	0.80	0.0523	2.96	0.02386	0.0002	151.98	1.24	
GB2-9	237.80	58.32	0.25	4.81	0.32	42.45	0.94	0.0515	3.50	0.02348	0.0002	149.62	1.43	
GB2-10	281.47	53.09	0.19	5.81	0.09	41.64	0.87	0.0498	3.28	0.02399	0.0002	152.84	1.36	

(continued)

TABLE 3. U-PB SENSITIVE HIGH-RESOLUTION ION MICROPROBE (SHRIMP) ISOTOPIC ANALYSES AND AGES (*continued*)

Grain	U (ppm)	Th (ppm)	Th/U	Pb† (ppm)	f206§ (%)	238U/206Pb#	% err (1σ)	207Pb/206Pb#	% err (1σ)	206Pb/238U**	err abs (1σ)	206Pb/238U††	err abs (1σ)	Weighted average age (Ma, 2σ)
Grey Eagle hornblende diorite														
08GE-1-1	342.38	199.18	0.58	7.25	-0.08	40.57	1.39	0.0486	2.62	0.02467	0.0003	157.10	2.17	157.1 ± 2.0 MSWD = 0.68
08GE-1-2	75.06	14.70	0.20	1.61	-0.21	40.07	1.84	0.0476	5.36	0.02501	0.0005	159.22	2.95	
08GE-1-3	138.47	53.41	0.39	2.95	0.21	40.36	1.59	0.0508	3.86	0.02472	0.0004	157.44	2.51	
08GE-1-4	98.94	34.28	0.35	2.15	0.23	39.56	1.71	0.0511	6.33	0.02522	0.0004	160.57	2.80	
08GE-1-5	132.16	56.00	0.42	2.80	-0.07	40.57	1.61	0.0486	4.11	0.02467	0.0004	157.10	2.54	
08GE-1-6	190.58	76.50	0.40	4.06	-0.17	40.31	1.50	0.0479	3.43	0.02485	0.0004	158.23	2.37	
08GE-1-7	162.52	56.95	0.35	3.39	-0.33	41.18	1.54	0.0465	3.68	0.02437	0.0004	155.19	2.39	
08GE-1-8	181.08	81.92	0.45	3.87	0.03	40.23	1.50	0.0495	3.38	0.02485	0.0004	158.24	2.38	
08GE-1-9	229.59	91.27	0.40	4.86	0.27	40.59	1.45	0.0513	3.01	0.02457	0.0004	156.49	2.27	
08GE-1-10	246.08	86.64	0.35	5.19	0.25	40.76	1.43	0.0512	2.89	0.02447	0.0004	155.86	2.24	
08GE-1-11	166.37	63.69	0.38	3.43	0.12	41.66	1.52	0.0501	3.47	0.02397	0.0004	152.73	2.33	
08GE-1-12	146.57	47.61	0.32	3.14	-0.12	40.14	1.58	0.0483	3.91	0.02494	0.0004	158.82	2.52	
Canyon Mountain trondhjemite														
GM-3-1-1	59.34	23.63	0.35	2.24	0.08	22.76	1.71	0.0524	5.28	0.04390	0.00077	276.97	4.75	267.0 ± 3.1 MSWD = 0.61
CM-3-2.1	34.92	7.00	0.35	1.25	0.09	24.01	1.98	0.0522	7.18	0.04162	0.00085	262.84	5.27	
CM-3-3.1	34.07	8.85	0.35	1.26	0.72	23.23	1.99	0.0574	6.46	0.04273	0.00088	269.76	5.44	
GM-3-4.1	275.40	164.36	0.35	10.76	0.02	21.98	0.76	0.0522	2.54	0.04548	0.00035	286.72	2.19	
CM-3-5.1	120.97	48.42	0.35	4.44	-0.21	23.42	1.08	0.0500	3.70	0.04278	0.00048	270.06	2.95	
CM-3-6.1	79.58	27.55	0.35	2.90	0.35	23.59	1.36	0.0544	4.99	0.04225	0.00060	266.74	3.68	
CM-3-7.1	50.97	14.36	0.35	1.91	5.18	22.88	1.67	0.0930	4.42	0.04144	0.00073	261.73	4.54	
CM-3-8.1	81.44	26.88	0.35	2.95	0.40	23.71	1.41	0.0548	4.61	0.04200	0.00061	265.25	3.79	
CM-3-9.1	58.67	21.37	0.35	2.17	0.44	23.21	1.59	0.0552	5.11	0.04290	0.00070	270.76	4.36	
CM-3-10.1	106.32	23.34	0.35	3.86	-0.10	23.66	1.15	0.0508	3.88	0.04230	0.00050	267.07	3.11	
CM-3-11.1	42.47	13.30	0.35	1.52	0.47	24.03	1.95	0.0552	6.11	0.04143	0.00083	261.67	5.15	
CM-3-12.1	39.47	10.62	0.35	1.46	0.14	23.21	1.99	0.0528	6.53	0.04303	0.00088	271.61	5.44	
CM-3-13.1	68.90	26.30	0.35	2.50	0.52	23.63	1.52	0.0557	4.83	0.04209	0.00066	265.80	4.07	
GM-3-14.1	27.08	6.48	0.35	0.92	0.18	25.17	2.43	0.0527	8.13	0.03966	0.00099	250.73	6.17	

Note: MSWD—mean square of weighted deviates.
*Errors are reported at 1σ level and refer to last digits.
†Radiogenic 206Pb.
§Fraction of total 206Pb that is common 206Pb.
#Uncorrected ratios.
**207Pb corrected ratios using age-appropriate Pb isotopic composition of Stacey and Kramers (1975).
††207Pb corrected age; spot analyses with strikethrough were excluded in age calculation due to open system behavior and/or analytical problems.

indicating top to the northwest (Fig. 2). In the footwall of the fault zone, Elkhorn Ridge Argillite is intensely brecciated within 2–3 km of the subterrane contact (cf. Fig. 2 and cross section). Although these brittle and semibrittle features overprint the penetrative slaty to spaced cleavage, they likely formed during the same event, as suggested by the similarity in orientations of fault surfaces, hinge lines, and fold axes in all rocks in the area (Fig. 7).

Cataclastic shear zones are common in metaplutonic rocks in the Vinegar Hill area, where they are variable in orientation but generally define two conjugate sets striking E-W and N-S, respectively (Fig. 7). Locally, these semibrittle shear zones are ultracataclastic and are characterized by extensive alteration of plagioclase and clinopyroxene to chlorite- and epidotegroup minerals. Cataclastic and ultracataclastic shear zones locally crosscut white clinozoisiterich veinlets (Fig. 5B), suggesting that they developed after these metamorphic veinlets.

Radiolarian Micropaleontology

Three samples from the Elkhorn Ridge Argillite (Bourne subterrane, southwest of Baker City) and one sample from the Vinegar Hill chert argillite (Greenhorn subterrane, Dixie Butte area) yielded sufficiently preserved radiolaria for faunal analysis. Sample locations are given in Table A1 (see footnote 1), and a selection of diagnostic Jurassic radiolarian taxa is presented in Figure 8.

Faunal assemblages recovered from the Elkhorn Ridge Argillite (Bourne subterrane) range in age from Middle Triassic to Early Jurassic. Sample 08FC-02 yielded *Triassocampe* sp. (Middle or Late Triassic), sample 08FC-05 yielded *Annulotriassocampe* sp. and *Triassocampe* sp. (Middle Triassic), and sample 08FC-08 included *Bagotum* sp., *?Broctus* sp., *Canoptum* sp., *Orbiculiformella* sp., *Paronaella* sp., *Praeconocaryomma* sp. cf. *magnimamma*, *Praeconocaryomma* spp., and *Thurstonia* sp., an assemblage of Early Jurassic age (within the late Sinemurian–early Toarcian interval, ca. 193–181 Ma).

The faunal assemblage recovered from the basal section of the Dixie Butte meta-andesite (Greenhorn subterrane, locality 08DBOJ4) includes *Haploaxon* sp. and *Pseudoalbaillella lomentaria* of Early Permian age (within the Sakmarian–Kungurian interval).

Geochemical Data

Meta-igneous and metasedimentary rocks in the Greenhorn subterrane are affected by varying degrees of greenschist-facies to lower-

Schwartz et al.

amphibolite-facies metamorphism. Consequently, we base our interpretation of these rocks primarily on relatively immobile trace elements. Metavolcanic rocks in the Greenhorn subterrane typically exhibit a narrow range in SiO_2 content, ranging from 46 to 54 wt%, but values have been reported to extend up to ~71 wt% in other studies (Fig. 9A; Ferns and Brooks, 1995). Chondrite-normalized rare earth element (REE) abundances for greenstones in the Greenhorn subterrane are flat to slightly depleted in light rare earth elements (LREEs) and have negative Eu anomalies (Fig. 10). In contrast, REE abundances for basalts from the Olive Creek unit (Bourne subterrane; Fig. 3) display LREE enrichment and steeply negative slopes, and they lack Eu anomalies (Fig. 10). Metaplutonic rocks from the Greenhorn subterrane are characterized as magnesian and calcic–calc-alkalic (Frost et al., 2001; Frost and Frost, 2008), and show flat to slightly LREE-depleted abundances with positive Eu anomalies.

Plutonic rocks that intrude fault boundaries are generally unaltered to weakly metamorphosed. Middle to early Late Jurassic gabbro to quartz diorite are characterized by 52–65 wt% SiO_2 and are typically magnesian and calcic–calc-alkalic (Fig. 9). They have Na_2O contents typically <4.0 wt%, Al_2O_3 <18 wt%, Sr <400 ppm, and high Y >20 ppm. Rare earth element abundances display weak LREE enrichment and have negative Eu anomalies (Fig. 10). A second suite of Late Jurassic tonalite and granodiorite plutonic rocks intrudes older Middle Jurassic plutons and is characterized by SiO_2 concentrations >70 w.%, and it is also characterized as magnesian and calcic–calc-alkalic (Fig. 9). In contrast to the older intrusive suite, these plutons have steeper REE abundances (La/Lu >140; Fig. 9), and Eu anomalies are weak or absent.

Metasedimentary rocks in the Greenhorn subterrane are characterized by LREE enrichment and flat heavy REE abundances and, typically, negative Eu anomalies (Fig. 10). Relative to North American shale composite (Gromet et al., 1984), these samples show flat REE abundances.

Isotopic Data

A sample of the Vinegar Hill chert-argillite unit has an initial (220 Ma) ε_{Nd} value of –2.4 and a corresponding initial $^{87}Sr/^{86}Sr$ value of 0.7062 (Fig. 11). The Nd model age for this sample is 1.5 Ga. Two Permian to Late (?) Triassic argillites from the Badger Creek metasedimentary unit are characterized by negative initial ε_{Nd} values of –2.4 to –3.8 and

TABLE 4. LASER-ABLATION–MULTICOLLECTOR–INDUCTIVELY COUPLED PLASMA–MASS SPECTROMETRY (LA-MC-ICP-MS) GEOCHRONOLOGIC ANALYSES

				Isotope ratios							Apparent ages (Ma)												Weighted average
Analysis	U (ppm)	$^{206}Pb/^{204}Pb$	U/Th	$^{206}Pb*/^{207}Pb*$	± (%)	$^{207}Pb*/^{235}U*$	± (%)	$^{206}Pb*/^{238}U$	± (%)	Error corr.	$^{206}Pb*/^{238}U$	± (Ma)	$^{207}Pb*/^{235}U$	± (Ma)	$^{206}Pb*/^{207}Pb*$	± (Ma)	Best age (Ma)	± (Ma)	Total $^{238}U/^{206}Pb$	% err	Total $^{207}Pb/^{206}Pb$	% err	(Ma, 2σ)
Greenhorn subterrane muscovite-biotite tonalite																							
08GH01-1	258	11440	2.1	18.4669	13.1	0.1682	13.3	0.0225	2.2	0.17	143.6	3.2	157.8	19.4	377.3	295.5	143.6	3.2	44.4	2.2	0.1	13.1	145.0 ± 2.8 (MSWD = 0.9)
08GH01-2	70	5905	3.8	22.1711	34.9	0.1500	35.2	0.0241	3.8	0.11	153.7	5.7	141.9	46.6	–50.1	873.7	153.7	5.7	41.5	3.8	0.0	34.9	
08GH01-5	911	13435	3.0	18.5775	4.3	0.1623	4.5	0.0219	1.3	0.29	139.5	1.8	152.7	6.3	369.9	96.2	139.5	1.8	45.7	1.3	0.1	4.3	
08GH01-6	275	14105	2.5	21.2326	5.3	0.1517	5.6	0.0234	1.7	0.30	148.8	2.5	143.4	7.5	54.1	127.3	148.8	2.5	42.8	1.7	0.0	5.3	
08GH01-7	292	32100	1.3	18.5697	2.3	0.4574	2.9	0.0616	1.9	0.64	385.4	7.0	382.4	9.4	364.8	51.0	385.4	7.0	16.2	1.9	0.1	2.3	
08GH01-8	360	31320	1.7	19.6796	5.3	0.1675	6.0	0.0239	2.9	0.49	152.3	4.4	157.2	8.8	232.4	122.0	152.3	4.4	41.8	2.9	0.1	5.3	
08GH01-9	1621	78635	3.2	20.1439	1.4	0.1609	2.1	0.0235	1.5	0.74	149.8	2.3	151.5	2.9	178.3	32.4	149.8	2.3	42.5	1.5	0.0	1.4	
08GH01-10	87	7610	3.5	23.1230	44.4	0.1309	44.5	0.0220	2.1	0.06	140.0	3.5	124.9	52.3	–153.4	1152.3	140.0	3.5	45.5	2.1	0.0	44.4	
08GH01-11	352	18520	2.2	21.2673	4.2	0.1474	4.9	0.0227	2.5	0.51	144.9	3.6	139.6	6.4	50.3	101.0	144.9	3.6	44.0	2.5	0.0	4.2	
08GH01-12	440	23425	3.9	20.3210	2.9	0.1583	4.4	0.0233	3.3	0.75	148.6	4.8	149.2	6.1	157.8	67.7	148.6	4.8	42.9	3.3	0.0	2.9	
08GH01-13	810	8725	4.6	17.1560	12.6	0.1820	12.8	0.0226	2.3	0.18	144.3	3.3	169.7	20.0	540.6	276.7	144.3	3.3	44.2	2.3	0.1	12.6	
08GH01-14	452	24635	3.8	20.4649	4.3	0.1568	5.4	0.0233	3.3	0.61	148.3	4.8	147.9	7.5	141.3	101.1	148.3	4.8	43.0	3.3	0.0	4.3	
08GH01-15	499	22465	3.8	20.9549	7.3	0.1468	8.4	0.0223	4.2	0.50	142.3	5.9	139.1	11.0	85.5	173.4	142.3	5.9	44.8	4.2	0.0	7.3	
08GH01-16	565	24905	2.6	20.6630	3.5	0.1484	3.7	0.0222	1.3	0.35	141.8	1.8	140.5	4.9	118.6	82.6	141.8	1.8	45.0	1.3	0.0	3.5	
08GH01-17	697	37440	5.2	20.2007	2.4	0.1549	3.8	0.0227	3.0	0.79	144.7	4.3	146.2	5.2	171.7	55.4	144.7	4.3	44.1	3.0	0.0	2.4	
08GH01-18	447	14840	2.7	18.7411	5.2	0.1620	5.9	0.0220	2.9	0.49	140.4	4.0	152.5	8.4	344.1	117.3	140.4	4.0	45.4	2.9	0.1	5.2	
08GH01-19	359	27730	4.2	20.1364	5.9	0.1551	7.5	0.0227	4.7	0.62	144.4	6.6	146.4	10.2	179.1	137.0	144.4	6.6	44.1	4.7	0.0	5.9	
08GH01-20	771	59905	4.1	21.2513	4.8	0.1333	5.2	0.0205	2.2	0.42	131.1	2.9	127.0	6.3	52.0	113.5	131.1	2.9	48.7	2.2	0.0	4.8	
08GH01-22	297	9415	3.2	18.9266	12.8	0.1686	13.2	0.0231	3.2	0.25	147.5	4.7	158.2	19.4	321.7	292.1	147.5	4.7	43.2	3.2	0.1	12.8	
08GH01-23	599	16390	3.6	19.2440	5.4	0.1681	7.9	0.0235	5.7	0.72	149.5	8.4	157.8	11.5	283.8	124.7	149.5	8.4	42.6	5.7	0.1	5.4	
08GH01-24	391	15270	3.4	19.1321	13.1	0.1647	13.8	0.0228	4.2	0.31	145.6	6.1	154.8	19.8	297.1	300.9	145.6	6.1	43.8	4.2	0.1	13.1	
08GH01-25	410	20765	4.9	21.4446	5.5	0.1476	6.5	0.0230	3.6	0.55	146.3	5.2	139.8	8.5	30.4	130.8	146.3	5.2	43.6	3.6	0.0	5.5	
08GH01-26	726	48585	4.1	20.4966	3.7	0.1491	5.2	0.0222	3.7	0.70	141.3	5.1	141.1	6.9	137.7	87.5	141.3	5.1	45.1	3.7	0.0	3.7	

Late Jurassic orogenesis in the Blue Mountains Province

TABLE 4. LASER-ABLATION–MULTICOLLECTOR–INDUCTIVELY COUPLED PLASMA–MASS SPECTROMETRY (LA-MC-ICP-MS) GEOCHRONOLOGIC ANALYSES (*continued*)

Analysis	U (ppm)	^{206}Pb/^{204}Pb	U/Th	^{206}Pb*/^{207}Pb*	± (%)	^{207}Pb*/^{235}U*	± (%)	^{206}Pb*/^{238}U	± (%)	Error corr.	^{206}Pb*/^{238}U (Ma)	± (Ma)	^{207}Pb*/^{235}U (Ma)	± (Ma)	^{207}Pb*/^{206}Pb* (Ma)	± (Ma)	Best age (Ma)	± (Ma)	Total ^{238}U/^{206}Pb	% err	Total ^{207}Pb/^{206}Pb	% err	Weighted average (Ma, 2σ)
Volcaniclastic breccia (Bourne subterrane)																							
OBM62-1	771	30405	1.0	19.3844	2.1	0.2739	2.7	0.0385	1.8	0.64	243.6	4.2	245.8	4.2	267.2	6.0	243.6	48.0	26.0	1.8	0.1	2.1	**244.4 ± 6.1 (MSWD = 1.4)**
OBM62-2	444	41375	1.3	19.7654	2.3	0.2580	2.5	0.0370	1.2	0.47	234.1	2.7	233.0	5.3	222.3	5.3	234.1	52.1	27.0	1.2	0.1	2.3	
OBM62-3	248	24040	1.4	19.7409	5.5	0.2827	5.9	0.0405	2.2	0.37	255.7	5.5	252.8	13.2	225.2	13.2	255.7	126.5	24.7	2.2	0.1	5.5	
~~OBM62-4~~	~~23~~	~~2555~~	~~4.1~~	~~26.5128~~	~~165.4~~	~~0.1915~~	~~165.5~~	~~0.0368~~	~~5.5~~	~~0.03~~	~~233.1~~	~~12.6~~	~~177.9~~	~~12.6~~	~~-505.0~~	~~276.7~~	~~233.1~~	~~2262.6~~	~~27.2~~	~~5.5~~	~~0.0~~	~~165.4~~	
OBM62-5	104	10120	1.9	19.7592	14.4	0.2685	14.6	0.0385	2.4	0.16	243.4	5.6	241.5	5.6	223.1	31.4	243.4	334.3	26.0	2.4	0.1	14.4	
OBM62-6	147	13680	3.0	20.6990	9.6	0.2579	9.9	0.0387	2.7	0.27	244.8	6.5	232.9	20.7	114.5	20.7	244.8	225.9	25.8	2.7	0.0	9.6	
OBM62-7	530	49805	0.9	19.6721	3.0	0.2773	3.6	0.0396	2.0	0.56	250.2	4.9	248.6	8.0	233.3	69.3	250.2	69.3	25.3	2.0	0.1	3.0	
OBM62-8	499	25125	1.2	19.4998	2.3	0.2718	2.9	0.0384	1.8	0.61	243.1	4.2	244.1	6.3	253.5	53.0	243.1	53.0	26.0	1.8	0.1	2.3	
OBM62-9	605	28185	0.7	19.4926	2.7	0.2714	3.9	0.0384	2.8	0.72	242.7	6.7	243.8	8.5	254.4	62.4	242.7	62.4	26.1	2.8	0.1	2.7	
OBM62-10	110	10595	1.1	20.1907	11.0	0.2785	12.0	0.0408	4.9	0.41	257.7	12.4	249.5	26.6	172.9	257.0	257.7	257.0	24.5	4.9	0.0	11.0	
OBM62-11	399	37415	1.3	19.5000	2.1	0.2762	2.7	0.0391	1.6	0.61	247.0	4.0	247.6	5.9	253.5	48.9	247.0	48.9	25.6	1.6	0.1	2.1	
OBM62-12	498	19835	0.9	19.7853	2.2	0.2642	3.1	0.0379	2.2	0.71	239.9	5.2	238.0	6.7	220.0	51.5	239.9	51.5	26.4	2.2	0.1	2.2	
OBM62-13	192	17305	1.6	19.4553	7.7	0.2753	8.0	0.0388	2.2	0.27	245.7	5.3	246.9	17.5	258.8	176.4	245.7	176.4	25.7	2.2	0.1	7.7	
OBM62-14	1063	33765	1.0	19.9420	2.4	0.2686	3.1	0.0388	1.9	0.62	245.7	4.7	241.6	6.7	201.7	56.7	245.7	56.7	25.7	1.9	0.1	2.4	
OBM62-15	234	13915	1.3	20.4830	5.6	0.2552	5.8	0.0379	1.4	0.24	239.9	3.3	230.8	12.0	139.2	132.7	239.9	132.7	26.4	1.4	0.0	5.6	
OBM62-16	505	25660	1.1	19.9841	2.8	0.2726	3.2	0.0395	1.5	0.47	249.8	3.7	244.8	7.0	196.8	66.1	249.8	66.1	25.3	1.5	0.1	2.8	
OBM62-17	153	15800	1.9	20.0292	10.0	0.2592	10.8	0.0377	4.1	0.38	238.3	9.5	234.0	22.5	191.6	232.3	238.3	232.3	26.6	4.1	0.0	10.0	
OBM62-18	1138	54610	1.1	19.3589	2.4	0.2696	2.9	0.0379	1.7	0.57	239.5	3.9	242.4	6.4	270.2	55.7	239.5	55.7	26.4	1.7	0.1	2.4	
OBM62-19	184	17740	1.9	19.7644	9.0	0.2538	9.8	0.0364	3.9	0.39	230.3	8.8	229.6	20.2	222.4	209.6	230.3	209.6	27.5	3.9	0.1	9.0	
OBM62-20	88	8130	2.8	20.0933	19.3	0.2524	19.7	0.0368	3.6	0.18	232.8	8.3	228.5	40.2	184.1	453.7	232.8	453.7	27.2	3.6	0.0	19.3	
~~OBM62-21~~	~~35~~	~~830~~	~~3.3~~	~~8.0827~~	~~47.3~~	~~0.7342~~	~~47.6~~	~~0.0430~~	~~4.9~~	~~0.10~~	~~271.6~~	~~13.0~~	~~559.0~~	~~207.4~~	~~2010.6~~	~~897.0~~	~~2010.6~~	~~897.0~~	~~23.2~~	~~4.9~~	~~0.1~~	~~47.3~~	
OBM62-22	600	30700	1.4	19.5048	2.5	0.2714	3.5	0.0384	2.5	0.71	242.8	5.9	243.8	7.5	252.9	56.4	242.8	56.4	26.1	2.5	0.1	2.5	
OBM62-23	399	41505	0.8	19.8164	3.5	0.2445	4.4	0.0351	2.6	0.58	222.6	5.6	222.1	8.7	216.4	82.1	222.6	82.1	28.5	2.6	0.1	3.5	
OBM62-24	390	20630	1.1	19.5472	4.5	0.2599	4.7	0.0382	1.5	0.32	241.6	3.7	234.6	9.9	165.3	104.8	241.6	104.8	26.2	1.5	0.0	4.5	
OBM62-25	311	22280	1.5	19.8421	6.9	0.2696	7.2	0.0388	2.1	0.29	245.4	5.0	242.4	15.4	213.4	158.9	245.4	158.9	26.2	2.1	0.1	6.9	
OBM62-26	1194	54450	0.8	19.5241	1.5	0.2780	2.5	0.0394	2.0	0.79	248.9	4.9	249.1	5.6	250.7	35.5	248.9	35.5	25.4	2.0	0.1	1.5	
OBM62-27	1314	29030	0.8	19.9007	1.7	0.2665	2.3	0.0385	1.6	0.69	243.3	3.9	239.9	5.0	206.5	39.4	243.3	39.4	26.0	1.6	0.1	1.7	
OBM62-28	1452	51460	0.7	19.7154	1.2	0.2683	2.3	0.0384	1.9	0.84	242.7	4.5	241.3	4.8	228.2	28.5	242.7	28.5	26.1	1.9	0.1	1.2	
OBM62-29	624	34685	0.8	20.0297	2.6	0.2663	2.9	0.0387	1.2	0.42	244.7	2.9	239.7	6.2	191.5	60.7	244.7	60.7	25.9	1.2	0.0	2.6	
OBM62-30	890	29155	0.9	19.4848	2.9	0.2819	3.0	0.0398	0.8	0.27	251.8	2.0	252.1	6.7	255.3	66.1	251.8	66.1	25.1	0.8	0.1	2.9	
OBM62-31	717	40090	0.8	19.9338	2.9	0.2639	3.4	0.0382	1.8	0.52	241.4	4.2	237.8	7.2	202.7	66.9	241.4	66.9	26.2	1.8	0.1	2.9	
OBM62-32	272	17755	1.3	20.2038	5.7	0.2589	6.6	0.0379	3.4	0.51	240.1	7.9	233.8	13.9	171.4	133.6	240.1	133.6	26.4	3.4	0.0	5.7	
OBM62-33	1143	38590	1.0	19.3917	1.6	0.2744	2.2	0.0386	1.5	0.70	244.1	3.7	246.2	4.8	266.3	36.1	244.1	36.1	25.9	1.5	0.1	1.6	
OBM62-34	549	22670	0.9	19.5472	1.5	0.2699	2.8	0.0383	2.3	0.84	242.1	5.6	242.6	6.0	247.9	35.0	242.1	35.0	26.1	2.3	0.1	1.5	
OBM62-35	282	17590	1.1	20.1636	6.1	0.2648	7.2	0.0387	3.8	0.53	244.9	9.2	238.5	15.3	176.0	142.0	244.9	142.0	25.8	3.8	0.0	6.1	
OBM62-36	162	18710	1.7	20.7608	6.5	0.2600	7.2	0.0392	3.1	0.43	247.6	7.6	234.7	15.1	107.5	153.8	247.6	153.8	25.5	3.1	0.0	6.5	
OBM62-37	121	10705	1.7	20.9127	20.5	0.2493	20.6	0.0378	2.7	0.13	239.3	6.2	226.0	41.8	90.2	489.3	239.3	489.3	26.4	2.7	0.0	20.5	
OBM62-38	22	1615	2.6	12.3440	30.5	0.4126	30.8	0.0369	3.9	0.13	233.9	9.0	350.8	91.5	1221.7	613.8	233.9	613.8	27.1	3.9	0.1	30.5	
OBM62-39	86	10500	3.0	20.5039	11.9	0.2482	12.2	0.0369	2.6	0.21	233.6	6.0	225.1	24.5	136.8	279.7	233.6	279.7	27.1	2.6	0.0	11.9	
OBM62-40	148	13705	1.6	20.3769	12.7	0.2571	13.0	0.0380	2.6	0.20	240.4	6.2	232.3	27.0	151.4	299.3	240.4	299.3	26.3	2.6	0.0	12.7	
OBM62-41	226	25405	1.1	19.5813	4.5	0.2661	6.9	0.0378	5.3	0.76	239.2	12.4	239.6	14.8	243.9	104.0	239.2	104.0	26.5	5.3	0.1	4.5	
OBM62-42	803	31310	0.6	19.5403	2.1	0.2728	2.8	0.0387	1.9	0.67	244.5	4.6	244.9	6.2	248.8	48.2	244.5	48.2	25.9	1.9	0.1	2.1	
OBM62-43	71	6360	2.4	18.7697	14.3	0.3116	14.7	0.0424	3.4	0.23	267.8	8.9	275.4	35.6	340.6	326.0	267.8	326.0	23.6	3.4	0.1	14.3	
OBM62-44	1072	28780	0.5	19.1300	1.9	0.2875	2.6	0.0399	1.8	0.67	252.2	4.3	256.6	5.9	297.4	44.3	252.2	44.3	25.1	1.8	0.1	1.9	
OBM62-45	653	28645	0.9	19.4931	2.1	0.2829	2.6	0.0400	1.6	0.61	252.8	4.0	252.9	5.8	254.3	47.4	252.8	47.4	25.0	1.6	0.1	2.1	
OBM62-46	213	13575	1.4	20.5262	6.8	0.2633	7.3	0.0392	2.7	0.37	247.9	6.5	237.3	15.4	134.3	159.5	247.9	159.5	25.5	2.7	0.0	6.8	
OBM62-47	1179	42910	0.7	19.1428	2.2	0.2799	2.9	0.0389	1.9	0.66	245.7	4.7	250.6	6.5	295.9	49.8	245.7	49.8	25.7	1.9	0.1	2.2	
OBM62-48	258	14135	1.2	20.1691	4.2	0.2659	5.4	0.0389	3.5	0.64	246.0	8.4	239.4	11.6	175.4	96.9	246.0	96.9	25.7	3.5	0.0	4.2	
OBM62-49	610	30390	1.1	19.7134	1.6	0.2636	3.0	0.0377	2.6	0.85	238.5	6.0	237.6	6.4	228.4	37.3	238.5	37.3	26.5	2.6	0.1	1.6	
OBM62-50	842	27330	0.9	19.5759	2.1	0.2682	2.8	0.0381	1.9	0.67	240.9	4.4	242.1	6.0	244.6	47.3	240.9	47.3	26.3	1.9	0.1	2.1	
OBM62-51	292	15295	1.2	20.0981	4.5	0.2671	5.1	0.0389	2.8	0.47	246.2	5.8	240.4	10.9	183.6	104.6	246.2	104.6	25.7	2.4	0.0	4.5	

Note: All uncertainties are reported at the 1σ level and include only measurement errors. Systematic errors would increase age uncertainties by 1%–2%. U concentration and U/Th are calibrated relative to our Sri Lanka zircon standard and are accurate to ~20%. Common Pb correction is from ^{204}Pb, with composition interpreted from Stacey and Kramers (1975), and uncertainties of 1.0 for ^{206}Pb/^{204}Pb, 0.3 for ^{207}Pb/^{204}Pb, and 2.0 for ^{208}Pb/^{204}Pb. U/Pb and ^{206}Pb/^{207}Pb fractionation is calibrated relative to fragments of a large Sri Lanka zircon of 563.5 ± 3.2 Ma (2σ). Spot analyses with strikethrough were excluded in age calculation due to open system behavior and/or analytical problems. U decay constants and composition are as follows: ^{238}U = 9.8485 × 10^{-10}, ^{235}U = 1.55125 × 10^{-10}, ^{238}U/^{235}U = 137.88. MSWD—mean square of weighted deviates.

Schwartz et al.
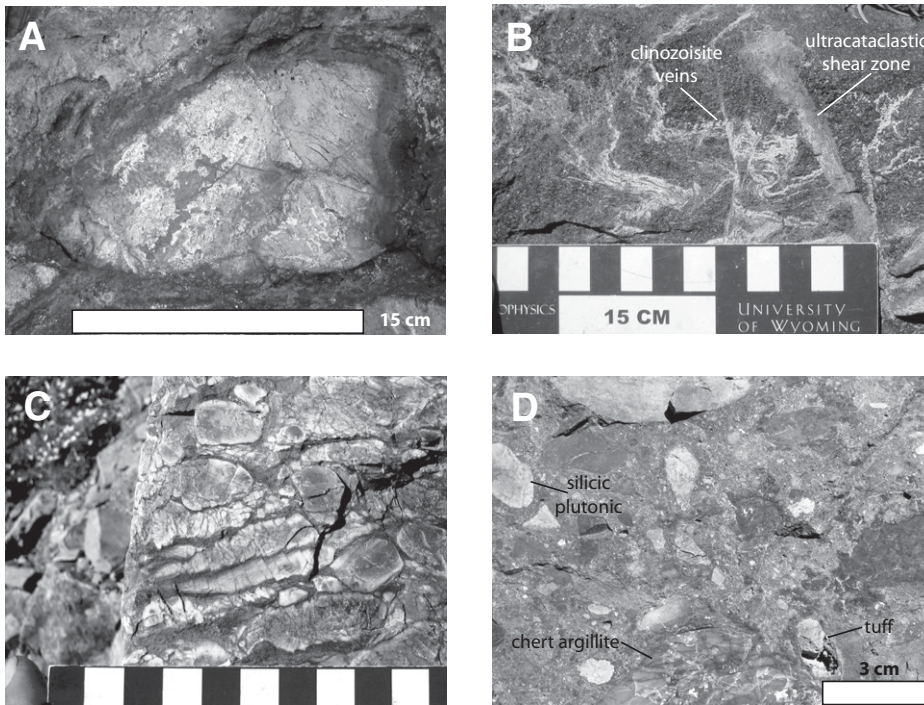
Figure 5. Photographs of various lithologic units of the Greenhorn subterrane. (A) Pillow basalt with chilled margin near the pinnacle on Vinegar Hill (Fig. 3). (B) Fine-grained diorite with white clinozoisite-rich veinlets cut by ultracataclastic shear zone on Black Butte, Vinegar Hill. (C) Brecciated siliceous chert-argillite of the Vinegar Hill chert-argillite unit exposed near the pinnacle of Vinegar Hill. (D) Conglomeratic unit of the Badger Creek metasedimentary unit with angular fragments of argillite, silicic plutonic rocks, and tuff, on eastern flank of Vinegar Hill.
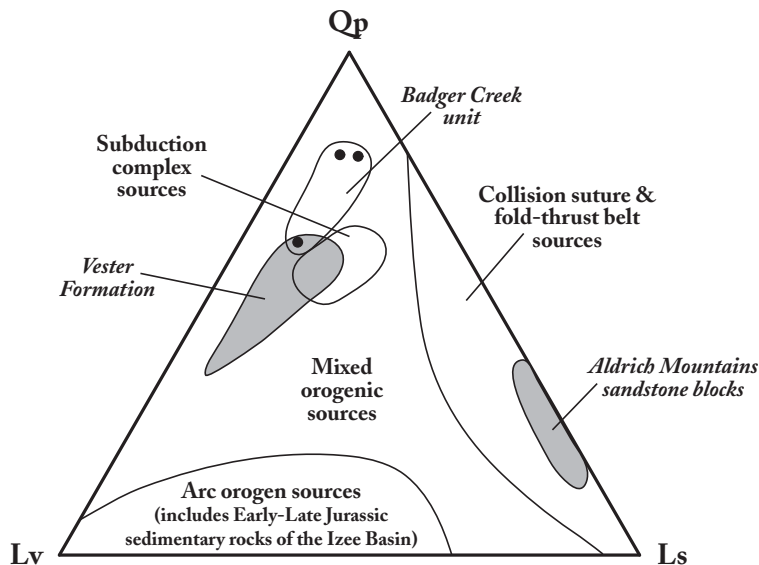
Figure 6. Qp-Ls-Lv sandstone discrimination diagram showing composition of the Badger Creek metasedimentary unit with respect to various depositional settings (fields after Dickinson et al., 1979). Qp—polycrystalline quartz, Ls—lithic sedimentary fragment, Lv—lithic volcanic fragment. Fields for the Late Triassic Vester Formation (Dickinson et al., 1979) and Aldrich Mountains sandstone mélange blocks (Carpenter and Walker, 1992) are depicted by gray fields.

Nd model ages ranging from 1.3 to 1.6 Ga (Fig. 11). Initial $^{87}Sr/^{86}Sr$ values for these rocks range from 0.7072 to 0.7073. The range in Sm/Nd exhibited by the Badger Creek unit samples (0.2121–0.2264) and Vinegar Hill chert-argillite (0.2279) is slightly higher than the North American shale composite (Sm/Nd = 0.1967; Gromet et al., 1984) and the Elkhorn Ridge Argillite of the adjacent Bourne subterrane (0.1908–0.1986).

U-Pb Zircon Geochronology

A trondhjemite (CM-05–3) from the Canyon Mountain complex yielded 13 concordant zircon spot analyses and one discordant analysis. The weighted average $^{206}Pb/^{238}U$ age of all individual spot analyses is 271.4 ± 5.5 Ma (mean square of weighted deviates [MSWD] = 6.2). The large MSWD of these data and their broad age range (35 m.y.) suggest a component of nonanalytical scatter in the data. Excluding the discordant analysis and the oldest (possibly inherited age, ca. 287 Ma) and the youngest ages (Pb-loss?, 250 Ma) yields a weighted average $^{206}Pb/^{238}U$ age of 267.0 ± 3.1 Ma (MSWD = 0.6; Fig. 12A). This age is similar within error to the weighted average age of the entire sample distribution, yet it has a lower MSWD. We interpret this age as the best approximation for the crystallization age.

A volcaniclastic breccia (08BM62) located north of the Bourne-Greenhorn subterrane boundary yielded 49 concordant individual zircon spot analyses with virtually identical ages, giving a weighted average $^{206}Pb/^{238}U$ age of 244.4 ± 6.1 Ma (MSWD = 1.4; Fig. 12B). Two analyses were strongly discordant; one of the two yielded a $^{207}Pb/^{206}Pb$ age of ca. 2010 Ma, i.e., an age similar to detrital zircon ages reported from the Baker terrane (Alexander and Schwartz, 2009).

A hornblende diorite (08GE-1) that intrudes Elkhorn Ridge Argillite and metagabbro thrust slices at the Baker-Wallowa terrane boundary at the Grey Eagle mine yielded 12 concordant zircon spot analyses giving a weighted average $^{206}Pb/^{238}U$ age of 157.1 ± 2.0 Ma (MSWD = 0.7; Fig. 12C). We interpret this age as the best approximation for the crystallization age.

A biotite-hornblende diorite (GB-07–02) from the Gold Bug pluton, which intrudes the Bourne-Greenhorn subterrane boundary (Fig. 2), gave 10 concordant spot analyses yielding a weighted average $^{206}Pb/^{238}U$ age of 154.2 ± 1.5 Ma (MSWD = 4.1). The large MSWD of these data and their broad age range (10 m.y.) suggest a component of nonanalytical scatter in the data. Excluding the two oldest (possibly inherited ages, ca. 159 Ma) and the two youngest

Late Jurassic orogenesis in the Blue Mountains Province

A. Badger Creek unit (Greenhorn subterrane)

N

- Poles to foliation (S0/S1), *n* = 37
- × Poles to foliation (S1), *n* = 37 (Ferns & Brooks, 1995)*
- ▲ Fold axis, T&P = 067/32

  *data not used in fold axis calculation

B. Elkhorn Ridge Argillite (Bourne subterrane)

N

- Poles to foliation (S0/S1), *n* = 20
- ■ Fold axis, T&P = 088/14
- ☆ Fold axis, T&P = 150/62, (Evans, 1995)

C. Serpentinite (Greenhorn subterrane)

N

- Poles to foliation (S1), *n* = 14
- ■ Fold axis, T&P = 123/45
- ○ Poles to foliation, *n* = 14 (Evans, 1995)*

  *data not used in fold axis calculation

D. Metaplutonic & metavolcaniclastic rocks (Greenhorn subterrane)

N

- Poles to foliation (S1), *n* = 17
- ▣ Fold axis, T&P = 096/35
- ◉ Fold hinges, *n* = 4 (Evans, 1995)

E. Cataclastic foliations (Greenhorn subterrane)

N

Figure 7. Structural data for various lithologic units in the Bourne-Greenhorn subterrane boundary region (Figs. 2 and 3). Plots are equal-area, lower-hemisphere projections shown with fold axes defined by the best-fit great circle to foliation. (A) Data from the Badger Creek unit, shown with data from Ferns and Brooks (1995). (B) Data from Elkhorn Ridge Argillite in the Desolation Butte area, shown with data from Evans (1995). (C) Data from serpentinite in the Desolation Butte area, shown with data from Evans (1995). (D) Data from metaplutonic and metavolcaniclastic rocks in the Desolation Butte area, shown with data from Evans (1995). (E) Data from cataclastic foliations in metaplutonic rocks on Vinegar Hill area (Fig. 3). T&P refers to trend and plunge.

ages (Pb-loss?), we find a weighted average $^{206}Pb/^{238}U$ age of 153.9 ± 1.3 Ma (MSWD = 0.9; Fig. 12D). This age is identical within error to the weighted average age of the entire sample distribution, yet it has a lower MSWD. We in-

terpret this age as the best approximation for the crystallization age.

A biotite tonalite (GB-07–1) that intrudes the ca. 154 Ma Gold Bug diorite (Fig. 2) yielded seven concordant spot analyses. The

majority of the analyses have $^{206}Pb/^{238}U$ ages of ca. 146 Ma, whereas one spot analysis is older than the rest, yielding an age of ca. 154 Ma, which is likely inherited from the older Gold Bug pluton. The weighted average $^{206}Pb/^{238}U$ age of the remaining six spots is 146.3 ± 1.5 Ma (MSWD = 0.6) and is interpreted as the best approximation for the crystallization age (Fig. 12E).

A muscovite-biotite tonalite (08GH01) northeast of Greenhorn intrudes the Bourne (Olive Creek unit) and Greenhorn subterranes (Fig. 3). Twenty-six zircon concordant spot analyses yield $^{206}Pb/^{238}U$ ages ranging from 131 to 385 Ma, with the majority of analyses giving ages of ca. 145 Ma. Older ages of ca. 152–154 and ca. 385 Ma likely reflect xenocrystic zircons derived from either plutonic basement or metasedimentary rocks. Two analyses give ages of 131 and 139 Ma, and these are interpreted to reflect small degrees of Pb loss. The remaining 22 zircon spot analyses yield a weighted average $^{206}Pb/^{238}U$ age of 145.0 ± 2.8 Ma (MSWD = 0.9; Fig. 12F), which we interpret as the best approximation for the crystallization age.

A biotite-hornblende tonalite (BMO-1) from the "Granodiorite of Anthony Lake" unit of the Bald Mountain batholith (Taubeneck, 1995) yielded 12 concordant spot analyses that give a weighted average $^{206}Pb/^{238}U$ age of 145.2 ± 2.3 Ma (MSWD = 1.8). One analysis is slightly younger than the rest of the population and may reflect Pb loss. Excluding that anomalous analysis, the remaining 11 analyses yield a weighted average $^{206}Pb/^{238}U$ age of 146.7 ± 2.1 Ma (MSWD = 1.3; Fig. 12G). We interpret this age as the best approximation for the igneous crystallization age of this sample.

The Lonesome Formation is the youngest deformed sedimentary sequence in the John Day area, and it provides a maximum age for the timing of deformation in the region. The age of the Lonesome Formation is well constrained by ammonite biostratigraphy (Dickinson and Vigrass, 1964, 1965; Imlay, 1986) as late Callovian (ca. 163–161 Ma using Gradstein et al., 2004; or ca. 160–157 Ma using Pálfy et al., 2000). The detrital zircon age distribution from a turbidite sandstone of the Lonesome Formation contains >50% Mesozoic ages, suggesting that deposition occurred in close proximity to the active Cordilleran margin arc (LaMaskin et al., 2009a, 2011). In addition, the youngest age distribution in the sample includes 20 single-grain ages that overlap at 1σ, ruling out the prospect of spurious, nonreproducible ages (cf. Dickinson and Gehrels, 2009). Thus, it is acceptable to use the youngest single-grain age of 159 ± 2 Ma as a measure of maximum depositional age for the Lonesome Formation.
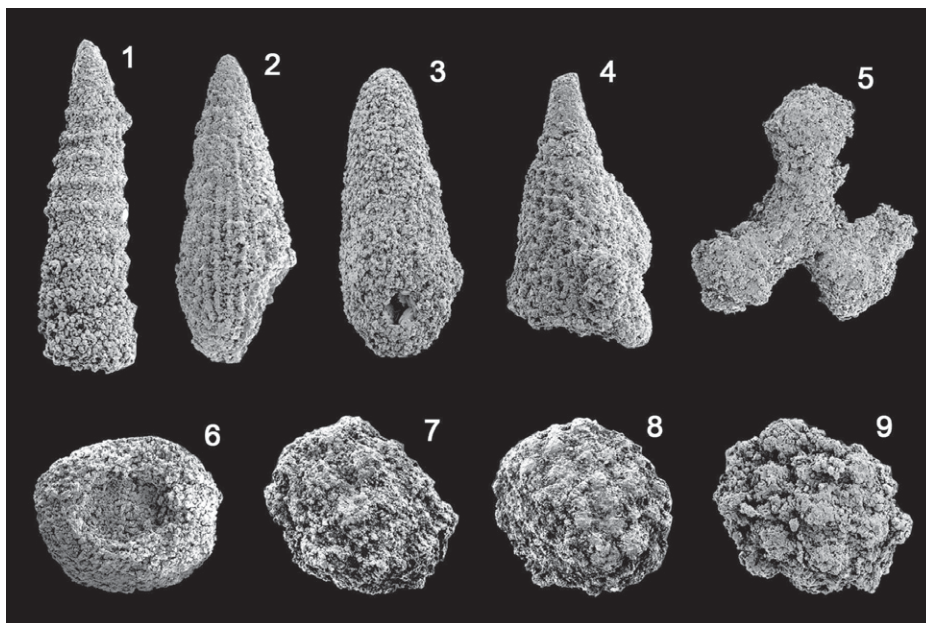
Figure 8. Jurassic radiolarians from the Elkhorn Ridge Argillite unit (Bourne subterrane) near Baboon Creek (locality 08FC08). Following numbers indicate the taxon, database picture number, and maximum width. 1—*Canoptum* sp., #08, 150 μm; 2—?*Broctus* sp., #19, 180 μm; 3—*Bagotum* sp., #07, 180 μm; 4—?*Canutus* sp., #28, 250 μm; 5—*Paronaella* sp., #04, 350 μm; 6—*Orbiculiformella* sp., #06, 280 μm; 7—*Praeconocaryomma* sp. cf. *magnimamma* (Rüst), #31, 350 μm; 8–9—*Praeconocaryomma* spp., #33, 280 μm and #01, 300 μm.

DISCUSSION

Origin of the Bourne and Greenhorn Subterranes: A Paired Accretionary Complex and Forearc

The Bourne and Greenhorn subterranes of the Baker terrane contain diverse and distinct rock types that are juxtaposed along an anastomosing, semibrittle to brittle, greenschist-facies fault zone. Whereas the Bourne subterrane consists primarily of fine-grained argillite (Elkhorn Ridge Argillite) and lesser contributions of volcanogenic material (e.g., tuff, tuffaceous argillite, and thin beds of altered mafic lavas; e.g., Gilluly, 1937), the Greenhorn subterrane contains a variety of metavolcanic, metaplutonic, and metasedimentary rocks associated with serpentinite-matrix mélange (Ferns and Brooks, 1995). Geochemically, the meta-igneous rocks in the Greenhorn subterrane are magnesian and calcic to calc-alkalic in character, display flat to LREE-depleted, chondrite-normalized REE patterns (Figs. 8 and 9), and show evidence for large ion lithophile element enrichment characteristic of magmas generated in a suprasubduction-zone setting (cf. Mullen, 1985). Previous workers have suggested that the diverse rock types in the Bourne and Greenhorn subterranes may have evolved as distinct and genetically unrelated subduction-related complexes that were
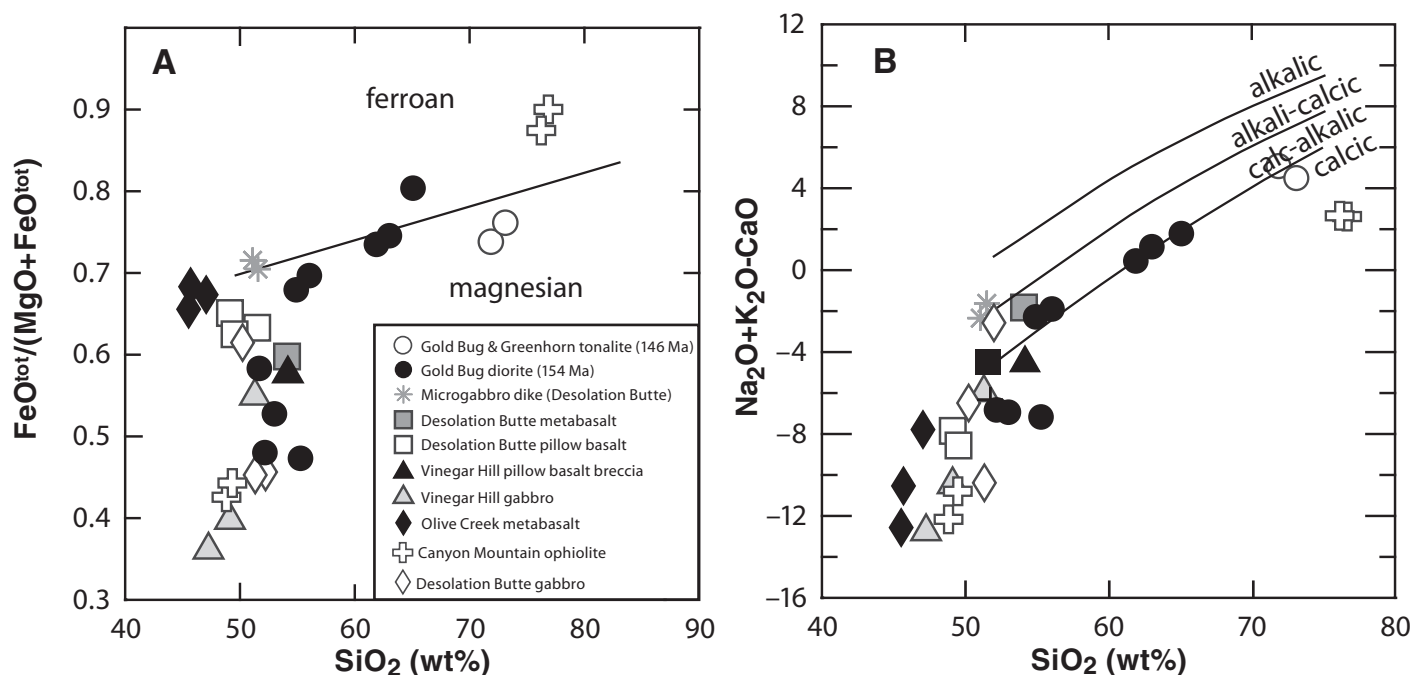
Figure 9. Major-element geochemical plots for igneous rocks in the Bourne and Greenhorn subterranes. (A) $FeO^{tot}/(FeO^{tot} + MgO)$ versus weight percent SiO_2 showing the magnesian character of igneous rocks. (B,) Plot of $Na_2O + K_2O–CaO$ versus SiO_2 showing the calcic–calc-alkalic character of igneous rocks.

Late Jurassic orogenesis in the Blue Mountains Province
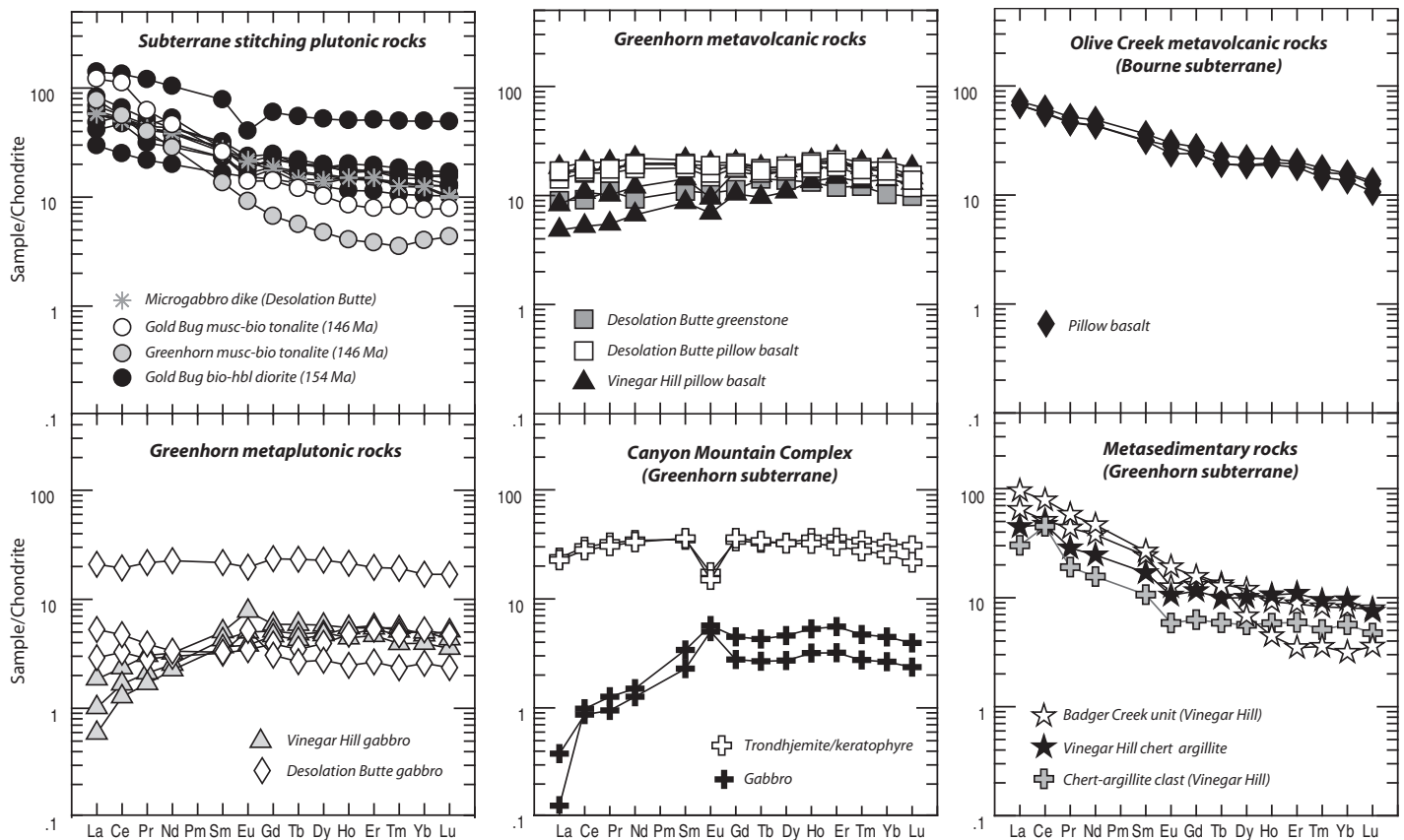
Figure 10. Chondrite-normalized rare earth element abundances for igneous and metasedimentary rocks of the Baker terrane. Samples are normalized to chondrite values of Sun and McDonough (1989). Bio—biotite; musc—muscovite; hbl—hornblende.

juxtaposed during tectonic amalgamation (Ferns and Brooks, 1995). Hence, the nature of these subterranes is of significance in understanding the origin of the Baker terrane, the location of crustal suture zones in the Blue Mountains Province, and mechanisms of upper-crustal strain localization during contractional deformation.

Our geochemical and isotopic data permit us to evaluate the relationships between the Bourne and Greenhorn subterranes, and the significance of the brittle to semibrittle fault zone that separates them. In particular, isotopic data from metasedimentary sequences in the Greenhorn subterrane (i.e., Vinegar Hill chert-argillite unit and Badger Creek metasedimentary unit: $^{87}Sr/^{86}Sr_i = 0.7062–0.7073$, $\varepsilon_{Nd} = -2.4$ to -3.8) provide strong evidence for significant involvement of an evolved, Proterozoic or older source during deposition (Fig. 11A). These evolved isotopic signatures are similar to those from the nearby Elkhorn Ridge Argillite ($^{87}Sr/^{86}Sr_i = 0.7073–0.7094$, $\varepsilon_{Nd} = -4.7$ to -7.8; Schwartz et al., 2010) in the Bourne subterrane, and they are consistent with a shared depositional source between the two subterranes. Isotopic modeling indicates that metasedimentary rocks of both

subterranes can be described as binary mechanical mixtures of a depleted-mantle arc source and average North American miogeoclinal rocks (Fig. 11A; see Schwartz et al. [2010] for details of binary mixture model). This suggestion is further supported by recent U-Pb detrital-zircon studies from the Greenhorn and Bourne subterranes, which demonstrate similar Precambrian and Phanerozoic detrital-zircon age distributions in the Badger Creek unit (Greenhorn subterrane) and Elkhorn Ridge Argillite (Bourne subterrane)(Alexander and Schwartz, 2009).

Although the Bourne and Greenhorn subterranes are separated by a greenschist-facies fault zone, we suggest, based on their similar isotopic signatures, detrital-zircon age populations, and shared deformational features (Fig. 7), that they are genetically related to each other as distinct, tectonically disrupted parts of a paired accretionary complex–forearc system (Fig. 13). In our model, the Greenhorn and Bourne subterranes developed as spatially distinct but related components of the fringing, continental-margin Olds Ferry island-arc terrane. This relationship is illustrated schematically in Figures 13 and 14. We suggest that the Permian–Triassic Badger

Creek unit formed in an extensional or transtensional forearc basin (as suggested by left-lateral mylonitic zones in the Olds Ferry terrane); however, we recognize that mélange formation and Late Jurassic contractional deformation obscure the original geometry of this basin.

We also propose that the partially age-correlative Permian–Triassic Badger Creek unit and Late Triassic Vester Formation (basal Triassic clastic sedimentary unit in the John Day region) are tectonically disrupted portions of the same forearc basin. This suggestion is supported by similar detrital zircon age distributions between the Vester Formation and Badger Creek unit (Alexander and Schwartz, 2009; LaMaskin et al., 2009b), and similar modal mineral content (e.g., Fig. 6) and lithic clasts (e.g., angular chert-argillite, metagabbro, greenstone, limestone, sandstone, and minor white quartzite).

Contractional Deformation during Arc-Arc Collision

Late Jurassic deformation in the Blue Mountains Province involved widespread faulting and folding within the Baker terrane and at

Schwartz et al.
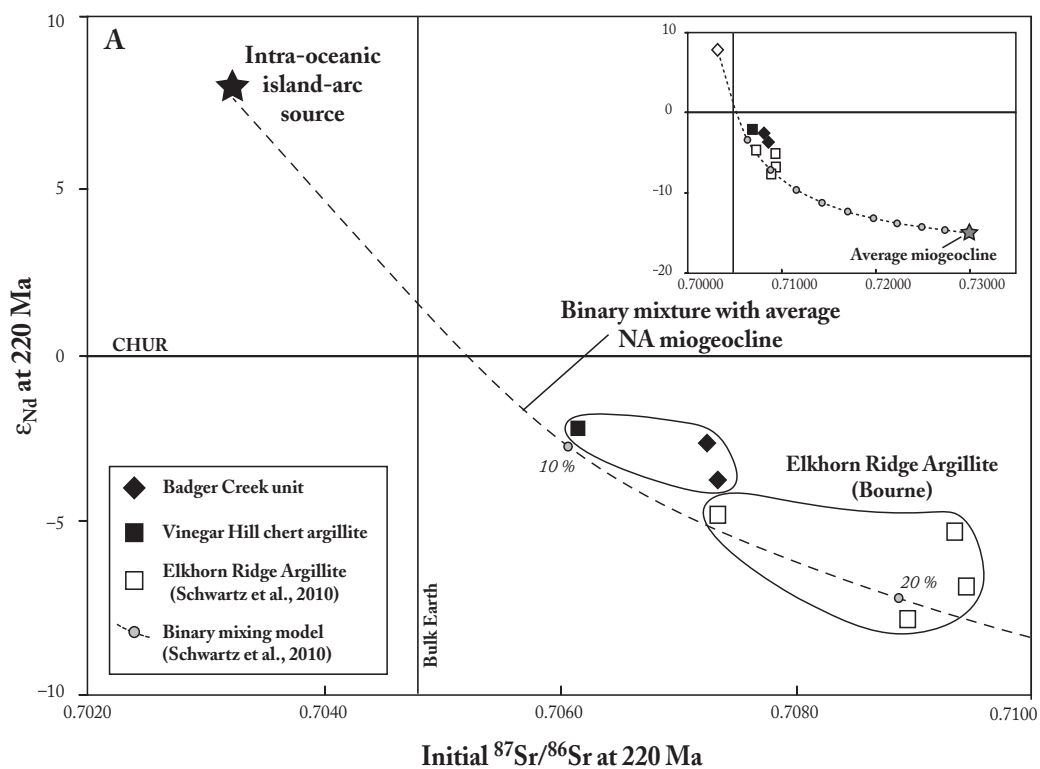
Figure 11. A, Plot of initial ε_{Nd} versus initial ^{87}Sr/^{86}Sr at 220 Ma for (meta)sedimentary rocks of the Baker terrane. A binary mixture model with average North American (NA) miogeocline and intra-oceanic island-arc rocks is shown as curved line. Metasedimentary rocks in the Greenhorn and Bourne subterrane may be described as mechanical binary mixtures of average depleted-mantle arc rocks mixed with average North American miogeocline (for mixture model details, see Schwartz et al., 2010). (B) Plot of initial ε_{Nd} versus ^{147}Sm/^{144}Nd for (meta)sedimentary rocks of the Baker terrane. Data from Klamath Mountains and Intermontane terranes are shown for comparison. CHUR refers to chondrite uniform reservoir.
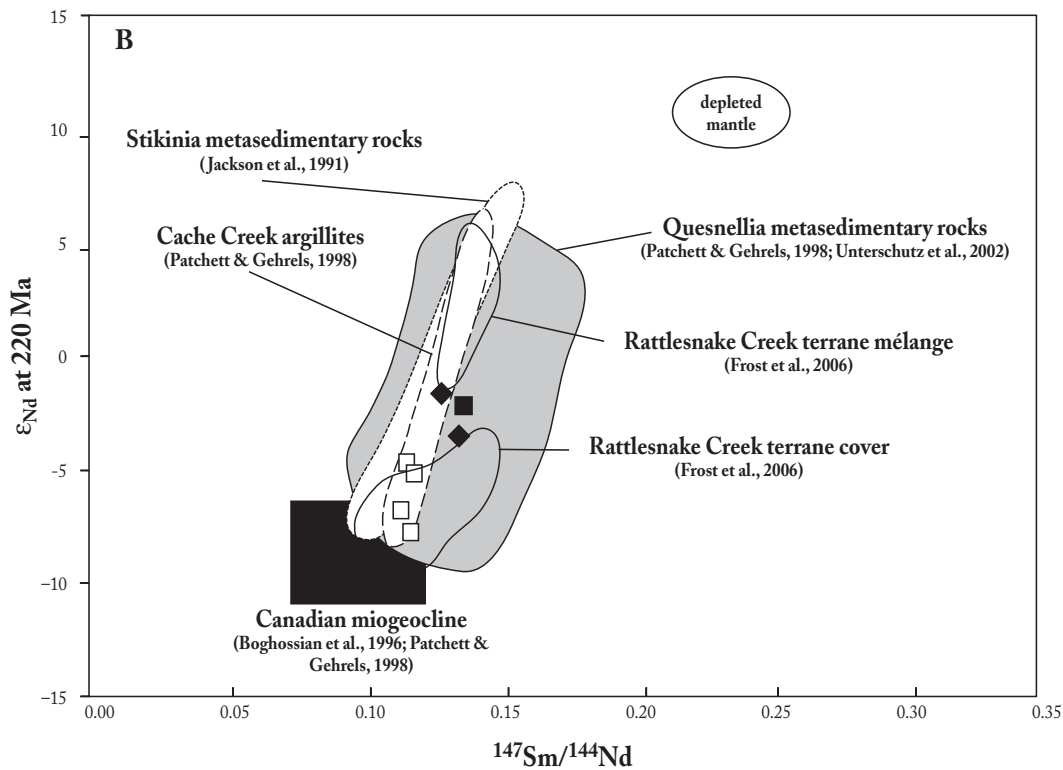
Late Jurassic orogenesis in the Blue Mountains Province
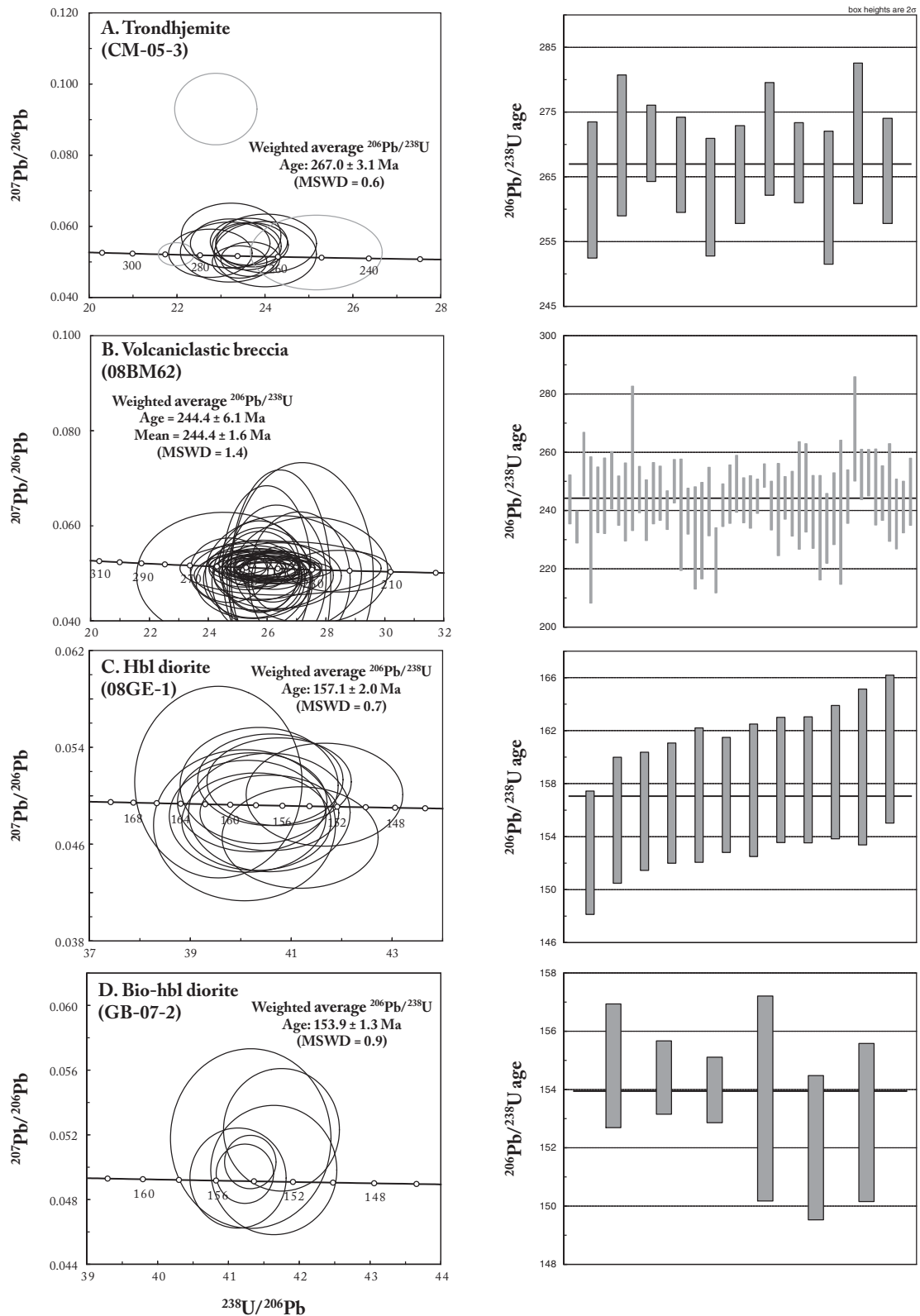
Figure 12 (*on this and following page*). U-Pb concordia plots for igneous rocks of the Bourne and Greenhorn subterranes. Data shown in A, C–E, and G were collected by ion microprobe at the Stanford–U.S. Geological Survey sensitive high-resolution ion microprobe (SHRIMP) facility, whereas data shown in B and F were collected by laser ablation–multicollector–inductively coupled plasma–mass spectrometry (LA-MC-ICP-MS) at the University of Arizona LaserChron Laboratory. MSWD—mean square of weighted deviates; bio—biotite; musc—muscovite; hbl—hornblende.
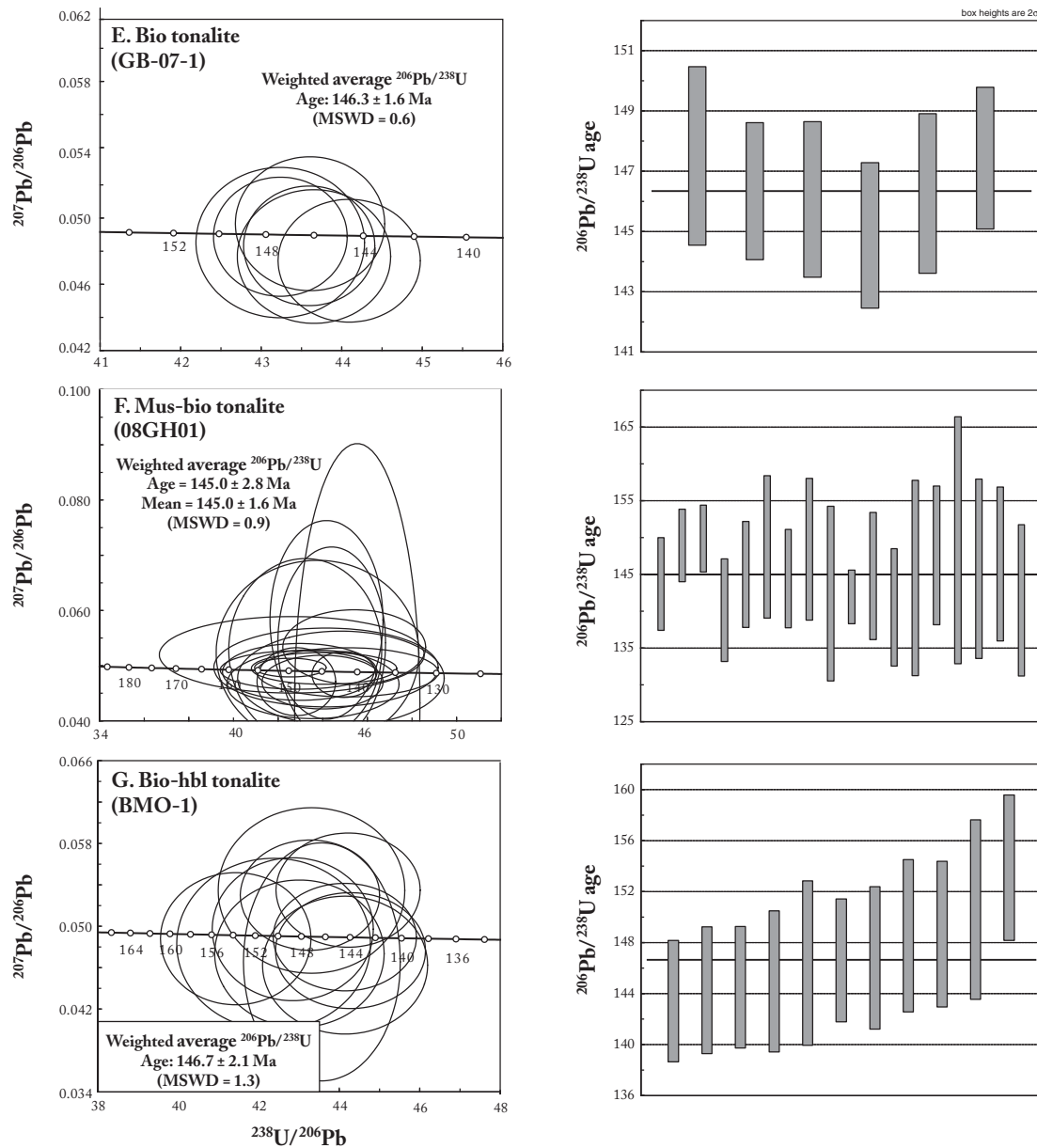
Figure 12 (*continued*).

terrane boundaries, where bivergent thrusting emplaced the Baker terrane structurally above the Olds Ferry and Wallowa island arcs along several brittle to semibrittle deformation zones (e.g., Baker-Wallowa terrane boundary, and Baker–Izee–Olds Ferry terrane boundary; Figs. 1 and 13). These contractional features record the oldest deformation to affect all terranes in the Blue Mountains Province (Avé Lallemant, 1995), and they preserve information about the mechanics of upper-crustal strain partitioning and deformation during terrane amalgamation. This deformational event has been interpreted by previous authors (e.g., Avé Lallemant,

1995; Ferns and Brooks, 1995; Schwartz et al., 2010) to signify the collision of the distal and allochthonous Wallowa island-arc terrane with the fringing continental-margin Olds Ferry island-arc terrane. Next, we discuss the nature of these brittle to semibrittle deformation zones (Bourne-Greenhorn subterrane boundary, Baker-Wallowa terrane boundary, and Baker–Izee–Olds Ferry terrane boundary) and their significance in Late Jurassic contractional orogenesis in the Blue Mountains Province.

Within the Baker terrane, widespread contractional deformation resulted in the development of E-W–oriented, penetrative slaty

to spaced cleavage in metasedimentary rocks in both subterranes. This prominent cleavage is locally overprinted by anastomosing, brittle to semibrittle faults, particularly at the Bourne-Greenhorn subterrane boundary, where contractional deformation involved thrusting of serpentinite-matrix mélange over argillite-matrix mélange, intense brecciation in chert-argillite units of the footwall (Elkhorn Ridge Argillite), and localized cataclastic shearing associated with greenschist-facies metamorphic veining in both hanging-wall and footwall rocks (Evans, 1989, 1995)(cf. Fig. 2). The presence of greenschist-facies metamorphic assemblages
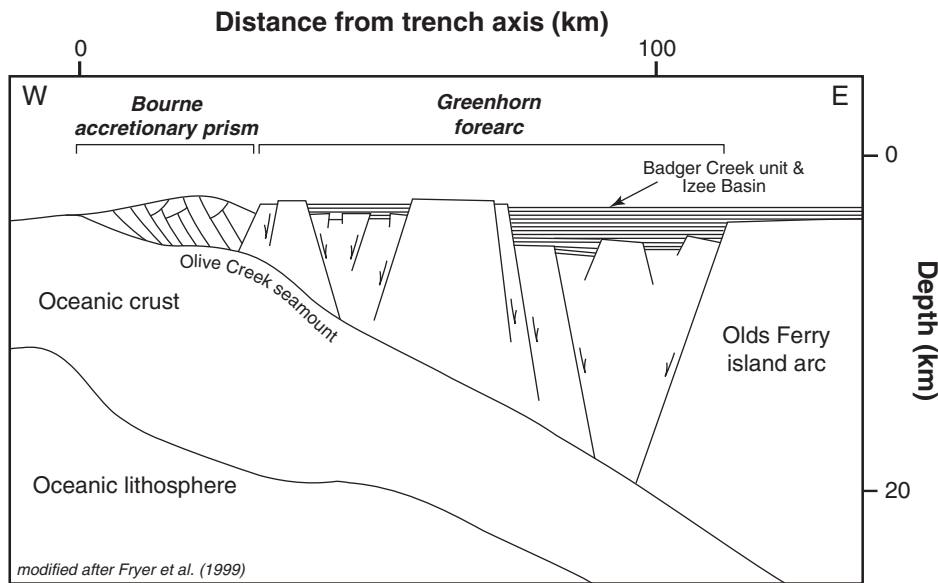
Figure 13. Schematic (pre–Late Jurassic contraction) reconstruction of Baker terrane in Permian to Late Triassic, illustrating our preferred interpretation of the relationship between the Bourne accretionary complex and Greenhorn forearc (modified after Fryer et al., 1999). We suggest that the Permian to Late Triassic (?) Badger Creek unit formed in an extensional forearc basin and may be genetically related to the partially age-correlative Vester Formation of the John Day region.

and clinozoisite veins supports previous suggestions that contractional deformation was accompanied by widespread fluid flow and dissolution (Avé Lallemant, 1983). Metamorphic mineral assemblages in the Greenhorn subterrane also indicate higher metamorphic conditions (lower amphibolites facies) versus the Bourne subterrane (lower greenschist facies), which are consistent with exposure of deeper structural levels in the hanging wall during thrusting.

Another zone of intense deformation in the Blue Mountains Province is the Baker-Wallowa terrane boundary, which is characterized by a broad zone (>25 km wide) of fault-bounded, imbricated slabs and slices of meta-igneous and metasedimentary rocks (interpreted to be derived from the Wallowa island-arc terrane; Fig. 4), which were faulted into chert-argillite mélange of the Elkhorn Ridge Argillite (Ferns and Brooks, 1995; Schwartz et al., 2010). Slabs of meta-igneous rocks in this zone consistently dip to the south (away from the Wallowa island-arc terrane) as a series of arc-directed thrusts. Metasedimentary and meta-igneous rocks in these fault slices are distinct and less isotopically evolved than those in the coeval Elkhorn Ridge Argillite, indicating that this fault zone is a fundamental tectonic and isotopic boundary that separates the distal Wallowa island-arc terrane from the Bourne accretionary complex. Ferns and Brooks (1995) and Schwartz et al.

(2010) suggested that the incorporation of these fault slices into the Bourne accretionary complex represents the collision of the Wallowa and Olds Ferry island-arc terranes, resulting in widespread imbrication of the southern margin of the Wallowa plate beneath the Bourne subterrane. This suggestion is supported by contrasting early (Permian–Early Jurassic) deformational histories of the Baker and Wallowa terranes prior to amalgamation (cf. Avé Lallemant, 1995; Kays et al., 2006) and contrasting isotopic and detrital zircon characteristics (LaMaskin et al., 2007; Alexander and Schwartz, 2009). North of this deformation zone (within the Wallowa island-arc terrane), E-W–oriented thrust faults and hinge lines are similar to observations at the Baker-Wallowa terrane boundary and suggest that these features may have also formed together in response to widespread Late Jurassic contractional deformation in the Blue Mountains Province.

Along the southern margin of the Baker terrane, Late Triassic to early Late Jurassic sedimentary rocks were deformed in response to contractional deformation. Deformation occurred throughout the region from eastern Oregon and western Idaho to the John Day region. The highest strain is preserved at the contact of the Baker–Izee–Olds Ferry terrane boundaries, northeast of Huntington, Oregon (cf. Fig. 1). Contractional structural features in the Weath-

erby Formation (north of Huntington) include mega- and mesoscale folds, overturned to the south and southeast, and the synchronous development of a NE-SW–striking axial-surface slaty to spaced cleavage. Folds were developed in association with N-dipping, S- to SE-directed thrust and/or reverse faults that emplaced the Baker terrane (Burnt River Schist) structurally above the Early to latest Middle Jurassic Weatherby Formation along the Connor Creek fault (Fig. 1; Brooks and Vallier, 1978; Avé Lallemant, 1983). The Weatherby Formation was in turn thrust over the Late Triassic to Early Jurassic Huntington Formation of the Olds Ferry arc-terrane along a highly imbricated fault zone (Avé Lallemant, 1983). Microstructural observations of quartz c-axis fabrics from this fault zone indicate NW-SE principal compressive stress directions associated with Late Jurassic contractional deformation (Avé Lallemant, 1983, 1995). Kinematic data from stretched-pebble conglomerates in the basal Weatherby Formation also indicate a component of left-lateral strike-slip displacement along a WNW-ESE–striking shear zone (Avé Lallemant, 1995). Folding and faulting of sedimentary rocks in both eastern Oregon–western Idaho and the John Day region were followed by a hiatus in deposition after ca. 159 ± 2 Ma (Oxfordian Lonesome Formation in the John Day region and Callovian Weatherby Formation in eastern Oregon–western Idaho; Dickinson and Thayer, 1978; Dickinson, 1979; Imlay, 1986; Dorsey and LaMaskin, 2007).

Other unconformities and faults (cf. Dickinson and Thayer, 1978; Dickinson, 1979) are also present between volcanogenic sedimentary rocks of the Olds Ferry island arc and overlying Jurassic sedimentary rocks (e.g., between the Huntington and Weatherby Formations at 187–181 Ma; Tumpane and Schmitz, 2009). Previous workers have interpreted the Early Jurassic unconformity in the John Day and Huntington regions as possibly representing nascent arc-arc collision between the Wallowa and Olds Ferry arcs (Dorsey and LaMaskin, 2007; Lamaskin et al., 2008b), or alternatively, as an episode of intraforearc, arc-directed back thrusting associated with E-dipping subduction (present-day coordinates) beneath the Olds Ferry fringing continental-margin island arc (Dickinson, 1979). We emphasize that this hiatus overlaps in age with deposition of radiolarian-bearing cherts in the adjacent Bourne subterrane (193–181 Ma; see "Radiolarian Micropaleontology" section). Hence, our structural observations, new U-Pb zircon geochronology, and micropaleontology are inconsistent with Early Jurassic arc-arc collision. We therefore prefer the interpretation of Late Triassic to Early Jurassic limited intraforearc deformation. This
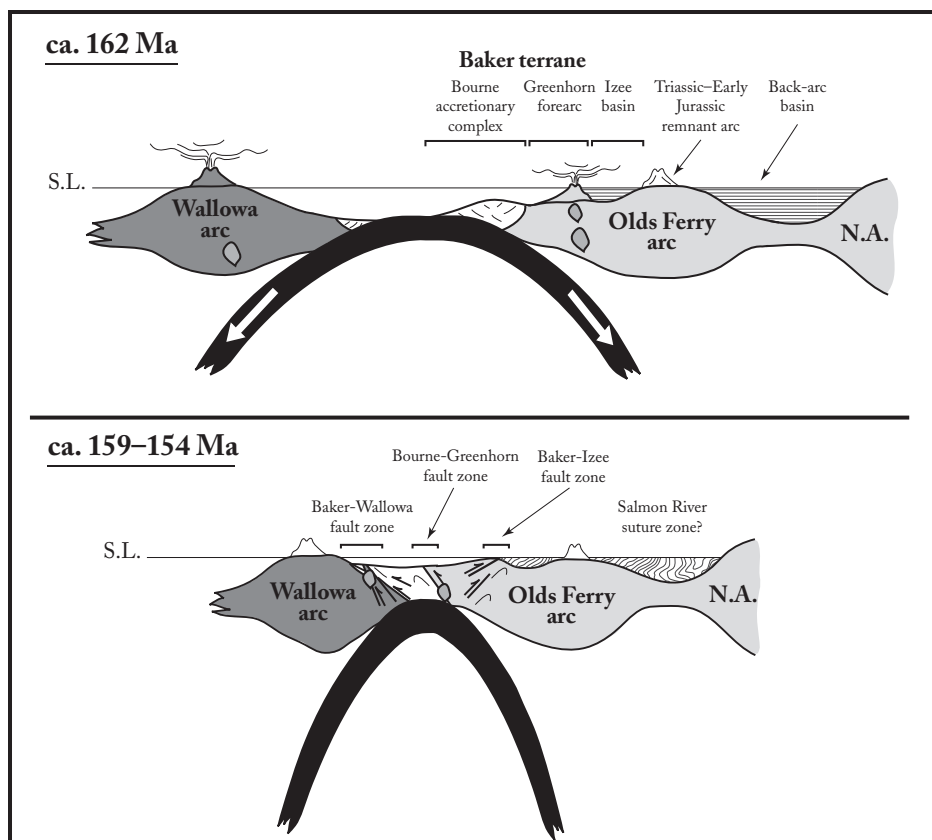
Figure 14. Schematic, precollisional (ca. 162 Ma) and collisional (159–154 Ma) scenarios for the Bourne and Greenhorn subterranes in the Middle to early Late Jurassic. The Bourne and Greenhorn subterranes are interpreted to be accretionary complex and forearc, respectively, of the fringing continental-margin, Olds Ferry island-arc terrane. Brittle to semibrittle deformation zones discussed in text are shown. S.L.—sea level; N.A.—North America.

In the John Day region, thin andesitic lavas, dikes, and sills of Early to Middle Jurassic age are locally present and are associated with andesitic volcaniclastic turbidites, which grade into subaqueous ash-flow tuffs of dacitic to rhyodacitic composition (Dickinson, 1979). Coeval latest Middle Jurassic andesitic magmatism is documented in the nearby Dixie Butte area (north of the John Day region) and is a potential local source for Jurassic volcanic and volcaniclastic rocks in the John Day region. Paleocurrent indicators (prior to ~60° of post–Early Cretaceous clockwise rotation) and thickness relations support derivation of volcaniclastic debris from a NE to NW source region (Dickinson and Thayer, 1978). Collectively, these features suggest ongoing magmatism and deposition in both the Baker terrane and John Day region of the Izee "terrane" during the latest Middle Jurassic. Furthermore, these data also suggest that the John Day region may have transitioned from a distal forearc basin in Late Triassic to Early Jurassic time to a back-arc setting in Middle to Early Jurassic time as magmatism migrated northwestward (present-day coordinates) from the Olds Ferry arc (Huntington Formation) to the Greenhorn subterrane (cf. Fig. 14). We suggest that our new data may record an ancient example of outboard arc-axis migration associated with arc-arc collision, a well-documented process in the modern southwest Pacific (e.g., Hall, 2002).

Widespread contractional features within the Baker terrane and at subterrane and terrane boundaries postdate Early Permian–Early Jurassic deposition and bedding-parallel extensional fabric development (Avé Lallemant, 1995). These structural features also deform Triassic–Late Jurassic sedimentary rocks in the John Day and eastern Oregon–western Idaho areas. The youngest deformed sedimentary rocks are the Oxfordian Lonesome Formation (ca. 159 ± 2 Ma; LaMaskin, 2009), providing a maximum age for Jurassic contractional deformation in the region. E-W–oriented contractional features in the Baker terrane are crosscut by postkinematic plutonic rocks at 157 ± 2 Ma (Grey Eagle pluton) at the Baker-Wallowa terrane boundary and 154 ± 1 Ma (Gold Bug pluton) at the Bourne-Greenhorn subterrane boundary. Collectively, these features bracket contractional deformation to between ca. 159 and ca. 157 Ma at the Baker-Wallowa terrane boundary and between ca. 159 and ca. 154 at the Bourne-Greenhorn subterrane boundary. Next, we discuss the significance of these results in terms of tectonic correlations and orogenic events in other parts of the western North American Cordillera (e.g., Canadian Intermontane superterrane and Klamath Mountains).

interpretation is more compatible with our geologic observations for this relatively brief and apparently focused episode of deformation (see following discussion).

Timing of Deposition, Development of Layer-Parallel Extensional Fabric, and Contractional Deformation in the Baker Terrane

Our new faunal ages from radiolarian-bearing thin-bedded chert in the Baker terrane (Bourne subterrane) indicate that deposition occurred over at least 100 m.y. from the Early Permian (Sakmarian) through Early Jurassic (Sinemurian–Toarcian). Based on the commonly inferred depositional setting of thin-bedded chert, this deposition occurred in a sediment-starved, deep-water marine basin. Layer-parallel extensional fabrics are ubiquitous in these rocks and likely formed syndepositionally in response to landsliding and/or slumping in a subduction-zone setting (cf. type II mélange of Cowan,

1985). Early Jurassic radiolarian-bearing cherts in the Baker terrane are similar in age to andesites, rhyolites, and tuffs in the Olds Ferry and Wallowa terranes (Tumpane and Schmitz, 2009), suggesting that sedimentation and extensional-fabric development occurred synchronous with arc-related magmatism during Early Jurassic time. Syndepositional, Late Triassic to Early Jurassic faulting is also recorded in the John Day region at this time and is interpreted to reflect intra-arc contraction during subduction (see previous discussion; Dickinson and Thayer, 1978; Dickinson, 1979). Early to Middle Jurassic volcaniclastic sedimentary rocks of the Mowich Group and Snowshoe Formation (Pliensbachian to basal Callovian) overlie older sedimentary rocks in the John Day region, indicating that syndepositional faulting was followed by continued arc-related magmatism that extended episodically through the latest Middle Jurassic (cf. Dickinson and Vigrass, 1965; Dickinson and Thayer, 1978; Dorsey and LaMaskin, 2007).

Tectonic Correlations and Middle–Late Jurassic Deformation along the Western North American Cordillera

Northern Cordillera Correlations: Intermontane Superterrane

North of the Blue Mountains Province, lithotectonic terranes of the Canadian Intermontane superterrane contain two contemporaneous late Paleozoic to Mesozoic island-arc terranes and an associated mélange terrane, which collectively bear broad similarities in rock type and age to terranes of the Blue Mountains Province. Island arc–related terranes consist of a Triassic to Early Jurassic fringing continental margin arc (Quesnellia) and a more distal, Triassic to Middle Jurassic island arc (Stikinia), both of which contain volcanic, volcaniclastic, and sedimentary rocks and associated cogenetic plutons (Marsden and Thorkelson, 1992; Anderson, 1993; Currie and Parrish, 1997; Patchett and Gehrels, 1998; MacIntyre et al., 2001; English and Johnston, 2005). These island-arc terranes are separated by a long-lived, argillite-matrix mélange terrane (Cache Creek) that contains remnants of oceanic plateaus tectonically intercalated with Permian–Middle Jurassic metasedimentary rocks consisting of ribbon chert, argillite, graywacke, sandstone, conglomerate, and limestone (Cordey et al., 1987; Nelson and Mihalynuk, 1993; Mihalynuk et al., 1994; Orchard et al., 2001; Struik, 2001; Struik et al., 2001; Tardy et al., 2001; Lapierre et al., 2003). Lateral tectonic collision of the Stikinia–Cache Creek–Quesnellia terranes may have been diachronous from north to south, associated with progressive oroclinal closure, with initial collision recorded by early Middle Jurassic deformation in the north and progressive southward younging of deformation and final closure between the Toarcian and Bajocian (Thomson et al., 1986; Ricketts et al., 1992; Anderson, 1993; Nelson and Mihalynuk, 1993; Mihalynuk et al., 1994).

Previous workers have noted faunal, age, and isotopic similarities between the Intermontane terranes and those in the Blue Mountains Province and have suggested that the Wallowa–Baker–Olds Ferry superterrane may represent a southern extension of the Stikinia–Cache Creek–Quesnellia superterrane (e.g., Mortimer, 1986; Stanley and Senowbari-Daryan, 1986). Similarities between the Cache Creek and Baker terranes are also compelling and include, (1) long-lived (Permian–Early-Middle Jurassic) deposition of chert-argillite, (2) intercalation of oceanic plateaus (e.g., Olive Creek unit in Baker terrane) into chert-argillite mélange, and (3) isotopic similarities between Baker and Cache Creek argillaceous rocks (cf. Fig. 11B). We note, however, that the Cache Creek terrane contains only Tethyan fauna, whereas the Baker terrane contains both Tethyan and McCloud fauna. Another difference is that contractional deformation in the Blue Mountains was somewhat younger (159–154 Ma) versus Middle Jurassic deformation in the southern Intermontane terrane.

Southern Cordillera Correlations: Klamath Terranes

Components of the Baker terrane bear a number of similarities to accreted terranes in the Klamath Mountains of northwestern California and southwestern Oregon. In particular, the Greenhorn subterrane shares similarities to the North Fork terrane, a composite Permian to Jurassic forearc terrane, which consists of serpentinized ultramafic rock, metagabbro, metabasalt, metavolcaniclastic breccia, argillite, chert-argillite, and limestone (e.g., Ando, 1979; Ando et al., 1983; Ernst, 1998, 1999; Scherer et al., 2006; Scherer and Ernst, 2008). Metasedimentary rocks in the North Fork terrane range in age from Permian to Early Jurassic and have McCloud faunal affinities (Wright, 1982; Ernst, 1998; Ernst et al., 2008). The North Fork terrane also lies inboard of the eastern Hayfork terrane, a subduction-related, argillite-matrix mélange terrane similar in composition to the Bourne subterrane (Wright, 1982; Wright and Fahan, 1988; Goodge and Renne, 1993; Ernst, 1999; Scherer et al., 2006; Snow and Scherer, 2006). Detrital zircons from the eastern Hayfork have also been interpreted to have derived from older continental crust (Scherer et al., 2006; Ernst et al., 2008). These broad lithologic and geochemical similarities between the North Fork and eastern Hayfork terranes in the Klamath Mountains and Greenhorn and Bourne subterranes in the Blue Mountains Province are compelling and suggest that they may have a similar tectonic origin.

The Rattlesnake Creek terrane, also located in the Klamath Mountains, shares a number of similarities with the Greenhorn subterrane in that it contains tectonic fragments of peridotite, metavolcanic rock, amphibolite, pillow basalt, mafic plutonic rocks, metachert, and limestone within a matrix of sheared serpentinite (Wright and Wyld, 1994). Much like their counterparts in the Greenhorn Mountains, metavolcanic rocks in the Rattlesnake Creek terrane were derived from normal mid-ocean-ridge basalt (N-MORB), enriched (E) MORB, and within-plate sources (Wright and Wyld, 1994). Initial ^{87}Sr/^{86}Sr and ε_{Nd} isotopic values for these mélange blocks range from 0.7000 to 0.7061 and 4.2 to –2.3, respectively (Frost et al., 2006). The Rattlesnake Creek terrane is also unconformably (?) overlain by an Upper Triassic to Lower Jurassic "cover sequence" consisting of metavolcanic and isotopically evolved metasedimentary rocks (Frost et al., 2006), which may correlate with sedimentary rocks in the John Day region of northeast Oregon and in eastern Oregon–western Idaho. Their strongly evolved isotopic characteristics have been interpreted to reflect derivation from eolian dust in the case of the Rattlesnake Creek mélange and proximal cratonic sources in the case of the cover sequence (Frost et al., 2006). Unlike the Greenhorn subterrane, the Rattlesnake Creek terrane lies outboard of argillite-matrix mélange rocks of the eastern Hayfork terrane (Wright, 1982; Wright and Fahan, 1988; Goodge and Renne, 1993; Ernst, 1999; Scherer et al., 2006; Snow and Scherer, 2006; Ernst et al., 2008). These contrasting spatial relationships between the Greenhorn-Bourne subterranes and Rattlesnake Creek–eastern Hayfork terranes are difficult to attribute to a single forearc and accretionary complex, unless mechanisms such as terrane transfer along strike-slip faults (e.g., Wright and Wyld, 2007) or intra-arc rifting (e.g., Ernst et al., 2008) are invoked.

Middle to Late Jurassic contractional deformation is also recognized in the Klamath Mountains and western Sierra Nevada foothills in the U.S. sector of the western North American Cordillera (e.g., Schweickert and Cowan, 1975; Schweickert et al., 1984; Wright and Fahan, 1988). Although originally conceived as a single, Late Jurassic Klamath–Sierra Nevada orogenic event ("Nevadan" orogeny, sensu lato), subsequent work has demonstrated that multiple Mesozoic deformational events have affected the Klamath–Sierra Nevada terranes, including a discrete Middle Jurassic event at ca. 169–161 Ma (Siskiyou orogeny; Coleman et al., 1988; Wright and Fahan, 1988; Wright and Wyld, 1994; Hacker et al., 1995), and a Late Jurassic event at ca. 153–150 Ma (Nevadan orogeny; e.g., Saleeby et al., 1982; Harper and Wright, 1984; Harper et al., 1994; Allen and Barnes, 2006; Chamberlain et al., 2006). The geodynamic significance of these contractional events is still controversial and may represent either (1) repeated collisions of distal island arc–related terranes, or (2) alternating periods of coupling between the subducting slab and the overriding plate (Wright and Fahan, 1988; Snoke and Barnes, 2006). Although certain structural and stratigraphic similarities exist between the Klamath and Blue Mountains Provinces (see previous), lithotectonic correlations are problematic because the Klamath terranes appear to lack a Wallowa-equivalent terrane, and the timing of regional deformation is apparently different (159–154 Ma in the Blue Mountains Province as compared to 169–161 Ma and 153–150 Ma in the Klamath Mountains).

Schwartz et al.

CONCLUSIONS

Late Jurassic contractional deformation in the Blue Mountains Province, northeast Oregon, involved the development of widespread, penetrative, approximately E-W–oriented slaty to spaced cleavage, approximately N-S–directed folding, and N- and S-dipping reverse and thrust faulting throughout the Baker, Izee, Olds Ferry, and Wallowa terranes. Deformation related to Late Jurassic contraction is localized in several brittle to semibrittle deformation zones within the Baker oceanic mélange terrane (e.g., Bourne-Greenhorn subterrane boundary) and at terrane boundaries (e.g., the Baker-Wallowa terrane boundary, and Baker–Izee–Olds Ferry terrane boundary). Within these brittle to semibrittle deformation zones, there are numerous brittle faults, intense brecciation of footwall rocks, and extensive networks of cataclastic shear zones developed within footwall and hanging-wall rocks at greenschist-facies metamorphic conditions. Detrital zircon ages from deformed sedimentary rocks (e.g., Oxfordian Lonesome Formation; LaMaskin, 2009), coupled with new U-Pb zircon ages of postkinematic fault-stitching plutons, allows us to tightly bracket contractional deformation between 159 and 157 Ma at the Baker-Wallowa terrane boundary and between 159 and 154 Ma at the Bourne-Greenhorn subterrane boundary within the Baker terrane.

Based on structural, geochemical, and isotopic data, we propose that the widespread, bivergent, approximately N-S–directed contractional features in the Baker terrane (and the broader Blue Mountains Province) record a short-lived episode of deformation related to the early Late Jurassic terminal collision of the distal Wallowa island arc with the fringing, continental-margin Olds Ferry island arc. We suggest that the brittle to semibrittle deformation zones in the Blue Mountains Province preserve an example of shallow- to midcrustal deformation related to inferred arc-arc collision, during which time the Baker terrane was thrust over both colliding island arcs and accommodated much of the contractional strain. Similar contractional features are observed in the Intermontane superterrane, Klamath Mountains, and western Sierra Nevada, suggesting widespread contraction and mountain building along much of the western North American Cordillera during Early–Middle Jurassic time.

ACKNOWLEDGMENTS

REFERENCES CITED

Alexander, R., and Schwartz, J.J., 2009, Detrital zircon geochronology of Permian-Triassic metasedimentary rocks in the Baker terrane, Blue Mountains Province, NE Oregon: Geological Society of America Abstracts with Programs, v. 41, no. 7, p. 294.

Allen, C.M., and Barnes, C.G., 2006, Ages and some cryptic sources of Mesozoic plutonic rocks in the Klamath Mountains, California and Oregon, *in* Snoke, A.W., and Barnes, C.G., eds., Geological Studies in the Klamath Mountains Province, California and Oregon: A Volume in Honor of William P. Irwin: Geological Society of America Special Paper 410, p. 223–245.

Anderson, R.G., 1993, A Mesozoic stratigraphic and plutonic framework for northwestern Stikinia (Iskut River area), northwestern British Columbia, Canada, *in* Dunne, C., and Mcdougall, K., eds., Mesozoic Paleogeography of the western United States: Pacific Section, Society of Economic Paleontologists and Mineralogists, Field Trip Guidebook, v. 71, p. 477–494.

Ando, C.J., 1979, Structural and Petrologic Analysis of the North Fork Terrane, Central Klamath Mountains, California [Ph.D. thesis]: Los Angeles, University of Southern California, 197 p.

Ando, C.J., Irwin, W.P., Jones, D.L., and Saleeby, J.B., 1983, The ophiolitic North Fork terrane in the Salmon River region, central Klamath Mountains, California: Geological Society of America Bulletin, v. 94, p. 236–252, doi: 10.1130/0016-7606(1983)94<236:TONFTI>2.0.CO;2.

Ashley, R.P., 1966, Metamorphic Petrology and Structure of the Burnt River Canyon Area, Northeastern Oregon [Ph.D. thesis]: Stanford, California, Stanford University, 193 p.

Ashley, R.P., 1995, Petrology and deformation history of the Burnt River Schist and associated plutonic rocks in the Burnt River Canyon area, northeastern Oregon, *in* Vallier, T.L., and Brooks, H.C., eds., Geology of the Blue Mountains Region of Oregon, Idaho, and Washington: Petrology and Tectonic Evolution of Pre-Tertiary Rocks of the Blue Mountains Region: U.S. Geological Survey Professional Paper 1438, p. 457–495.

Avé Lallemant, H.G., 1983, The kinematic insignificance of mineral lineations in a Late Jurassic thrust and fold belt in eastern Oregon, U.S.: Tectonophysics, v. 100, p. 389–404, doi: 10.1016/0040-1951(83)90195-6.

Avé Lallemant, H.G., 1995, Pre-Cretaceous tectonic evolution of the Blue Mountains Province, northeastern Oregon, *in* Vallier, T.L., and Brooks, H.C., eds., Geology of the Blue Mountains Region of Oregon, Idaho and Washington: Petrology and Tectonic Evolution of Pre-Tertiary Rocks of the Blue Mountains Region: U.S. Geological Survey Professional Paper 1438, p. 271–304.

Barnes, C.G., Snoke, A.W., Harper, G.D., Frost, C.D., McFadden, R.R., Bushey, J.C., and Barnes, M.A.W., 2006, Arc plutonism following regional thrusting: Petrology and geochemistry of syn- and post-Nevadan plutons in the Siskiyou Mountains, Klamath Mountains province, California, *in* Snoke, A.W., and Barnes, C.G., eds., Geological Studies in the Klamath Mountains Province, California and Oregon: A Volume in Honor of William P. Irwin: Geological Society of America Special Paper 410, p. 357–376.

Bishop, E.M., 1995a, High-pressure, low-temperature schistose rocks of the Baker terrane, northeastern Oregon, *in* Vallier, T.L., and Brooks, H.C., eds., Geology of the Blue Mountains Region of Oregon, Idaho and Washington: Petrology and Tectonic Evolution of Pre-Tertiary Rocks of the Blue Mountains Region: U.S. Geological Survey Professional Paper 1438, p. 211–245.

Bishop, E.M., 1995b, Mafic and ultramafic rocks of the Baker terrane, eastern Oregon, and their implications for terrane origin, *in* Vallier, T.L., and Brooks, H.C., eds., Geology of the Blue Mountains Region of Oregon, Idaho and Washington: Petrology and Tectonic Evolution of Pre-Tertiary Rocks of the Blue Mountains Region: U.S. Geological Survey Professional Paper 1438, p. 221–245.

Blackwelder, E., 1914, A summary of the orogenic epochs in the geologic history of North America: The Journal of Geology, v. 22, p. 633–654, doi: 10.1086/622180.

Blome, C.D., and Nestell, M.K., 1991, Evolution of a Permo-Triassic sedimentary mélange, Grindstone terrane, east-central Oregon: Geological Society of America Bulletin, v. 103, p. 1280–1296, doi: 10.1130/0016-7606(1991)103<1280:EOAPTS>2.3.CO;2.

Blome, C.D., Jones, D.L., Murchey, B.L., and Liniecki, M., 1986, Geologic implications for radiolarian-bearing Paleozoic and Mesozoic rocks from the Blue Mountains Province, eastern Oregon, *in* Vallier, T.L., and Brooks, H.C., eds., Geology of the Blue Mountains Region of Oregon, Idaho, and Washington—Geological Implications of Paleozoic and Mesozoic Paleontology and Biostratigraphy, Blue Mountains Province, Oregon and Idaho: U.S. Geological Survey Professional Paper 1435, p. 79–101.

Boghossian, N.D., Patchett, P.J., Ross, G.M., and Gehrels, G.E., 1996, Nd isotopes and the source of sediments in the miogeocline of the Canadian Cordillera: The Journal of Geology, v. 104, p. 259–277, doi: 10.1086/629824.

Bostwick, D.A., and Koch, G.S., 1962, Permian and Triassic rocks of northeastern Oregon: Geological Society of America Bulletin, v. 73, p. 419–421, doi: 10.1130/0016-7606(1962)73[419:PATRON]2.0.CO;2.

Bostwick, D.A., and Nestell, M.K., 1965, A new species of *Polydiexodina* from central Oregon: Journal of Paleontology, v. 39, p. 611–614.

Brooks, H.C., 1979, Geologic map of the Huntington and part of the Olds Ferry quadrangles, Baker and Malheur Counties, Oregon: Oregon Department of Geology and Mineral Industries Geologic Map Series, GMS-13, scale 1:62,500.

Brooks, H.C., and Vallier, T.L., 1978, Mesozoic rocks and tectonic evolution of eastern Oregon and western Idaho, *in* Howell, D.G., and McDougall, K.A., eds., Mesozoic Paleogeography of the Western United States: Los Angeles, Pacific Section, Society of Economic Paleontologists and Mineralogists, p. 133–145.

Brooks, H.C., Ferns, M.L., Coward, R.I., Paul, E.K., and Nunlist, M., 1982a, Geology and Gold Deposits of the Bourne Quadrangle, Baker and Grant Counties, Oregon: Oregon Department of Geology and Mineral Industries Geological Map Series GMS–19, scale 1:24,000, 1 sheet.

Brooks, H.C., Ferns, M.L., and Mullen, E.D., 1982b, Geology and Gold Deposits Map of the Granite Quadrangle, Grant County, Oregon: Oregon Department of Geology and Mineral Industries Geological Map Series GMS–25, scale 1:24,000, 1 sheet.

Brooks, H.C., Ferns, M.L., and Avery, D.G., 1984, Geology and Gold Deposits Map of the Southwest Quarter of the Bates Quadrangle, Grant County, Oregon: Oregon Department of Geology and Mineral Industries Geological Map Series GMS–35, scale 1:24,000, 1 sheet.

Carpenter, P.S., and Walker, N.W., 1992, Origin and tectonic significance of the Aldrich Mountains serpentinite matrix mélange, northeastern Oregon: Tectonics, v. 11, p. 690–708, doi: 10.1029/91TC03013.

Chamberlain, K.R., Snoke, A.W., Barnes, C.G., and Bushey, J.C., 2006, New U-Pb radiometric dates of the Bear Mountain intrusive complex, Klamath Mountains, California, *in* Snoke, A.W., and Barnes, C.G., eds., Geological Studies in the Klamath Mountains Province, California and Oregon: A Volume in Honor of William P. Irwin: Geological Society of America Special Paper 410, p. 317–332.

Coleman, R.G., 1963, Serpentinites, rodingites, and Tectonic Inclusions in Alpine-Type Mountain Chains: Geological Society of America Special Paper 73, 130 p.

Coleman, R.G., Manning, C.E., Mortimer, N., Donato, M.M., and Hill, L.B., 1988, Tectonic and regional metamorphic framework of the Klamath Mountains and adjacent Coast Ranges, California and Oregon, *in* Ernst, W.G., ed., Metamorphism and Crustal Evolution of the Western United States—Rubey Volume 7: Englewood Cliffs, New Jersey, Prentice Hall, p. 1059–1097.

Cordey, F., Mortimer, N., DeWever, P., and Monger, J.W.H., 1987, Significance of Jurassic radiolarians from the Cache Creek terrane, British Columbia: Geology, v. 15, p. 1151–1154, doi: 10.1130/0091-7613(1987)15 <1151:SOJRFT>2.0.CO;2.

Coward, R.I., 1983, Structural Geology, Stratigraphy and Petrology of the Elkhorn Ridge Argillite, in the Sumpter Area, Northeastern Oregon [Ph.D. thesis]: Houston, Texas, Rice University, 144 p.

Currie, L.D., and Parrish, R.R., 1997, Paleozoic and Mesozoic rocks of Stikinia exposed in northwestern British Columbia: Implications for correlations in the northern Cordillera: Geological Society of America Bulletin, v. 109, p. 1402–1420, doi: 10.1130/0016-7606 (1997)109<1402:PAMROS>2.3.CO;2.

Dickinson, W.R., 1979, Mesozoic forearc basin in central Oregon: Geology, v. 7, p. 166–170, doi: 10.1130/ 0091-7613(1979)7<166:MFBICO>2.0.CO;2.

Dickinson, W.R., 1982, Compositions of sandstones in circum-Pacific subduction complexes and fore-arc basins: American Association of Petroleum Geologists Bulletin, v. 66, p. 121–137.

Dickinson, W.R., 2004, Evolution of the North American Cordillera: Annual Review of Earth and Planetary Sciences, v. 32, p. 13–45, doi: 10.1146/annurev .earth.32.101802.120257.

Dickinson, W.R., and Gehrels, G.E., 2009, Use of U-Pb ages of detrital zircons to infer maximum depositional ages of strata: A test against a Colorado Plateau Mesozoic database: Earth and Planetary Science Letters, v. 288, p. 115–125, doi: 10.1016/j.epsl.2009.09.013.

Dickinson, W.R., and Thayer, T.P., 1978, Paleogeographic and paleotectonic implications of Mesozoic stratigraphy and structure in the John Day inlier of central Oregon, *in* Howell, D.G., and McDougall, K.A., eds., Mesozoic paleogeography of the western United States: Society of Economic Paleontologists and Mineralogists, Pacific Section, Paleogeography Symposium 2, p. 147-161.

Dickinson, W.R., and Vigrass, L.W., 1965, Geology of the Suplee-Izee Area, Crook, Grant, and Harney Counties, Oregon: Oregon Department of Geology and Mineral Industries Bulletin 58, 109 p.

Dickinson, W.R., Helmold, K.P., and Stein, J.A., 1979, Mesozoic lithic sandstones in central Oregon: Journal of Sedimentary Research, v. 49, p. 501–516.

Dorsey, R.J., and LaMaskin, T.A., 2007, Stratigraphic record of Triassic–Jurassic collisional tectonics in the Blue Mountains Province, northeastern Oregon: American Journal of Science, v. 307, p. 1167–1193, doi: 10.2475/10.2007.03.

English, J.M., and Johnston, S.T., 2005, Collisional orogenesis in the northern Canadian Cordillera: Implications for Cordilleran crustal structure, ophiolite emplacement, continental growth, and the terrane hypothesis: Earth and Planetary Science Letters, v. 232, p. 333–344, doi: 10.1016/j.epsl.2005.01.025.

Ernst, W.G., 1998, Geologic Map of the Sawyers Bar Area: Geochemical/Petrotectonic Evolution of an Oceanic Island Arc, Central Klamath Mountains, California: California Division of Mines and Geology Map Sheet 47, scale 1:48,000, with 59 p. pamphlet.

Ernst, W.G., 1999, Mesozoic petrotectonic development of the Sawyers Bar suprasubduction-zone arc, central Klamath Mountains, northern California: Geological Society of America Bulletin, v. 111, p. 1217–1232, doi: 10.1130/0016-7606(1999)111<1217:MPDOTS> 2.3.CO;2.

Ernst, W.G., Snow, C.A., and Scherer, H.H., 2008, Contrasting early and late Mesozoic petrotectonic evolution of northern California: Geological Society of America Bulletin, v. 120, p. 179–194, doi: 10.1130/B26173.1.

Evans, J.G., 1989, Geologic Map of the Desolation Butte Quadrangle, Grant and Umatilla Counties, Oregon:

Reston, Virginia, U.S. Geological Survey Geologic Quadrangle GQ-1654, scale 1:62,500, 1 sheet.

Evans, J.G., 1995, Pre-Tertiary deformation in the Desolation Butte Quadrangle, northeastern Oregon, *in* Vallier, T.L., and Brooks, H.C., eds., Geology of the Blue Mountains Region of Oregon, Idaho and Washington: Petrology and Tectonic Evolution of Pre-Tertiary Rocks of the Blue Mountains Region: U.S. Geological Survey Professional Paper 1438, p. 305–330.

Ferns, M.L., and Brooks, H.C., 1995, The Bourne and Greenhorn subterranes of the Baker terrane, northeastern Oregon; implications for the evolution of the Blue Mountains island-arc system, *in* Vallier, T.L., and Brooks, H.C., eds., Geology of the Blue Mountains Region of Oregon, Idaho and Washington: Petrology and Tectonic Evolution of Pre-Tertiary Rocks of the Blue Mountains Region: U.S. Geological Survey Professional Paper 1438, p. 331–358.

Ferns, M.L., and Ramp, L., 1988, Investigations of Talc in Oregon: Oregon Department of Geology and Mineral Industries Special Paper 18, 52 p.

Ferns, M.L., Brooks, A.C., and Avery, D.G., 1983, Geology and Gold Deposits Map of the Greenhorn Quadrangle, Baker and Grant Counties, Oregon: Oregon Department of Geology and Mineral Industries Geological Map Series GMS–28, scale 1:24,000, 1 sheet.

Ferns, M.L., Brooks, H.C., Avery, D.G., and Blome, C.D., 1987, Geology and Mineral Resources Map of the Elkhorn Peak Quadrangle, Baker County, Oregon: Oregon Department of Geology and Mineral Industries Geological Map Series GMS–41, scale 1:24,000, 1 sheet.

Frost, B.R., and Beard, J., 2007, On silica activity and serpentinization: Journal of Petrology, v. 48, p. 1351–1368, doi: 10.1093/petrology/egm021.

Frost, B.R., and Frost, C.D., 2008, A geochemical classification for feldspathic igneous rocks: Journal of Petrology, v. 49, p. 1955–1969, doi: 10.1093/petrology/ egn054.

Frost, B.R., Barnes, C.G., Collins, W.J., Arculus, R.J., Ellis, D.J., and Frost, C.D., 2001, A geochemical classification for granitic rocks: Journal of Petrology, v. 42, p. 2033–2048, doi: 10.1093/petrology/42.11.2033.

Frost, C.D., Barnes, C.G., and Snoke, A.W., 2006, Nd and Sr isotopic data from argillaceous rocks of the Galice Formation and Rattlesnake Creek terrane, Klamath Mountains: Evidence for the input of Precambrian sources, *in* Snoke, A.W., and Barnes, C.G., eds., Geological Studies in the Klamath Mountains Province, California and Oregon: A Volume in Honor of William P. Irwin: Geological Society of America Special Paper 410, p. 103–120.

Fryer, P., Wheat, C.G., and Mottl, M.J., 1999, Mariana blueschist mud volcanism: Implications for conditions within the subduction zone: Geology, v. 27, p. 103–106, doi: 10.1130/0091-7613(1999)027<0103:MBMVIF> 2.3.CO;2.

Gerlach, D.C., Ave Lallemant, H.G., and Leeman, W.P., 1981, An island arc origin for the Canyon Mountain ophiolite complex, eastern Oregon, U.S.: Earth and Planetary Science Letters, v. 53, p. 255–265, doi: 10.1016/0012-821X(81)90158-8.

Gilluly, J., 1937, Geology and Mineral Resources of the Baker Quadrangle, Oregon: U.S. Geological Survey Bulletin 879, 199 p.

Goldstein, S.L., O'Nions, R.K., and Hamilton, P.J., 1984, A Sm-Nd isotopic study of atmospheric dusts and particulates from major river systems: Earth and Planetary Science Letters, v. 70, p. 221–236.

Goodge, J.W., and Renne, P.R., 1993, Mid-Paleozoic olistoliths in eastern Hayfork terrane mélange, Klamath Mountains: Implications for late Paleozoic–early Mesozoic Cordilleran forearc development: Tectonics, v. 12, p. 279–290, doi: 10.1029/92TC01325.

Gradstein, F.M., Ogg, J.G., and Smith, A.G., 2004, A Geologic Time Scale 2004: Cambridge, UK, Cambridge University Press, 589 p.

Gray, K.D., and Oldow, J.S., 2005, Contrasting structural histories of the Salmon River belt and Wallowa terrane: Implications for terrane accretion in northeastern Oregon and west-central Idaho: Geological Society of America Bulletin, v. 117, p. 687–706, doi: 10.1130/ B25411.1.

Gromet, L.P., Dymek, R.F., Haskin, L.A., and Korotev, R.L., 1984, The "North American shale composite": Its compilation, major and trace element characteristics: Geochimica et Cosmochimica Acta, v. 48, p. 2469–2482, doi: 10.1016/0016-7037(84)90298-9.

Hacker, B.R., Donato, M.M., Barnes, C.G., McWilliams, M.O., and Ernst, W.G., 1995, Timescales of orogeny; Jurassic construction of the Klamath Mountains: Tectonics, v. 14, p. 677–703, doi: 10.1029/94TC02454.

Hall, R., 2002, Cenozoic geological and plate tectonic evolution of SE Asia and the SW Pacific: Computer-based reconstructions, models and animations: Journal of Asian Earth Sciences, v. 20, p. 353–431, doi: 10.1016/ S1367-9120(01)00069-4.

Hamilton, W., 1979, Tectonics of the Indonesian Region: U.S. Geological Survey Professional Paper 1078, 345 p.

Harper, G.D., and Wright, J.E., 1984, Middle to Late Jurassic tectonic evolution of the Klamath Mountains, California-Oregon: Tectonics, v. 3, p. 759–772, doi: 10.1029/TC003i007p00759.

Harper, G.D., Saleeby, J.B., and Heizler, M., 1994, Formation and emplacement of the Josephine ophiolite and the Nevadan orogeny in the Klamath Mountains, California-Oregon: U/Pb zircon and ^{40}Ar/^{39}Ar geochronology: Journal of Geophysical Research, v. 99, p. 4293–4321, doi: 10.1029/93JB02061.

Housen, B.A., 2007, Paleomagnetism of Mesozoic-Cenozoic rocks of the Blue Mountains, Oregon: Geological Society of America Abstracts with Programs, v. 39, no. 6, p. 207–208.

Housen, B.A., and Dorsey, R.J., 2005, Paleomagnetism and tectonic significance of Albian and Cenomanian turbidites, Ochoco Basin, Mitchell Inlier, central Oregon: Journal of Geophysical Research, v. 110, p. B07102, doi: 10.1029/2004JB003458.

Imlay, R.W., 1986, Jurassic ammonites and biostratigraphy of eastern Oregon and western Idaho, *in* Vallier, T.L., and Brooks, H.C., eds., Geology of the Blue Mountains Region of Oregon, Idaho, and Washington: Geologic Implications of Paleozoic and Mesozoic Paleontology and Biostratigraphy, Blue Mountains Province, Oregon and Idaho: U.S. Geological Survey Professional Paper 1435, p. 53–57.

Jackson, J.L., Gehrels, G.E., Patchett, P.J., and Mihalynuk, M.G., 1991, Stratigraphic and isotopic link between the northern Stikine terrane and an ancient continental margin assemblage, Canadian Cordillera: Geology, v. 19, p. 1177–1180, doi: 10.1130/0091-7613 (1991)019<1177:SAILBT>2.3.CO;2.

Johnson, K., and Barnes, C.G., 2002, Jurassic magmatism prior to and during terrane accretion in the Blue Mountains Province, NE Oregon: Geological Society of America Abstracts with Programs, v. 34, no. 5, p. 21–22.

Johnson, K., and Schwartz, J.J., 2009, Overview of Jurassic–Cretaceous magmatism in the Blue Mountains Province (NE Oregon & W Idaho): Insights from new Pb/U (SHRIMP-RG) age determinations: Geological Society of America Abstracts with Programs, v. 41, no. 7, p. 182.

Johnson, K., Barnes, C.G., and Miller, C.A., 1997, Petrology, geochemistry, and genesis of high-Al tonalite and trondhjemites of the Cornucopia stock, Blue Mountains, northeastern Oregon: Journal of Petrology, v. 38, p. 1585–1611, doi: 10.1093/petrology/38.11.1585.

Johnson, K., Schwartz, J.J., and Walton, C., 2007, Petrology of the Late Jurassic Sunrise Butte Pluton, eastern Oregon; a record of renewed Mesozoic arc activity?: Geological Society of America Abstracts with Programs, v. 39, no. 6, p. 209.

Jones, D.L., Pessagno, E.A., Jr., Force, E.R., and Irwin, W.P., 1977, Jurassic radiolarian chert from near John Day, Oregon: Geological Society of America Abstracts with Programs, v. 8, p. 386.

Kays, M.A., Stimac, J.P., and Goebel, P.M., 2006, Permian-Jurassic growth and amalgamation of the Wallowa composite terrane, northeastern Oregon, *in* Snoke, A.W., and Barnes, C.G., eds., Geological Studies in the Klamath Mountains Province, California and Oregon: A Volume in Honor of William P. Irwin: Geological Society of America Special Paper 410, p. 465–494.

Schwartz et al.

Kurz, G.A., Northrup, C.J., and Schmitz, M.D., 2009, High-precision U-Pb dating of neoblastic sphene from mylonitic rocks of the Cougar Creek complex, Blue Mountains Province, Oregon–Idaho: Implications for the interplay between deformation and arc magmatism: Geological Society of America Abstracts with Programs, v. 41, no. 7, p. 182.

LaMaskin, T.A., 2009, Stratigraphy, Provenance, and Tectonic Evolution of Mesozoic Basins in the Blue Mountains Province, Eastern Oregon and Western Idaho [Ph.D. thesis]: Eugene, Oregon, University of Oregon, 232 p.

LaMaskin, T.A., Dorsey, R.J., and Vervoort, J.D., 2007, Insights into the Mesozoic tectonic history of the Blue Mountains Province, eastern Oregon, from initial results of detrital zircon dating: Geological Society of America Abstracts with Programs, v. 39, no. 6, p. 208.

LaMaskin, T.A., Dorsey, R., and Vervoort, J., 2008a, Early Mesozoic paleogeography and tectonic evolution of the western United States: Insights from detrital zircon U-Pb geochronology, Blue Mountains Province, NE Oregon: Geological Society of America Abstracts with Programs, v. 41, no. 5, p. 9.

LaMaskin, T.A., Dorsey, R.J., and Vervoort, J.D., 2008b, Tectonic controls on mudrock geochemistry, Mesozoic rocks of eastern Oregon and western Idaho, U.S.A.: Implications for Cordilleran tectonics: Journal of Sedimentary Research, v. 78, p. 765–783, doi: 10.2110/jsr.2008.087.

LaMaskin, T.A., Dorsey, R.J., and Vervoort, J.D., 2009a, Initiation of the Cretaceous, Andean-type margin of the western U.S. Cordillera: Insights from detrital-zircon ages of the Coon Hollow Formation, Idaho, U.S.A.: Geological Society of America Abstracts with Programs, v. 41, no. 7, p. 183.

LaMaskin, T.A., Schwartz, J.J., Dorsey, R.J., Snoke, A.W., Johnson, K., and Vervoort, J.D., 2009b, Mesozoic sedimentation, magmatism, and tectonics in the Blue Mountains Province, northeastern Oregon, *in* O'Connor, J.E., Dorsey, R.J., and Madin, I.P., eds., Volcanoes to Vineyards: Geologic Field Trips through the Dynamic Landscape of the Pacific Northwest: Boulder, Colorado, Geological Society of America, Field Guide 15, p. 187–202.

LaMaskin, T.A., Vervoort, J.D., Dorsey, R.J., and Wright, J.E., 2011, Early Mesozoic paleogeography and tectonic evolution of the western United States: Insights from detrital zircon U-Pb geochronology, Blue Mountains Province, northeastern Oregon: Geological Society of America Bulletin (in press), doi: 10.1130/B30260.1.

Lanphere, M.A., Irwin, W.P., and Hotz, P.E., 1968, Isotopic age of the Nevadan orogeny and older plutonic and metamorphic events in the Klamath Mountains, California: Geological Society of America Bulletin, v. 79, p. 1027–1052, doi: 10.1130/0016-7606(1968)79[1027:IAOTNO]2.0.CO;2.

Lapierre, H., Bosch, D., Tardy, M., and Struik, L.C., 2003, Late Paleozoic and Triassic plume-derived magmas in the Canadian Cordillera played a key role in continental crust growth: Chemical Geology, v. 201, p. 55–89, doi: 10.1016/S0009-2541(03)00224-9.

Leeman, W.P., Ave Lallemant, H.G., Gerlach, D.C., Sutter, J.F., and Arculus, R.J., 1995, Petrology of the Canyon Mountain complex, eastern Oregon, *in* Vallier, T.L., and Brooks, H.C., eds., Geology of the Blue Mountains Region of Oregon, Idaho and Washington: Petrology and Tectonic Evolution of Pre-Tertiary Rocks of the Blue Mountains Region: U.S. Geological Survey Professional Paper 1438, p. 1–43.

Lund, K., 1995, Metamorphic and structural development of island-arc rocks in the Slate Creek–John Day Creek area, west-central Idaho, *in* Vallier, T.L., and Brooks, H.C., eds., Geology of the Blue Mountains Region of Oregon, Idaho, and Washington: Petrology and Tectonic Evolution of Pre-Tertiary Rocks of the Blue Mountains Region: U.S. Geological Survey Professional Paper 1438, p. 517–540.

MacIntyre, D.G., Villeneuve, M.E., and Schiarizza, P., 2001, Timing and tectonic setting of Stikine terrane magmatism, Babine-Takla lakes area, central British Columbia: Canadian Journal of Earth Sciences (Revue Canadienne des Sciences de la Terre), v. 38, p. 579–601.

Mailloux, J.M., Starns, E.C., Snoke, A.W., and Frost, C.D., 2009, An isotopic study of the Burnt River Schist: Implications for the development of the composite Baker terrane, Blue Mountains Province, NE Oregon: Geological Society of America Abstracts with Programs, v. 41, no. 7, p. 441.

Marsden, H., and Thorkelson, D.J., 1992, Geology of the Hazelton volcanic belt in British Columbia; implications for the Early to Middle Jurassic evolution of Stikinia: Tectonics, v. 11, p. 1266–1287, doi: 10.1029/92TC00276.

Mihalynuk, M.G., Nelson, J., and Diakow, L.J., 1994, Cache Creek terrane entrapment; oroclinal paradox within the Canadian Cordillera: Tectonics, v. 13, p. 575–595, doi: 10.1029/93TC03492.

Morris, E., and Wardlaw, B.R., 1986, Conodont ages for limestones of eastern Oregon and their implications for pre-Tertiary mélange terranes, *in* Vallier, T.L., and Brooks, H.C., eds., Geology of the Blue Mountains Region of Oregon, Idaho, and Washington: Paleontology and Biostratigraphy: U.S. Geological Survey Professional Paper 1435, p. 59–64.

Mortimer, N., 1986, Late Triassic, arc-related, potassic igneous rocks in the North American Cordillera: Geology, v. 14, p. 1035–1038, doi: 10.1130/0091-7613(1986)14<1035:LTAPIR>2.0.CO;2.

Mullen, E.D., 1978, Geology of the Greenhorn Mountains, Northeastern Oregon [M.S. thesis]: Corvallis, Oregon State University, 372 p.

Mullen, E.D., 1980, Temperature-pressure progression in high pressure Permo-Triassic metamorphic rocks of N.E. Oregon: Eos (Transactions, American Geophysical Union), v. 61, p. 70–71.

Mullen, E.D., 1983, Petrology and Regional Setting of Peridotite and Gabbro of the Canyon Mountain Complex, Northeast Oregon [Ph.D. thesis]: Corvallis, Oregon State University, 277 p.

Mullen, E.D., 1985, Petrologic character of Permian and Triassic greenstones from the mélange terrane of eastern Oregon and their implications for terrane origin: Geology, v. 13, p. 131–134, doi: 10.1130/0091-7613(1985)13<131:PCOPAT>2.0.CO;2.

Nelson, J., and Mihalynuk, M., 1993, Cache Creek ocean: Closure or enclosure?: Geology, v. 21, p. 173–176, doi: 10.1130/0091-7613(1993)021<0173:CCOCOE>2.3.CO;2.

Nestell, M.K., 1983, Permian foraminiferal faunas of central and eastern Oregon: Geological Society of America Abstracts with Programs, v. 15, no. 5, p. 371.

Nestell, M.K., and Nestell, G.P., 1998, Middle Permian conodonts and Tethyan fusulinaceans associated with possible seamount debris in Oregon: Geological Society of America Abstracts with Programs, v. 30, no. 7, p. 151–152.

Nestell, M.K., and Orchard, M.J., 2000, Late Paleozoic and middle Late Triassic conodont assemblages from the Baker terrane, eastern Oregon: Geological Society of America Abstracts with Programs, v. 32, no. 6, p. 59.

Nestell, M.K., Lambert, L.L., and Wardlaw, B.R., 1995, Pennsylvanian conodonts and fusulinaceans of the Baker terrane, eastern Oregon: Geological Society of America Abstracts with Programs, v. 27, no. 3, p. 76.

Orchard, M.J., Cordey, F., Rui, L., Bamber, E.W., Mamet, B., Struik, L.C., Sano, H., and Taylor, H.J., 2001, Biostratigraphic and biogeographic constraints on the Carboniferous to Jurassic Cache Creek terrane in central British Columbia: Canadian Journal of Earth Sciences, v. 38, p. 551–578, doi: 10.1139/cjes-38-4-551.

Pálfy, J., Smith, P.L., Mortensen, J.K., 2000, A U-Pb and ^{40}Ar/^{39}Ar time scale for the Jurassic: Canadian Journal of Earth Sciences, v. 37, p. 923–944.

Pardee, J.T., and Hewett, D.F., 1914, Geology and Mineral Resources of the Sumpter Quadrangle, Oregon: Oregon, Oregon Bureau of Mines and Geology, v. 1, no. 6, p. 3–128.

Parker, K.O., Schwartz, J.J., Johnson, K., and Anonymous, 2008, Petrology and age of Dixie Butte plutonic rocks, Blue Mountains, NE Oregon: Geological Society of America Abstracts with Programs, v. 40, no. 6, p. 154–155.

Patchett, P.J., and Gehrels, G.E., 1998, Continental influence of Canadian Cordilleran terranes from Nd isotopic study, and significance for crustal growth processes: The Journal of Geology, v. 106, p. 269–280, doi: 10.1086/516021.

Prostka, H.J., and Bateman, R.L., 1962, Geology of the Sparta Quadrangle, Oregon: Oregon Department of Geology and Mineral Industries Geological Map Series GMS-1, scale 1:62,500, 1 sheet.

Ricketts, B.D., Evenchick, C.A., Anderson, R.G., and Murphy, D.C., 1992, Bowser Basin, northern British Columbia: Constraints on the timing of initial subsidence and Stikinia–North America terrane interactions: Geology, v. 20, p. 1119–1122, doi: 10.1130/0091-7613(1992)020<1119:BBNBCC>2.3.CO;2.

Saleeby, J.B., Harper, G.D., Snoke, A.W., and Sharp, W.D., 1982, Time relations and structural-stratigraphic patterns in ophiolite accretion, west central Klamath Mountains, California: Journal of Geophysical Research, v. 87, p. 3831–3848, doi: 10.1029/JB087iB05p03831.

Scherer, H.H., and Ernst, W.G., 2008, North Fork terrane, Klamath Mountains, California: Geologic, geochemical, and geochronologic evidence for an early Mesozoic fore-arc, *in* Wright, J.E., and Shervais, J.W., eds., Ophiolites, Arcs and Batholiths: A Tribute to Cliff Hopson: Geological Society of America Special Paper 438, p. 289–309.

Scherer, H.H., Snow, C.A., and Ernst, W.G., 2006, Geologic-petrochemical comparison of early Mesozoic oceanic terranes: Western Paleozoic and Triassic Belt, Klamath Mountains, and Jura-Triassic arc, Sierran Foothills, *in* Snoke, A.W., and Barnes, C.G., eds., Geological Studies in the Klamath Mountains Province, California and Oregon: A Volume in Honor of William P. Irwin: Boulder, Colorado, Geological Society of America Special Paper 410, p. 377–392.

Schwartz, J.J., and Johnson, K., 2009, Origin of paired Late Jurassic high and low Sr/Y magmatic belts in the Blue Mountains Province, NE Oregon: Geological Society of America Abstracts with Programs, v. 41, no. 7, p. 182.

Schwartz, J.J., Snoke, A.W., Frost, C.D., Barnes, C.G., Gromet, L.P., and Johnson, K., 2010, Analysis of the Baker-Wallowa terrane boundary: Implications for tectonic accretion in the Blue Mountains Province, northeastern Oregon: Geological Society of America Bulletin, v. 122, p. 517–536, doi: 10.1130/B26493.1.

Schweickert, R.A., and Cowan, D.S., 1975, Early Mesozoic tectonic evolution of the western Sierra Nevada, California: Geological Society of America Bulletin, v. 86, p. 1329–1336, doi: 10.1130/0016-7606(1975)86<1329:EMTEOT>2.0.CO;2.

Schweickert, R.A., Bogen, N.L., Girty, G.H., Hanson, R.E., and Merguerian, C., 1984, Timing and structural expression of the Nevadan orogeny, Sierra Nevada, California: Geological Society of America Bulletin, v. 95, p. 967–979, doi: 10.1130/0016-7606(1984)95<967:TASEOT>2.0.CO;2.

Silberling, N.J., Jones, D.L., Blake, M.C., and Howell, D.G., 1987, Lithotectonic Terrane Map of the Western Conterminous United States: U.S. Geological Survey Miscellaneous Field Studies Map MF-1874-C, scale 1:250,000, with 20 p. pamphlet.

Snee, L.W., Lund, K., Sutter, J.F., Balcer, D.E., and Evans, K.V., 1995, An ^{40}Ar/^{39}Ar chronicle of the tectonic development of the Salmon River suture zone, western Idaho, *in* Vallier, T.L., and Brooks, H.C., eds., Geology of the Blue Mountains Region of Oregon, Idaho and Washington: Petrology and Tectonic Evolution of Pre-Tertiary Rocks of the Blue Mountains Region: U.S. Geological Survey Professional Paper 1438, p. 359–414.

Snoke, A.W., 1977, A thrust plate of ophiolitic rocks in the Preston Peak area, Klamath Mountains, California: Geological Society of America Bulletin, v. 88, p. 1641–1659, doi: 10.1130/0016-7606(1977)88<1641:ATPOOR>2.0.CO;2.

Snoke, A.W., and Barnes, C.G., 2006, The development of tectonic concepts for the Klamath Mountains province, California and Oregon, *in* Snoke, A.W., and Barnes, C.G., eds., Geological Studies in the Klamath

Late Jurassic orogenesis in the Blue Mountains Province

Mountains Province, California and Oregon: A Volume in Honor of William P. Irwin: Geological Society of America Special Paper 410, p. 1–29.

Snow, C.A., and Scherer, H., 2006, Terranes of the western Sierra Nevada foothills metamorphic belt, California; a critical review: International Geology Review, v. 48, p. 46–62, doi: 10.2747/0020-6814.48.1.46.

Stacey, J.S., and Kramers, J.D., 1975, Approximation of terrestrial lead isotope evolution by a two stage model: Earth and Planetary Science Letters, v. 26, p. 207–221, doi: 10.1016/0012-821X(75)90088-6.

Stanley, G.D., and Senowbari-Daryan, B., 1986, Upper Triassic, Dachstein-type, reef limestone from the Wallowa Mountains, Oregon: First reported occurrence in the United States: Palaios, v. 1, p. 172–177, doi: 10.2307/3514511.

Stanley, G.D., Jr., McRoberts, C.A., and Whalen, M.T., 2008, Stratigraphy of the Triassic Martin Bridge Formation, Wallowa terrane: Stratigraphy and depositional setting, *in* Blodgett, R.B. and Stanley, G.D., Jr., eds., The terrane puzzle: New perspectives on paleontology and stratigraphy from North American Cordillera: Boulder, Colorado, Geological Society of America Special Paper 442, p. 227–250.

Stimson, E.J., 1980, Geology and Metamorphic Petrology of the Elkhorn Ridge Area, Northeastern Oregon [M.S. thesis]: Eugene, University of Oregon, 123 p.

Struik, L.C., 2001, Tethyan fragments in the central Canadian Cordillera trapped during continental growth: Gondwana Research, v. 4, p. 790–791, doi: 10.1016/S1342-937X(05)70573-6.

Struik, L.C., Schiarizza, P., Orchard, M.J., Cordey, F., Sano, H., MacIntyre, D.G., Lapierre, H., and Tardy, M., 2001, Imbricate architecture of the Upper Paleozoic to Jurassic oceanic Cache Creek terrane, central British Columbia: Canadian Journal of Earth Sciences, v. 38, p. 495–514, doi: 10.1139/cjes-38-4-495.

Sun, S.S., and McDonough, W.F., 1989, Chemical and isotopic systematics of oceanic basalts: Implications for mantle composition and processes, *in* Saunders, A. D., and Norry, M. J., eds., Magmatism in the Ocean Basins: Geological Society of London Special Publication 42, p. 313–345, doi: 10.1144/GSL.SP.1989.042.01.19.

Taliaferro, N.L., 1942, Geologic history and correlation of the Jurassic of southwestern Oregon and California: Geological Society of America Bulletin, v. 53, p. 71–112.

Tardy, M., Lapierre, H., Struik, L.C., Bosch, D., and Brunet, P., 2001, The influence of mantle plume in the genesis of the Cache Creek oceanic igneous rocks: Implications for the geodynamic evolution of the inner accreted terranes of the Canadian Cordillera: Canadian Journal of Earth Sciences, v. 38, p. 515–534, doi: 10.1139/cjes-38-4-515.

Taubeneck, W.H., 1964, Cornucopia stock, Wallowa Mountains, northeastern Oregon: Field relations: Geological Society of America Bulletin, v. 75, p. 1093–1115, doi: 10.1130/0016-7606(1964)75[1093:CSWMNO]2.0.CO;2.

Taubeneck, W.H., 1967, Petrology of the Cornucopia Tonalite Unit, Cornucopia Stock, Wallowa Mountains, Northeastern Oregon: Geological Society of America Special Paper, 56 p.

Taubeneck, W.H., 1995, A closer look at the Bald Mountain batholith, Elkhorn Mountains, and some comparisons with the Wallowa batholith, Wallowa Mountains,

northeastern Oregon, *in* Vallier, T.L., and Brooks, H.C., eds., Geology of the Blue Mountains Region of Oregon, Idaho, and Washington: Petrology and Tectonic Evolution of Pre-Tertiary Rocks of the Blue Mountains Region: U.S. Geological Survey Professional Paper 1438, p. 45–138.

Thomson, R.C., Smith, P.L., and Tipper, H.W., 1986, Lower to Middle Jurassic (Pliensbachian to Bajocian) stratigraphy of the northern Spatsizi area, north-central British Columbia: Canadian Journal of Earth Sciences (Revue Canadienne des Sciences de la Terre), v. 23, p. 1963–1973.

Tulloch, A.J., and Kimbrough, D.L., 2003, Paired plutonic belts in convergent margins and the development of high Sr/Y magmatism; Peninsular Ranges Batholith of Baja California and Median Batholith of New Zealand, *in* Johnson, S.E., Paterson, S.R., Fletcher, J.M., Girty, G.H., Kimbrough, D.L., and Martin-Barajas, A., eds., Tectonic Evolution of Northwestern Mexico and the Southwestern USA: Geological Society of America Special Paper 374, p. 275–295.

Tumpane, K.P., and Schmitz, M.D., 2009, New geochronological constraints on the timing of deposition in the Coon Hollow and Weatherby Formations, and correlations between the Wallowa and Olds Ferry terranes, Blue Mountains Province, northern U.S. Cordillera: Geological Society of America Abstracts with Programs, v. 41, no.7, p. 182.

Unruh, D.M., Lund, K., Kuntz, M.A., and Snee, L.W., 2008, Uranium-Lead Zircon Ages and Sr, Nd, and Pb Isotope Geochemistry of Selected Plutonic Rocks from Western Idaho: U.S. Geological Survey Open-File Report 1142, 37 p.

Unterschutz, J.L.E., Creaser, R.A., Erdmer, P., Thompson, R.I., and Daughtry, K.L., 2002, North American margin origin of Quesnel terrane strata in the southern Canadian Cordillera: Inferences from geochemical and Nd isotopic characteristics of Triassic metasedimentary rocks: Geological Society of America Bulletin, v. 114, p. 462–475, doi: 10.1130/0016-7606(2002)114<0462:NAMOOQ>2.0.CO;2.

Vallier, T.L., 1977, The Permian and Triassic Seven Devils Group, Western Idaho and Northeastern Oregon: U.S. Geological Survey Bulletin 1437, 58 p.

Vallier, T.L., 1995, Petrology of pre-Tertiary igneous rocks in the Blue Mountains region of Oregon, Idaho, and Washington; implications for the geologic evolution of a complex island arc, *in* Vallier, T.L., and Brooks, H.C., eds., Geology of the Blue Mountains Region of Oregon, Idaho and Washington: Petrology and Tectonic Evolution of Pre-Tertiary Rocks of the Blue Mountains Region: U.S. Geological Survey Professional Paper 1438, p. 125–209.

Vallier, T.L., and Batiza, R., 1978, Petrogenesis of spilite and keratophyre from a Permian and Triassic volcanic arc terrane, eastern Oregon and western Idaho, U.S.: Canadian Journal of Earth Sciences, v. 15, p. 1356–1369.

Vallier, T.L., Brooks, H.C., and Thayer, T.P., 1977, Paleozoic rocks of eastern Oregon and western Idaho: Los Angeles, California, Pacific Section, Society of Economic Paleontologists and Mineralogists, p. 455–466.

Walker, N.W., 1986, U/Pb geochronologic and petrologic studies in the Blue Mountains terrane, northeastern Oregon and westernmost-central Idaho: Implications

for pre-Tertiary tectonic evolution [Ph.D. dissertation]: Santa Barbara, University of California, 224 p.

Walker, N.W., 1989, Early Cretaceous initiation of post-tectonic plutonism and the age of the Connor Creek fault, northeastern Oregon: Geological Society of America Abstracts with Programs, v. 21, no. 5, p. 155.

Walker, N.W., 1995, Tectonic implications of U-Pb zircon ages of the Canyon Mountain complex, Sparta complex, and related metaplutonic rocks of the Baker terrane, northeastern Oregon, *in* Vallier, T.L., and Brooks, H.C., eds., Geology of the Blue Mountains Region of Oregon, Idaho, and Washington: Petrology and Tectonic Evolution of Pre-Tertiary Rocks of the Blue Mountains Region: U.S. Geological Survey Professional Paper 1438, p. 247–269.

Wardlaw, B.R., Nestell, M.K., and Dutro, J.T., 1982, Biostratigraphy and structural setting of the Permian Coyote Butte Formation of central Oregon: Geology, v. 10, p. 13–16, doi: 10.1130/0091-7613(1982)10<13:BASSOT>2.0.CO;2.

Wheeler, G.R., 1976, Geology of the Vinegar Hill Area, Grant County, Oregon [Ph.D. dissertation]: Seattle, University of Washington, 94 p.

White, W.H., 1973, Flow structure and form of the Deep Creek stock, southern Seven Devils Mountains, Idaho: Geological Society of America Bulletin, v. 84, p. 199–210, doi: 10.1130/0016-7606(1973)84<199:FSAFOT>2.0.CO;2.

Wilson, D., and Cox, A., 1980, Paleomagnetic evidence for tectonic rotation of Jurassic plutons in Blue Mountains, eastern Oregon: Journal of Geophysical Research, v. 85, p. 3681–3689, doi: 10.1029/JB085iB07p03681.

Wright, J.E., 1982, Permo-Triassic accretionary subduction complex, southwestern Klamath Mountains, northern California: Journal of Geophysical Research, v. 87, p. 3805–3818, doi: 10.1029/JB087iB05p03805.

Wright, J.E., and Fahan, M.R., 1988, An expanded view of Jurassic orogenesis in the western United States Cordillera; Middle Jurassic (pre-Nevadan) regional metamorphism and thrust faulting within an active arc environment, Klamath Mountains, California: Geological Society of America Bulletin, v. 100, p. 859–876, doi: 10.1130/0016-7606(1988)100<0859:AEVOJO>2.3.CO;2.

Wright, J.E., and Wyld, S.J., 1994, The Rattlesnake Creek terrane, Klamath Mountains, California; an early Mesozoic volcanic arc and its basement of tectonically disrupted oceanic crust: Geological Society of America Bulletin, v. 106, p. 1033–1056, doi: 10.1130/0016-7606(1994)106<1033:TRCTKM>2.3.CO;2.

Wright, J.E., and Wyld, S.J., 2007, Alternative tectonic model for Late Jurassic through Early Cretaceous evolution of the Great Valley Group, California, *in* Cloos, M., Carlson, W.D., Gilbert, M.C., Liou, J.G., and Sorensen, S.S., eds., Convergent Margin Terranes and Associated Regions: A Tribute to W.G. Ernst: Geological Society of America Special Paper 419, p. 81–95.